LBL-1800
c.1

THE CRYSTALLOGRAPHY AND STRUCTURE OF DEFORMATION INDUCED EPSILON AND ALPHA MARTENSITE IN Fe-Ni-Cr SINGLE CRYSTALS

Glen Andrew Stone
(Ph.D. thesis)

September, 1974

Prepared for the U. S. Atomic Energy Commission
under Contract W-7405-ENG-48

For Reference

Not to be taken from this room

LAWRENCE BERKELEY LABORATORY • UNIVERSITY OF CALIFORNIA • BERKELEY

LBL-1800
c.1

DISCLAIMER

This document was prepared as an account of work sponsored by the United States Government. While this document is believed to contain correct information, neither the United States Government nor any agency thereof, nor the Regents of the University of California, nor any of their employees, makes any warranty, express or implied, or assumes any legal responsibility for the accuracy, completeness, or usefulness of any information, apparatus, product, or process disclosed, or represents that its use would not infringe privately owned rights. Reference herein to any specific commercial product, process, or service by its trade name, trademark, manufacturer, or otherwise, does not necessarily constitute or imply its endorsement, recommendation, or favoring by the United States Government or any agency thereof, or the Regents of the University of California. The views and opinions of authors expressed herein do not necessarily state or reflect those of the United States Government or any agency thereof or the Regents of the University of California.

0 0 0 0 3 9 0 0 7 3 8

THE CRYSTALLOGRAPHY AND STRUCTURE OF DEFORMATION INDUCED EPSILON AND ALPHA MARTENSITE IN Fe-Ni-Cr SINGLE CRYSTALS

Contents

ABSTRACT v

PART I. THE CRYSTALLOGRAPHY OF α MARTENSITE IN Fe-15wt%Ni-15wt%Cr SINGLE CRYSTALS

I. INTRODUCTION 1

A. Principles of the Phenomenological Theory 1

II. EXPERIMENTAL PROCEDURES 6

A. Habit Plane Measurements 6

B. Shape Change Measurements 9

III. EXPERIMENTAL RESULTS 16

A. Computer Calculations of Habit Plane and Shape Strain Using the AB Two-Shear Model 16

B. Habit Plane Measurement Results 19

C. Shape Change Measurement Results 21

IV. DISCUSSION 24

A. Comparison of the AB Theory and Experimental Results 24

B. Factors that Effect the Accuracy of Habit Plane and Shape Strain Calculations 26

V. CONCLUSIONS 31

PART II. THE STRUCTURE AND MECHANICAL PROPERTIES OF DEFORMATION INDUCED ε AND α MARTENSITE IN Fe-15Ni-15Cr SINGLE CRYSTALS

I. INTRODUCTION 33

II. STRUCTURE AND PROPERTIES 38

A. General Features of the Microstructure 38

B. Relationship Between ε Martensite and Slip in the Austenite 40

C. Why Deformation Induced ε Martensite Partitions the Austenite Matrix 41

D. Volume Fraction Measurements of Deformation Induced ε Martensite as a Function of Crystal Orientation, Temperature and Strain 43

E. Volume Fraction Measurements of Deformation Induced α Martensite as a Function of Crystal Orientation 45

F. Discussion of the Volume Fraction Measurements and Mechanical Property Results 46

G. Conclusions 51

III. THE DEFORMATION INDUCED MARTENSITE-AUSTENITE INTERFACE 54

ACKNOWLEDGEMENTS 56

REFERENCES 57

APPENDICES

A. A Computer Program to Calculate the Exact Specimen Normal from Indexed Back Reflection Laue Photographs. . 60

B. A Computer Program to Calculate the Direction of a Trace on the Surface of a Single Crystal 65

C. A Computer Program to Calculate the Magnitude and Direction of the Shape Change Associated with the γ→α Martensitic Transformations 72

D. The Mechanism of the γ→ε Deformation Induced Phase Transformation 77

E. The Volume Fraction of ε and α Martensite as a Function of Strain 81

FIGURES 99

THE CRYSTALLOGRAPHY AND STRUCTURE OF DEFORMATION INDUCED EPSILON AND ALPHA MARTENSITE IN Fe-Ni-Cr SINGLE CRYSTALS

Glen Andrew Stone

Inorganic Materials Research Division, Lawrence Berkeley Laboratory and Department of Materials Science and Engineering, College of Engineering; University of California, Berkeley, California

ABSTRACT

A comprehensive study of the crystallography and structure of deformation induced ε and α martensite (from austenite) in a low stacking fault energy Fe-15wt%Ni-15wt%Cr alloy has been completed. The martensite needle axis, magnitude of the shape change and direction of the shape change have been measured. When these results were compared to the Acton-Bevis two shear phenomenological theory, using two slip shears, the following result was obtained for the habit plane normal (assuming the long axis of the needles lie in the habit plane and the habit plane is perpendicular to the slip plane),

$$\vec{h} = \langle 0.333,\ 0.812,\ 0.479 \rangle_{\gamma} \quad \text{Experimental}$$

$$\vec{h} = \langle 0.341,\ 0.812,\ 0.475 \rangle_{\gamma} \quad \text{Theoretical}$$

for the direction of the shape change vector,

$$\vec{u} = \langle 0.822,\ 0.129,\ 0.555 \rangle_{\gamma} \quad \text{Experimental}$$

$$\vec{u} = \langle 0.825,\ 0.158,\ 0.542 \rangle_{\gamma} \quad \text{Theoretical}$$

and for the magnitude of the shape change experimental values varied between 0.21 to 0.30 and theoretical values varied between 0.25 to 0.39.

Studies of the microstructure show that in this alloy ε martensite will not form independently of α martensite by quenching. This is because the ε martensite start temperature (Es_γ) is less than or equal to the α martensite start temperature (Ms_γ). The deformation start temperature for ε martensite (Ed_γ) is greater than 300°K in this alloy. The α martensite start temperature (Md_γ) is 190±5°K for specimens deformed in tension with a $[100]_\gamma$ tensile axis. Deformation induced ε martensite forms as thin sheets parallel to active $\{111\}_\gamma$ slip planes. The ε phase at all temperatures partitions the austenite matrix with parallel sheets of ε 0.5 to 2.5 microns apart. This forces the α martensite to form in packets that are sandwiched between two ε sheets. The α martensite in this alloy is acicular and dislocated. Separate volumes of α martensite needles always meet at a $\{112\}_\alpha$ twin boundary. The internal structure is dislocated martensite, not twinned, even though the material exhibits the $\{252\}_\gamma$ habit plane commonly associated with twinned Fe-C, Fe-Mn-C and Fe-Cr-C alloys.

The magnitude of the critical resolved shear stress (CRSS) on possible α martensite habit planes controls which variants of the habit that can form. Measurements of the habits present in deformed single crystals agree well with the CRSS model of Patel and Cohen. The variants of the Kurdjumov-Sachs (KS) orientation relation present for α martensite were always the variants that contained both the active slip planes and slip directions. This result demonstrates that the K-S variants that are present also depend on the CRSS.

The sequence of transformations in the temperature range studied are $\gamma \rightleftharpoons \varepsilon$ and $\gamma \rightarrow \alpha$. The $\varepsilon \rightarrow \alpha$ transformation was not observed. The ease of these transformations above Es_γ and Ms_γ depends on the magnitude of the CRSS on potential habits. The $\gamma \rightarrow \varepsilon$ transformation is believed always to occur first. The $\varepsilon \rightarrow \gamma$ (reversion) occurs at large plastic strains after a significant amount of α martensite has formed. In addition to the $\varepsilon - \alpha$ interface formed by ε sheets parallel to $\{111\}_\gamma$ planes, ε martensite surrounding the entire α martensite needle has been observed. This situation is formed during accommodation deformation of the austenite adjacent to the growing α martensite needle.

PART I. THE CRYSTALLOGRAPHY OF α MARTENSITE IN Fe-15wt%Ni-15wt%Cr SINGLE CRYSTALS

I. INTRODUCTION

The great majority of steels exhibit either the $\{3,15,10\}_\gamma$ or $\{252\}_\gamma$ interface plane (habit). The phenomenological theory[1-4] has been successfully applied to explain the crystallographic features of $\{3,15,10\}_\gamma$ martensite. However the $\{252\}_\gamma$ habit that is observed in many low stacking fault energy steels (Fe-Mn-C, Fe-Cr-C and Fe-C alloys for example) has not been effectively explained, mainly because of the absence in the literature of measurements of the martensite shape strain and habit plane for these alloys. The objective in Part I is to obtain such measurements for an Fe-15Ni-15Cr alloy (alloy compositions are weight percent unless otherwise specified) and to test those measurements against results obtained from a new generalized phenomenological theory by Acton and Bevis (AB)[5] and Ross and Crocker (RC).[6] The objective is to test the theory to see if the generalized theory can effectively describe the crystallography of steels with the $\{252\}_\gamma$ habit plane.

A. Principles of the Phenomenological Theory

The martensitic phase transformation requires the motion of many atoms over short distances in the absence of diffusion. The change in crystal structure is accomplished by a homogeneous deformation of the crystal lattice and the experimentally observed change in shape is accomplished by a lattice invariant shear in the martensite. The

magnitude and direction of the lattice invariant shear must have values that preserve the experimentally observed orientation relationship and interface plane (habit plane) between the austenite and martensite phases. The habit plane is observed to be undistorted or nearly undistorted and unrotated with respect to the original crystal matrix.

The formulation of the present phenomenological theory of martensite crystallography developed from experimental studies of Greninger and Troiano.[1,2] They observed the existence of irrational habit planes in Fe-C and Fe-Ni alloys. Studies of the shape deformation in an Fe-22 Ni-0.8C alloy indicated the observed surface relief could be described by a homogeneous shear on the habit plane of the martensite plate. When the shape deformation alone was applied to the fcc lattice, the b.c.c. or b.c.t. lattice was not generated. It was concluded that two deformations must be required: a homogeneous deformation that produces the required change in the crystal structure and secondly, a lattice invariant shear which leaves the habit plane undistorted and unrotated to comply with the experimental results.

Wechsler, Lieberman and Read (WLR),[3] and Bowles and MacKenzie (BM)[4] independently developed mathematical models of the phenomenological theory to describe martensite crystallography. Both theories may be represented by the matrix equation

$$F = RPS \tag{1}$$

where F is the overall shape strain of the martensite crystal, R is a rigid body rotation often referred to in the literature as the

orientation relationship, P is the lattice deformation and S is the lattice invariant shear. The lattice deformation P contains the lattice correspondence and allied deformations that describe the motion of each parent lattice site into the product structure. The lattice correspondence that appears most likely for steels was proposed by Bain[7] and is shown in Fig. 1. The lattice invariant shear S is assumed to be a normal deformation mode such as slip or twinning. It is easily shown that a lattice deformation and lattice invariant shear can produce an undistorted interface plane, however the plane is no longer related to its original interface position in the lattice. To make the interface plane indeed invariant to agree with experimental observations a rigid body rotation was added to the theory. The rotation matrix R can be calculated for any combination of lattice invariant line and habit plane normal. This will determine the invariant line strain associated with lattice invariant shear S.

Before one can say the phenomenological theory is valid, it is necessary that the calculated and experimental orientation relationships between the austenite and martensite matrix, the habit plane and the magnitude and direction of the overall shape change of the martensite crystal all agree. The success (the $\{3,15,10\}_\gamma$ habit planes) and failure (the $\{252\}_\gamma$ habit planes) of this theory as applied to numerous alloy systems is throughly reviewed by Christian[8,9] and Wayman.[10-12] The problem of particular interest in this thesis which has not been described in any acceptable way by the WLR and BM models is the $\{252\}_\gamma$ habit plane observed in many low stacking fault austenitic stainless steels.

The (AB) and (RC) model of the theory evolved around the concept that perhaps a multiple lattice invariant shear in the martensite is occurring during the phase transformation. This theory is expressed by the matrix equation

$$F = RPTS \tag{2}$$

where T is an additional lattice invariant shear. The mode of shear as before may be by slip or twinning of the martensite. Observations of multiple twinning shears have been made by Oka and Wayman,[13] Das and Thomas[14] and Thomas and Das.[15] Wayman,[16] is careful to point out that there is no sure way one can prove that the multiple twinning shear observed in the martensite is due to the transformation or is an accommodation effect. The transformation shears are the homogeneous deformation and lattice invariant shear defined in the theory. The shears associated with accommodation deformation are those caused by impingment of adjacent martensite needles in regions of high volume fraction of martensite. Clearly if accommodation deformation is present in the martensite or austenite, agreement between the measure and calculated magnitude and direction of the shape change would not be expected.

This is a serious problem and the only way to effectively show that the shears observed in alloys that appear to have a multiple lattice invariant twinning shear is to carefully measure both the overall shape strain and the habit plane in alloys were a low volume fraction of α

martensite can be produced. As far as this author knows this is the first comprehensive study using single crystals to measure these parameters and apply the results to the generalized theory. Acton and Bevis[5] use published data[13,16,17,18] to test their theory and obtained what can be considered encouraging results in explaining martensite crystallography of alloys exhibiting the $\{252\}_\gamma$ habit plane.

The magnitude and direction of the shape strain and the habit plane have been measured using single crystals of a Fe-15Ni-15Cr alloy. Numerous computer calculations using the (AB) model have been made and a summary is presented in this thesis; the purpose is to test the two shear version of their theory. It is interesting to note that the lattice invariant shear (s) in this alloy, are not twinning shears even though the habit appears to be near the $\{252\}_\gamma$. Studies of microstructure of this alloy in the electron microscope reveal that the internal structure of the α martensite is dislocated, not twinned. A typical electron micrograph showing the dislocated martensite is shown in Fig. 2. Detailed analysis of the microstructures will be presented in Part II.

II. EXPERIMENTAL PROCEDURES

A. Habit Plane Measurements

The habit plane for martensite in a particular alloy is usually established by cutting specimens to expose two surfaces 90 degrees apart. If the martensite is lenticular and exhibits a structural feature such as a mid-rib, which is believed to be the trace of the habit plane, the Miller indices of the habit plane can be obtained. The α martensite in this Fe-15Ni-15Cr alloy is acicular. Two surface analysis of this alloy shows the needle type morphology and also shows the habit plane cannot be established directly by this method. An example of a two surface study using the optical and electron microscopes is shown in Fig. 3.

A habit plane must exist. To establish what it is in this alloy requires a combination of consistent observation between experiment and theory. Kelly[19] has observed in similar alloys that the habit planes near the $\{252\}_\gamma$ always appear to be perpendicular to a $\{111\}_\gamma$ plane. It also appears that the long axis of the needle lies in the habit plane. Computer calculations using the AB theory generates many variants of the habit plane of the type $\{0.340, 0.812, 0.474\}_\gamma$ (these results to be presented in detail later). Clearly habit planes of this type will be nearly perpendicular to specific $\{111\}_\gamma$ planes. If it can be shown the microstructure of this alloy is consistent with the observations made by Kelly[19] and calculation made using the AB theory, it will be possible to define the habit plane for each martensite needle present.

The objective is then to measure the direction of the needle axis from optical micrographs of the slip plane, to define the habit plane as being perpendicular to the active slip plane, and then to see if habit planes defined in this way are consistent with the theory. It is important the reader remembers this assumption during the following discussion, because the claimed agreement which will be demonstrated between the AB theory and experimental measurements is in fact agreement if and only if the assumption that the habit plane normal is perpendicular to the active slip plane is valid.

Measurements were made from single crystals deformed in tension in an easy glide orientation at a temperature between Md_γ and Ms_γ. The temperature Md_γ is defined as the α martensite start temperature for deformation induced α martensite. Above Md_γ deformation will not induce the α phase. The temperature Ms_γ is the α martensite start temperature observed upon cooling in the absence of any external loads.[20] Specifically the crystals were pulled to 5% strain with a $[\bar{2}\bar{1}3]_\gamma$ tensile axis at 185°K. The slip system for this tensile axis is the $(\bar{1}11)_\gamma$ $[01\bar{1}]_\gamma$. Specimens tested in this manner produce stress induced α martensite needles that are associated with only one $\{111\}_\gamma$ plane, the slip plane. The α martensite needles are packed between parallel ε martensite sheets that are parallel to the active slip plane. The ε martensite sheets are seen as vertical dark lines in Fig. 3a. By using specimens prepared in this manner the measurements can be made with ease because of the simple microstructure.[21]

The method used to calculate the long axis of the needle and the vector perpendicular to it on the slip plane follows. An accurate line of reference was needed on the polished surface of the crystal and in general there was no crystallographic feature on the polished and etched surface that can be used. To generate a reference line, a vector parallel to the cut edge of two 90° surfaces was calculated. To do this, back reflection Laue photographs of each surface were taken at a specimen to film distances of 5 cm. The spots on the Laue photographs were indexed in the conventional manner. The exact normals to these two polished surfaces were then calculated analytically using computer PROGRAM LAUE, discussed in Appendix A. The cross product of these two normals produces the indices of a vector defining the line of intersection between the two surfaces. This line of intersection is used as a reference line to calculate the direction of the long axis of the needles. The calculations are made by computer PROGRAM TRACE, discussed in Appendix B. To insure that optical micrographs of the etched austenite-martensite interface are correctly orientated with respect to the reference line, micrographs at the working magnification (usually x500) were taken; then without moving the microscope stage, a low magnification micrograph was taken showing the edge of the cut crystal and therefore defining the direction of the reference line. All angular measurements were made with respect to this reference line with a vernier protractor capable of measuring angles to five minutes of arc.

Because the polished surface was not the exact $(\bar{1}11)_\gamma$ plane, a correction was required to resolve the direction of the vector on the polished surface onto the $(\bar{1}11)_\gamma$ plane. To accomplish this, a rectangular geometry was assumed for the martensite needles and measurements were made only on plates where both sides were parallel. Justification for using this geometry can be seen in Fig. 3a. It was also assumed that the vector defining the trace on the polished surface was in an interface plane also containing the $[\bar{1}11]_\gamma$ direction. The vector normal to the interface plane is obtained by simply taking the vector product of the vectors defining the direction of the trace on the polished surface with the $[\bar{1}11]_\gamma$ direction. The vector parallel to the long axis of the needle is simply the vector product of the interface plane normal and the $[\bar{1}11]_\gamma$ direction.

B. Shape Change Measurements

1. Theory

The shape deformation due to a martensite plate in the austenite matrix is shown schematically in Fig. 4.[22] Experimentally it is observed that a straight line $\overline{ABCD}$ scribed on the austenite surface will remain continuous after the transformation. The surface EFGH is planar and is tilted about $\overline{EF}$ and $\overline{GH}$ which are vectors laying in the interface planes (habit plane) EFJI and HGKL respectively. The observed shape deformation is the result of a transformation where vectors in the austenite transform to vectors in the martensite and planes in the austenite transform to planes in the martensite. Such a transformation

can be treated as a linear homogeneous transformation. The shape strain, S, which is an invariant plane strain on the habit plane may be expressed by the matrix equation

$$S = \frac{1}{\delta}(I)(I + m\hat{d}\hat{h}), \tag{3}$$

where δ is the dilatation parameter and will be set equal to one in this study. The parameter δ was introduced in the BM theory and allows for the possibility that an isotropic distortion up to 2% in the interface plane may be present. For testing the AB model it will be assumed $\delta = 1$, i.e., no isotropic distortions are present. m is a scalar factor defining the magnitude of the displacement vector, $\hat{d}$ is a unit vector defining the direction of the shear and $\hat{h}$ is the unit normal to the habit plane. When $\hat{h}$ is known, m and $\hat{d}$ can be calculated from measured displacements of a single fiducial line on the crystal surface.

Bowles and Morton[23] have presented a general solution for the determinations of the shape strain. An arbitrary basis J that is related to the martensite crystallography is selected. Figure 5 is a sterographic projection showing the geometry that in fact corresponds to one calculation made from Fig. 6 to be discussed next. In Fig. 5 the unit vector $\hat{J}_3$ is the specimen normal, determined in this study using 5 cm back reflection Laue photographs (see Appendix A). The habit plane normal and normal to the tilted surface are plotted to lie in the same zone with $\hat{J}_3$. The unit vector $\hat{J}_1$ is then the intersection of the habit plane with the specimen surface and $\hat{J}_2 = \hat{J}_3 \times \hat{J}_1$. The habit plane normal in terms of the J basis is

$$(h;J) = (0;\sin\theta;\cos\theta)_J \tag{4}$$

where θ is the angle between the pole of the habit plane and the specimen normal. The shape strain is therefore given as

$$S = (JSJ) \begin{pmatrix} 1 & md_1\sin\theta & md_1\cos\theta \\ 0 & 1+md_2\sin\theta & md_2\cos\theta \\ 0 & md_3\sin\theta & 1+md_3\cos\theta \end{pmatrix} \tag{5}$$

where the unit vector defining the direction of shear is $[J,\hat{d}] = [d_1,d_2,d_3]$. To evaluate d_1, d_2 and d_3 four equations are required. The first is obtained by taking the determinant of S giving

$$r = 1+md_2\sin\theta + md_3\cos\theta \tag{6}$$

which is equal to the ratio of the final and initial volume of the fcc and bcc unit cells

$$r = 2\left(\frac{a}{a_o}\right)^3 = 2\left(\frac{2.87143}{3.58356}\right)^3 = 1.0289176$$

a and a_o being the martensite and austenite lattice parameters respectively.[21] The dashed line in Fig. 5 represents a fiducial line on the crystal surface which can be expressed as

$$[J;X] = [\cos\rho,\sin\rho,0]_J = [1,\tan\rho,0]_J \tag{7}$$

which will transform by the strain S to

$$(JSJ)[J:X] = \tan\rho[\cot\rho + md_1\sin\theta;\ 1+md_2\sin\theta;\ md_3\sin\theta]_J \tag{8}$$

The trace of this line is shown as a dotted line. From the geometry of Fig. 5 an independent equation for $S\hat{X}$ can be obtained.

$$S\hat{X} = [\cos\alpha;\cos\beta;\cos\gamma]_J \tag{9}$$

where α, β and γ are the angles between $S\hat{X}$ and $\hat{J}_1$, $\hat{J}_2$ and $\hat{J}_3$ respectively. Taking the vector $\hat{X}$ as always equal to unity,

$$\left.\begin{aligned} \cos\alpha &= \cos\rho'\sin\gamma = \lambda_1\cos\rho' \\ \cos\beta &= \sin\rho'\sin\gamma = \lambda_1\sin\rho' \\ \cos\beta &= \cos\phi\ \sin\alpha = \lambda_2\cos\phi \\ \cos\gamma &= \sin\phi\ \sin\alpha = \lambda_2\sin\phi \end{aligned}\right\} \tag{10}$$

From the two equations relating $\cos\beta$,

$$\lambda_1 = \frac{\lambda_2\ \cos\phi}{\sin\rho'} \tag{11}$$

giving in terms of measurable angles from the electron micrographs

$$(JSJ)[J:X] = \lambda_1\ [\cos\phi\cos\rho';\ \cos\phi;\ \sin\phi]_J\ . \tag{12}$$

Using Eqs. (8) and (12) three equations in terms of λ_1 may be obtained.

$$\lambda_1 = \frac{\cot\rho + md_1\sin\theta}{\cos\phi\cot\rho'} \tag{13a}$$

$$\lambda_1 = \frac{1 + md_2\sin\theta}{\cos\phi} \tag{13b}$$

$$\lambda_1 = \frac{md_3\sin\theta}{\sin\phi} \tag{13c}$$

to evaluate md_2 and md_3 take the ratio of Eq. (13b) and Eq. (13c) and using Eq. (6),

$$md_3 = r/(\sin\theta\cot\phi + \cos\theta) \tag{14a}$$

evaluate λ_1 in Eq. (13c) and set equal to Eq. (13b) gives

$$md_2 = \frac{r \cot\phi}{(\sin\theta\cot\phi+\cos\theta)} \tag{14b}$$

and λ_1 in Eq. (13a) gives

$$md_1 = \frac{r \cot\phi\cot\rho'}{\sin\theta\cot\phi+\cos\theta} - \cot\rho\csc\theta \tag{14c}$$

Because $[d_1,d_2,d_3]_J$ is a unit vector the value of scalar m, the magnitude of the shear can be calculated. The final result $[d_1d_2d_3]$ is obtained by a simple rotation of axes to the austenite basis shown in Fig. 5. The computer program, PROGRAM SHAPE use to make the shape change calculations is given in Appendix C.

2. Fiducial Lines

Experimentally the difficulty with shape strain measurements is placing fiducial lines on the polished austenite. Two methods were used in this study. Electropolished crystals were cemented on a glass slide, the straight edge of the slide being used as a reference for X-ray orientation of the crystal and as a guide to scratch the crystal by drawing over microcloth saturated with 0.05μ Al_2O_3 particles. This procedure produced a high density of parallel fiducial lines, the direction of which could be defined to ±0.5° on the austenite surface.

The second type of fiducial line, slip traces on the polished austenite surface, were favored in this work. Slip lines were generated on the electropolished surface of crystals by prestrains of 2-3% or were formed by accommodation deformations of the austenite during the martensitic transformation. Examples showing a gold shadowed carbon

replica of a $(001)_\gamma$ surface are given in Fig. 6. The spheres on the surface are 0.264±0.006 microns in diameter. The fiducial lines in the example are austenite $\langle 110 \rangle_\gamma$ slip traces produced by accommodation deformation. It was possible to define the change in direction of the fiducial line to ±0.2°. The angle of tilt (ϕ) of the martensite crystal was measurable to an accuracy of ±1°. All calculations of the shape strain and direction of shape strain vector assume the habit plane to be of the type $\{0.812, 0.479, 0.333\}_\gamma$. These habit plane normals are consistent with experimental measurements presented in this thesis.

3. Angle of tilt

To calculate the angle of tilt of the α martensite crystal with respect to the austenite surface it is not required to know the actual size of the spheres. However their uniformity is important so that good statistical information can be obtained. The procedure first involves calculating the shadow angle which is

$$\alpha = \tan^{-1} \left(\frac{d}{x}\right) \tag{15}$$

where d is the diameter of the sphere and x the length of the shadow on the electron micrograph. If a sphere is sitting on an α martensite surface tilted above the austenite, the length of the shadow on the tilted surface (y) is less than x. The tilt angle ϕ_s in the direction of the shadow is then,

$$\phi_s = \tan^{-1} \left\{ \left(\frac{x-y}{y}\right) \left(\tan\alpha\right) \right\} \tag{16}$$

When the α martensite surface is tilted below the austenite surface $y > x$ and

$$\phi_s = \tan^{-1}\left\{\left(\frac{y-x}{y}\right)\left(\tan\alpha\right)\right\} \tag{17}$$

The tilt in a second direction (usually the $[110]_\gamma$) was obtained from the geometry on the micrograph and both points plotted on a sterographic projection. The great circle cutting both points defines the trace of the tilted plane and the plane normal is located. Because the habit plane normal and the normal to the tilted surface must lie on the same great circle, the habit plane normal for the needle in question is clearly defined. These measurements were made from micrographs shown in Fig. 6.

III. EXPERIMENTAL RESULTS

A. Computer Calculations of Habit Plane and Shape Strain Using the AB Two-Shear Model

The FORTRAN version of the generalized martensite crystallography[5] was translated from Acton-Bevis ALGOL version by Schoen,[24] and further modified by the author. The program was checked by reproducing results obtained by Wayman[10] and Acton and Bevis.[5] Exact agreement was obtained thereby insuring that the new martensite two shear FORTRAN program was correct. The only input data required are the austenite and martensite lattice parameters, (measured for the Fe-15Ni-15Cr alloy by the author[21]), the two shears to be considered and the maximum value of the first (termed the S shear) and second shear (termed the T shear) to be allowed in the calculation. All possible combinations of shears of the type $\{110\}_\alpha \langle 111\rangle_\alpha$ in pairs were tested by the computer program. Twinning shears will not be considered in this study because no internal twinning of the α martensite was observed in the alloy. In each case the magnitude of the S shear was varied between +0.40 and -0.40 in steps of 0.02. The solution was rejected if the magnitude of the T shear exceeded 0.40, if the magnitude of the overall shape strain exceeded 0.40 or the K-S orientation relationship was not satisfied to within ±1.5°.

The variant of the Bain correspondence matrix use for these calculations was,

$$ {}^{b}U_{f} = \begin{pmatrix} \frac{1}{2} & -\frac{1}{2} & 0 \\ \frac{1}{2} & \frac{1}{2} & 0 \\ 0 & 0 & 1 \end{pmatrix} $$

and is the same variant as that shown in Fig. 1. This variant corresponds to the following three orientation relationships between the austenite and martensite lattice.

(1) $(111)_\gamma \parallel (011)_\alpha$; $[01\bar{1}]_\gamma \parallel [\bar{1}\bar{1}1]_\alpha$

(2) $(111)_\gamma \parallel (011)_\alpha$; $[10\bar{1}]_\gamma \parallel [\bar{1}1\bar{1}]_\alpha$

(3) $(111)_\gamma \parallel (011)_\alpha$; $[11\bar{2}]_\gamma \parallel [01\bar{1}]_\alpha$

The numbers (1), (2) and (3) corresponding to the three orientation relationships above will be use to identify which of the three correspond to a particular solution in results to follow.

Three types of solutions using lattice invariant slip shears were found that produced the $\{252\}_\gamma$ martensite habit. These were, first, solutions where one shear (the S or T) was equal to zero; second, solutions where the $\{252\}_\gamma$ was satisfied over a wide range of values for the S and T shears; and third, solutions that produced a pair of $\{252\}_\gamma$ habits that are twin related.

For the first type of situation where the magnitude of the S or T shear was zero, only two unique solutions were found. These solutions tended to converge rapidly on the K-S orientation relationship and are not minimized with respect to the magnitude of the shape change. The image of the computer print-out for the two solutions of this type is given in Table I.

Four different shear pairs were found where the magnitude of the S and T shears were non-zero. Two of these shear pairs each have one shear listed in Table I and therefore also reproduce these

solutions. The two shear solutions are presented in Table II.

The third type of solution given in Table III is of considerable interest. It is shown that the AB two-shear model can produce a twin related pair of $\{252\}_\gamma$ habits, which is observed experimentally, using the <u>same two slip shears</u>. Only the sign and magnitude of the two shears are different and the magnitude of the shape change for both habits are realistic. It appears the martensite in this alloy is always present in twin related needle pairs, in the same manner that is suggested by these calculations (this will be proved later).

It should be noted that changing the order of the shears produces exactly the same results. Therefore the order of the two lattice invariant slip shears is not important as far as AB formulation is concerned.

To summarize these data, for the Bain correspondence used, and all possible combinations of $\{110\}_\alpha \langle 111\rangle_\alpha$ lattice invariant slip shears, only four unique habit plane normals $(\vec{h})$ and directions of the shape change $(\vec{u})$ consistent with experimental observations were generated. These four are in fact two sets of twin related martensite habits. They are:

$$\left.\begin{array}{ll} (1)\quad \vec{h} = \begin{bmatrix} -0.341 \\ -0.812 \\ -0.475 \end{bmatrix}_\gamma ; & \vec{u} = \begin{bmatrix} -0.158 \\ -0.542 \\ 0.826 \end{bmatrix}_\gamma \\ \\ (2)\quad \vec{h} = \begin{bmatrix} 0.475 \\ 0.812 \\ 0.341 \end{bmatrix}_\gamma ; & \vec{u} = \begin{bmatrix} -0.826 \\ 0.542 \\ 0.158 \end{bmatrix}_\gamma \end{array}\right\} \text{Twin Pair}$$

$$\left.\begin{array}{lll} (3) & \vec{h} = \begin{bmatrix} -0.812 \\ -0.341 \\ -0.475 \end{bmatrix}_\gamma ; & \vec{u} = \begin{bmatrix} -0.542 \\ -0.158 \\ 0.826 \end{bmatrix}_\gamma \\ (4) & \vec{h} = \begin{bmatrix} 0.812 \\ 0.475 \\ 0.341 \end{bmatrix}_\gamma ; & \vec{u} = \begin{bmatrix} 0.542 \\ -0.826 \\ 0.158 \end{bmatrix}_\gamma \end{array}\right\} \text{Twin Pair}$$

It remains to be seen if these calculated habit plane normals and direction of shape change will be consistent with the experimentally measured values that follow.

B. Habit Plane Measurement Results

The habit plane normal measurements produced a vector that can be represented by

$$\vec{h} = \langle 0.333,\ 0.812,\ 0.479 \rangle_\gamma \pm 1.5^\circ \ .$$

This can be compared to the habit plane normal calculated using the AB two shear theory, which is

$$\vec{h} = \langle 0.341,\ 0.812,\ 0.475 \rangle_\gamma \ .$$

Keeping in mind the assumptions used to make the habit plane normal measurements, which was based on experimental observations made by Kelly,[19] it appears that outstanding agreement between theory and experiment exist. It is possible this result is fortuitous; however, using what is believed to be the best information available, the assumption that the habit plane is perpendicular to the active slip plane in the austenite is a logical statement. The data showing the experimentally measured habit plane normal and α martensite needle axis is given in Table IV.

To help the reader interpret consistency of these data in Table IV, the angle between the habit plane normal and the $[211]_\gamma$ direction is given. Each line of data in Table IV is of a single α martensite needle. No effort was made to average the data and no results were discarded. The data have been grouped to show what is believed to be a real variation in crystallographic direction of needles with seemingly the same long axis. All the measurements were made from four micrographs from the same crystal that was strained to 5% tensile strain at 185°K with a $[\bar{2}\bar{1}3]_\gamma$ tensile axis. When a crystal is strained under these conditions, α martensite forms only on the $(\bar{1}11)_\gamma$ plane.[21]

The first point to consider about these results is their accuracy. All the micrographs used for these calculations contained a rare linear feature; an ε martensite sheet cutting the polished surface shown in Fig. 7, whose trace direction was always $[0.69551347, 0.02264272, 0.71815619]_\gamma \pm 0.25°$ on the polished surface. It was observed that if this trace was assumed to be the intersection of an ε martensite plate on the $(11\bar{1})_\gamma$ plane cutting the polished surface the above trace was obtained. This result was fortuitous in that a crystallographic feature that could be used to check the precision of the measurement was unexpected. This outstanding agreement between the observed and correct line of intersection of a ε plate parallel to the $(11\bar{1})_\gamma$ plane and the polished surface indicates the precision of the experimental method used here is of the order of ± 0.25°. The data was tabulated to eight places in Table I for convenience and is not the implied accuracy. The variations observed in Table I are real within the experimental constraints of the measurement.

C. Shape Change Measurement Results

The measured direction of the shape change vector using the habit plane normal deduced in the previous section in the calculation for α martensite crystals in this Fe-15Ni-15Cr alloy can be represented as,

$$\vec{u} = \langle 0.822,\ 0.129,\ 0.555 \rangle_{\gamma} \pm 3^{\circ} \quad .$$

The general form of the result obtain from the AB two shear theory is consistent with experimental measurements, and is,

$$\vec{u} = \langle 0.825,\ 0.158,\ 0.542 \rangle_{\gamma} \quad .$$

The magnitude of the measured shape change varied between 0.21 and 0.30 where as the AB theory indicated the shape change varied between 0.25 and 0.39. A value of the shape change of 0.28 was typical for calculated solutions of $\vec{u}$ that best agreed with the experimental measurements. The magnitude of the shape change obtained experimentally was a little less than that calculated by the AB model. Until the errors associated with shape change calculations can be reduced, this error is not considered significant.

The ideal experimental conditions for these measurements are electron micrographs of isolated α martensite needles surrounded on all sides by austenite and the presence of one or more of the latex spheres on the tilted surface so the angle of tilt (ϕ) of the martensite plate can be calculated. Satisfying all of these conditions at the same time proved to be difficult. Figure 6 contains the best examples obtained during this phase of the study.

Before calculations of the magnitude and directions of the shape change can be made from electron micrographs of the type shown in Fig. 6, it is important that the morphology of the structure be clearly defined. The α martensite in this alloy is acicular. The habit planes are perpendicular to a $\{111\}_\gamma$ plane and the vector defining the long axis of a needle lies in the same $\{111\}_\gamma$ plane. With this in mind consider the pair of needles cutting the $(001)_\gamma$ surface in Fig. 6A. These needles will be shown to be twin related in Part II. In this example the needles intersect the surface with retained austenite between the needle pair. In Fig. 6B the twin pair is joined at the surface of the specimen.

If, for the twin orientated needles in 6A the habit planes are defined as,

$$(1) \qquad \hat{h}_1 = [0.812,\ 0.333,\ 0.479]_\gamma$$

$$(2) \qquad \hat{h}_2 = [0.812,\ 0.479,\ 0.333]_\gamma$$

the needles must then lie on the $(\bar{1}11)_\gamma$ plane and the fiducial line must be the $[110]_\gamma$ when using a $(001)_\gamma$ standard sterographic projection. If the selected habit planes are correct, and measurements of the projected deviation of the fiducial line and the angle of surface tilt are accurate, a solution for the magnitude and direction of the shape change will result. Because of symmetry, the same general form of the $\langle hkl \rangle_\gamma$ vector defining the direction of the shape change will be obtained for any of the possible $\{hkl\}$'s of the habit plane as long as the correct $\{111\}_\gamma$ plane and correct $\langle 110 \rangle_\gamma$ fiducial line, consistant

with the known morphology,are selected for the calculation.

It is possible to prove the symmetry of these solutions by simply rotating the micrographs in Fig. 6 about the $[110]_\gamma$, $[\bar{1}10]_\gamma$ and $[001]_\gamma$ and observing if in fact symmetrical solutions result. This was done, and the results are tabulated in Table V. It was not possible to measure the surface tilt for martensite needles B and D, however, study of Fig. 6A and 6B shows that the angles which produced experimental values of the magnitude and direction of the shape change are in good agreement with the general form of the solutions predicted by the AB two shear theory.

The accuracy of the calculation depends on knowledge of the habit plane normal and the ability to measure the angle of tilt ϕ of the α martensite crystal. Where the tilt was measurable, the range of confidence is indicated in Table V. The measurements are believed to be quite good, considering the experimental difficulties and are believed to be the first published data of the magnitude and direction of the shape change for α martensite crystals that are 1-2 microns in cross section.

IV. DISCUSSION

A. Comparison of the AB Theory and Experimental Results

For the first time a material that exhibits the $\{252\}_\gamma$ habit plane has been shown to be consistent with the generalized martensite crystallography theory developed by Acton and Bevis.[5] The consistency lies in the fact that theory predicts the general form of the habit plane to within one degree of the experimentally obtained value, assuming that the habit plane is correctly defined. The theory predicts the general form of the direction of the shape change to within two degrees of the experimentally obtained value. The calculated and experimental values for the magnitude of the shape change are clearly in reasonable agreement.

With all this consistency of experiment and theory there still exists a perplexing problem that seems insurmountable at this time. Clearly exact agreement with theory can be demonstrated if and only if the exact variants of the habit plane, magnitude and direction of the shape strain and the orientation relationship match with experimental results. For every martensite needle studied in this thesis, if the variants of orientation relationship and habit plane predicted by theory are applied to the experimental shape change measurement, the wrong variant for the direction of the shape change is obtained, even though the magnitude and general form of the vector are correct.

It is believed that the problem lies in the shape change calculation. The difficulty seems to be a problem of symmetry. It is possible experimental solutions of the shape change vector matching

the AB model would result if all possible variants of the habit plane, that could be rotated to the standard variant without destroying the orientation relationship, were used to make shape change calculations. One of these variants should result in a matching solution. A computer program to aid in these calculations is being prepared and the results of this effort will be reported in the near future.

The last serious effort by other researchers to define the problems as to why the $\{252\}_\gamma$ could not be satisfactorily explained by the present single and double shear models of the phenomenological theory was made by Dunne and Wayman.[12] Efforts to explain $\{252\}_\gamma$ martensite concentrated around the fact that in all the alloys studied, electron microscopy results showed the martensite microstructure was twinned. In nearly all of Wayman's publications a concern as to whether the twinning observed was a transformation shear or accommodation shear has been expressed. The evidence that twinning was a transformation shear was so strong that no one, not even Acton and Bevis,[5] considered trying all possible combinations of pairs of $\{110\}_\alpha \langle 111\rangle_\alpha$ lattice invariant shears. If this would have been done, the data on Fe-1.2C published by Dunne and Bowles[18] could have been explained. Dunne and Bowles shape strain results of their twinned Fe-1.2C microstructure effectively mirrors the results obtained in this thesis for dislocated martensite in a Fe-15Ni-15Cr carbon free alloy. The only difference being that Dunne and Bowles used a different K-S variant in their calculations. The data presented in this thesis on $\{252\}_\gamma$ martensite suggests strongly that the lattice invariant shears involved in the

transformation are slip shears, and that twinning observed in the Fe-1.2C,[18] Fe-6.14Mn-0.95C[18] and Fe-7.9Cr-1.11C[17] was caused by accommodation deformation in the martensite.

One very exciting result that presented itself in the calculations made using the AB model was the fact that a twin related pair of martensite habits with the same K-S orientation relations resulted for the same pair of lattice invariant shears (see Table III). This result has not been previously reported. This twin relationship between martensite needles was observed to be a consistent characteristic of the microstructure as shown in the habit plane measurements presented in Table IV. This remarkable agreement between experiment and theory demonstrates the basic soundness of the AB theory and its ability to predict the habit plane, direction of the shape change and magnitude of the shape change providing the correct pair of lattice invariant shears are selected.

B. Factors that Effect the Accuracy of Habit Plane and Shape Strain Calculations

The variation in crystallographic direction of the martensite needles in the austenite matrix shown in Table IV is felt to be unrealistic considering the apparent accuracy of the method used in this study. The cause for the observed variation is believed to be the present inability of x-ray methods to measure the exact austenite orientation next to the α martensite needle. Because only 7% of the crystal volume has been transformed to α martensite[21] and the fact that all the α martensite are located in isolated regions of nearly 100% α martensite throughtout the austenite matrix,[25] the Laue back reflection method is effective

in measuring the orientation of the untransformed austenite. The accommodation deformation of the austenite next to the α martensite crystal can cause significant lattice rotation of the austenite. This lattice rotation is clearly seen in the optical micrograph of the $(\bar{1}11)_\gamma$ surface in Fig. 7 and the electron micrograph of a gold shadowed carbon replica in Fig. 6b and c. The reader is asked to place a straight edge on the third ε martensite trace from the bottom of Fig. 7; the trace cutting the α martensite needle. Note that the trace on the left side of the needle is bent with respect to the right side of the needle. Now place the straight edge on one of the $[110]_\gamma$ slip traces on the right side of the tilted surface of Fig. 6b. Note as the α martensite needle is approached, the $[110]_\gamma$ trace is bending by several degrees. The bending is even more dramatic in the austenite near needle E of Fig. 6c. Clearly the data tabulated in Table IV reflects this experimental difficulty.

The only significant effort this author is aware of to resolve this problem was made by Rowlands, et al.[26] Here the back-reflection Kossel method was applied to study a Fe-32%Ni alloy. This experimental method could possibly be applied to the Fe-15Ni-15Cr alloy in an effort to resolve the magnitude of errors present due to austenite lattice rotations caused by accommodation deformation adjacent to martensite crystals. Electron beam spot sizes of about 1/2 micron would be required so that the divergent beam of x-rays required for the formation of the Kossel pattern from a single α martensite crystal and the adjacent austenite would result. The author attempted to

resolve this problem by using the pseudo-Kikuchi pattern that is generated in the Scanning Electron Microscope (SEM). The idea was to locate a martensite-austenite interface like that seen in Fig. 6A. With one scan axis off in the SEM, scan across the interface to produce a superimposed micrograph of the pseudo-Kikuchi image for each crystal (the austenite and martensite). By controlling the spot size and scanning across the interface $\pm 0.1\ \mu$ it was felt an exact orientation relationship between the α needle and the γ matrix would be obtained. The experiment failed for an unexpected reason. The surfaces of the crystals were electropolished to a mirror finish before they were transformed partially to α martensite. It seems the surface was so shiny that it was not possible to resolve the austenite-martensite interface in the SEM.[27] If this experiment would have worked, the logical extension would have been to deposit the small sphears on the surface of the partially transformed crystal, shadow in the same manner as use for the replica studies and obtain in one sitting at the SEM the orientation relationship and data needed to calculate the magnitude and direction of the shape change. If this were possible any ambiguities associated with the two shear martensite crystallographic model could be resolved. Additional effort must be made in the future to master this important experimental method.

The small scatter observed for the ε sheet on the $(11\bar{1})_\gamma$ plane cutting the polished surface of the crystal is because the dislocation density in the region of the ε plates is quite low. An example of the austenite - ε martensite structure is given in Fig. 9. This

electron micrograph shows the typical microstructure in a $(01\bar{1})_\gamma$ symmetrical orientation of the $[\bar{2}\bar{1}3]_\gamma$ tensile axis specimen where α martensite has not formed.

The primary error associated with the shape change measurements presented in Table V is one's ability to measure the tilt of the martensite surface with respect to the austenite surface. Because only one or two spheres were located on the tilted surface, satisfactory statistical analysis was not possible. It was therefore necessary to indicate a rather large error of ±1° for the direction of tilt of the α martensite needles, to give the reader a feeling for the sensitivity of the direction of the shape change vector as a function of tilt let's consider the first calculation for needle A in Table V. The best fit with theory for this particular variant was for a surface tilt of 10.0°. A variation of ±1° for this calculation would show the following variation in the shape change vector.

$$\vec{u} = \begin{bmatrix} 0.125475 & \begin{matrix} +\,0.036628 \\ -\,0.043114 \end{matrix} \\ -0.521830 & \begin{matrix} -\,0.040875 \\ +\,0.041920 \end{matrix} \\ 0.844787 & \begin{matrix} +\,0.016842 \\ -\,0.022959 \end{matrix} \end{bmatrix} \quad \text{or} \quad \begin{matrix} +\,2.28^\circ \\ -\,2.82^\circ \end{matrix}$$

The accuracy of these results are about the same as those reported by Dunne and Bowles,[18] who used a Leitz Wetzear two-beam interfermeter to measure the tilt of the exposed α martensite crystal on the surface.

It is clear the accuracy of this measurement must be improved. A method to improve this measurement, however, does not appear to be obvious at the present time.

V. CONCLUSIONS

A detailed examination of the crystallography of α martensite formed in a Fe-15Ni-15Cr single crystals has been completed. Measurement of the habit plane, the direction of the shape change and the magnitude of the shape change were made, and the results found to be in good agreement with the two shear crystallographic theory. The theory predicts accurately the orientation relationship, the habit plane, the magnitude of the shape change and the general form of the shape change vector. The fact that the experimental results presented in this thesis show a different variant of the shape change vector than that predicted by the theory may possibly be trivial, if it can be shown to be a problem of symmetry. This difficulty with the theory cannot be consider trivial however, until this important point is resolved.

It has been clearly demonstrated that martensite with the $\{252\}_\gamma$ habit plane can be effectively described by using two lattice invariant slip shears of the type $\{110\}_\alpha \langle 111 \rangle_\alpha$. All known previous studies of $\{252\}_\gamma$ have assumed the shears to be $(112)_\alpha\ [\bar{1}\bar{1}1]_\alpha$ and $(110)_\alpha\ [1\bar{1}\bar{1}]_\alpha$, as applied to the standard KS variant $(111)_\gamma \parallel (011)_\alpha$, in an effort to explain the experimental results. The selection of a twinning shear as one of the lattice invariant shears was logical because the Fe-C, Fe-Mn-C and Fe-Cr-C alloys studied all produced α martensite that is internally twinned. There is no question that the martensite formed in the Fe-Ni-Cr alloy used in this study is dislocated and produces

almost exactly the same results of the magnitude and direction of the shape change as that observed for twinned Fe-C martensite by Dunne and Bowles.[18] This strongly suggests the twinning observed in these alloys is due to accommodation deformation, and the transformation shears responsible for the observed shape change are slip shears.

Future work should be to resolve the symmetry problem, if it is in fact a problem of symmetry that produces the wrong variant of the shape change vector; to develope the scanning electron microscope analysis so the habit plane, the orientation relationship, and the magnitude and direction of the shape change can be obtained from a single α martensite crystal; and to develope an accurate method to measure the angle of tilt of the α martensite crystal with respect to the austenite matrix.

PART II. THE STRUCTURE AND MECHANICAL PROPERTIES OF DEFORMATION INDUCED ε AND α MARTENSITE IN Fe-15Ni-15Cr SINGLE CRYSTALS

I. INTRODUCTION

It is believed the formation of the ε (hcp) martensitic phase in association with α martensite in low stacking fault energy steels was first reported by Cina[28] (1954). The first single crystal studies were reported by Breedis and Robertson[29] using a Fe-12Ni-16Cr alloy. They reported the orientation relationship for ε martensite as $(0001)_\varepsilon \parallel (111)_\gamma$; $[\bar{1}2\bar{1}0]_\varepsilon \parallel [\bar{1}10]_\gamma$, the α martensite was dislocated, had a lenticular shape, exhibited a $\{252\}_\gamma$ habit plane and that pairs of α martensite crystals joined a $(112)_\alpha$ twin plane. The specific habits were of the form:

$$\left.\begin{aligned} \hat{h} &= \begin{pmatrix} 0.3367 \\ 0.3709 \\ 0.8655 \end{pmatrix}_\gamma \\ \hat{h} &= \begin{pmatrix} 0.3709 \\ 0.3367 \\ 0.8655 \end{pmatrix}_\gamma \end{aligned}\right\} \text{twin pair}$$

As shown in Part I the Fe-15Ni-15Cr alloy also exhibits a habit near the $\{252\}_\gamma$ (assuming the habit is perpendicular to the active austenite slip plane[19]), the α martensite is dislocated and that separate volumes of α martensite join at a $\{112\}_\alpha$ twin boundary with habit planes of the form:

$$\left.\begin{array}{l} \hat{h} = \begin{pmatrix} 0.812 \\ 0.479 \\ 0.333 \end{pmatrix}_{\gamma} \\ \\ \hat{h} = \begin{pmatrix} 0.812 \\ 0.333 \\ 0.479 \end{pmatrix}_{\gamma} \end{array}\right\} \text{Twin pair}$$

The martensite crystals are not lenticular in shape however but exhibit an acicular geometry. Results reported by Kelly and Nutting[30] using a commercial stainless steel (Fe-18Cr-8Ni) are consistent with these studies including the acicular geometry of the α martensite.

The sequence of the martensite transformations is of considerable interest and was reviewed by Breedis and Robertson[29] (1962). At that time the evidence suggested the sequence of the transformation was f.c.c. $\rightarrow$ h.c.p. $\rightarrow$ b.c.c. An example of this evidence was presented by Guntner and Reed[31] (1962). Using a polycrystalline Fe-18Cr-9Ni alloy, they deformation induced the ε and α phase at - 196°C. It was observed that the volume fraction increased from zero to 0.35 in about 9% tensile strain, then dropped to 0.10 at 26% tensile strain, the apparent strain at fracture. The volume fraction of α martensite increased from about 0.04 at zero strain to about 0.90 at 26% tensile strain. Thus at fracture the alloy was nearly 100% martensite, 10% ε and 90% α. The reduction of ε from 0.35 to 0.10 during the deformation strongly suggested the $\varepsilon \rightarrow \alpha$ transformation was taking place. Later observations by Breedis,[32] Kelly,[19] and this study strongly suggests that the $\varepsilon \rightarrow \alpha$ transformation does not exist. In all the electron microscopy studies

the author is aware of to date, α martensite has never been observed to replace regions that were clearly at one time ε martensite. It has been suggested that because the stacking fault energy in these alloys is positive,[32,33] the hcp phase is unstable and therefore the ε → γ will occur. Also that once the ε sheet has formed in the austenite matrix it will not completely revert to γ. The observed variations of the volume fraction of ε is due to thickening or thinning of the ε sheets.

It appears that the γ → ε transformation occurs only when the austenite is plastically deformed. In these Fe-Ni-Cr alloys, ε can exist by itself in plastically deformed specimens, but α is never observed in the absence of ε in quenched or deformed crystals. This is demonstrated in a Fe-18.5Cr-13.7Ni alloy by Thomas[33] and is consistent with observations in this single crystal study. Goldman, et al.[34] have shown that the martensite start temperature for the ε phase (Es_γ), if it exists in a Fe-15Cr-11.7Ni alloy is lower than Ms_γ. Thus by quenching type heat treatments ε martensite can not be formed by itself.

The thermodynamics of the γ-ε transformation have been studied in detail by Schumann[35,36] and Breedis and Kaufman.[20] Breedis and Kaufman concluded that at atmospheric pressure the ε → α transformation is not expected at temperatures below 500°K. The γ → ε and γ → α transformations therefore occur jointly in the Fe-Ni-Cr alloys consider here.

The effect of stress on the formation of α as a function of crystal orientation is of particular interest in this single crystal study. Patel and Cohen (1953)[37] and Richman and Bolling (1971)[38] showed how the action of an applied stress can aid or hinder the formation of α martensite crystals in the austenite matrix. Calculations were made using Patel and Cohen's model[37] in the same way discussed by Goodchild, et al.,[39] in an effort to identify which variants of the potential habit plane would be expected if the crystal was deformed between $Md\gamma$ and $Ms\gamma$. However, the experimental results clearly showed that many habits that were favored by the above calculations were not present in the crystal and as shown in the present paper all the α martensite appeared to have the same K-S variant of the orientation relationship. In order to study this apparent singularity associated with the direction of an applied stress, an x-ray experiment was designed,[21] using a Schulz goniometer,[40] that would allow the experimentor to locate and measure the volume fraction of α martensite in the austenite matrix associated with each variant of the K-S orientation relationship. The procedure was also used to measure the volume fraction of ε martensite associated with each $\{111\}_\gamma$ plane in the crystal. The results and discussion of these measurements follow.

The mechanical response of these crystals with various tensile axes pulled between $Md\gamma$ and $Ms\gamma$ is also of interest. Goodchild, et al.[39] observed in plastically deformed 303 and 305 stainless steel that grains with a tensile axis near $\{001\}_\gamma$ contained no α nor ε martensite. The absence of α martensite was also observed in single crystals with a

$[100]_\gamma$ tensile axis. The Patel and Cohen model[37] explains these results very well. Epsilon martensite was observed in $[100]_\gamma$ tensile axis crystals, which is in conflict with the polycrystalline studies. An explanation of these polycrystalline results based on the observed stress strain curves of single crystals pulled in tension with various tensile axes is presented.

The overall objective of this chapter is to describe as clearly as possible the structural relationships between γ, ε and α phase formed in this Fe-15Ni-15Cr single crystal alloy, and how the structure relates to the crystallography of the $\gamma \rightarrow \varepsilon$ and $\gamma \rightarrow \alpha$ martensitic phases transformations. Ideas as to how plastic deformation aids in the formation of ε martensite will be presented, and interesting observations as to how ε martensite controls the formation of α martensite crystals will be discussed. For the first time a detailed analysis of the γ-ε-α interface will be presented and discussed.

II. STRUCTURE AND PROPERTIES

A. General Features of the Microstructure

Single crystals were tested in tension with easy glide and multiple slip orientations at temperatures between 185°K and 273°K. The objective was to develop a clear understanding as to how plastic deformation, and deformation induced phases control the microstructure of the transformed material. Crystals tested with an easy glide orientation had the $[\bar{2}\bar{1}3]_\gamma$ tensile axis producing deformation for the first several percent stain on the $(\bar{1}11)_\gamma[01\bar{1}]_\gamma$ slip system. It was observed that all the α martensite had a rectangular geometry and appeared to be contained in parallel bands bounded by the $(\bar{1}11)_\gamma$ planes when the $(01\bar{1})_\gamma$ surface was viewed optically. When the $(\bar{1}11)_\gamma$ plane of the crystal was viewed, the α martensite appeared in the form of clusters of needles. Studies of this type clearly established that the α martensite crystals were needles (acicular martensite). Electron microscope studies of the same orientations confirmed the optical results and also demonstrated that the clusters of α martensite needles are bounded on both sides by parallel sheets of ε martensite. The orientation relationship between γ, ε and α is the well known Kurdjumov-Sachs (K-S) orientation relationship $(01\bar{1})_\gamma \parallel (\bar{1}11)_\alpha \parallel (\bar{2}110)_\varepsilon$ and $[\bar{1}11]_\gamma \parallel [110]_\alpha \parallel [0001]_\varepsilon$. A good example of this structure showing both electron and optical micrographs of the $(01\bar{1})_\gamma$ and $(\bar{1}11)_\gamma$ surface is presented in Fig. 3. Dark vertical lines seen in Fig. 3A that have a $[211]_\gamma$ trace on the $(01\bar{1})_\gamma$ surface are ε martensite sheets cutting the $(01\bar{1})_\gamma$ surface that have the specific

K-S variant of the orientation relationship just presented. A detailed study of these ε sheets was made by dark field electron microscopy using the $(01\bar{1}1)_\varepsilon$ reflection in $(01\bar{1})_\gamma$ thin foils. An example is shown in Fig. 8B. Figure 8D clearly demonstrates the K-S orientation relationship for this alloy.

The α martensite in this alloy has the $\{252\}_\gamma$ habit as demonstrated in Part I. Previous studies of alloys exhibiting the $\{252\}_\gamma$ habit were internally twinned.[12-18] Breedis (1962)[29] and Kelly (1965)[19] reported the habit plane in low stacking fault energy stainless steels was $\{252\}_\gamma$ and the martensite had a dislocated microstructure. Not one paper on the crystallography of $\{252\}_\gamma$ martensite published between 1962 and the present, including the most up to date review by Dunne and Wayman,[12] reference this result. The crystallographers were clearly convinced that one lattice invariant shear associated with the $\gamma \rightarrow \alpha$ transformation had to be a twinning shear. Because of this, considerable effort was expended trying to find internal twinning in the α martensite of this alloy. It was concluded the internal structure of the α martensite formed in this Fe-15Ni-15Cr carbon free alloy is that of dislocated martensite; no internal twins are present. This dislocated structure can be seen in Fig. 2, 3, 8 and 10.

Individual needles however were found to join in a bcc twin orientation. This was proved with thin foil electron microscopy specimens taken from a $[\bar{2}\bar{1}3]_\gamma$ tensile axis specimen pulled in tension at 185°K. In this type of specimen all the α martensite is confined between ε sheets parallel to the $(\bar{1}11)_\gamma$ slip plane. Initial optical observations

of specimens of this type were cut to expose the $(\bar{1}11)_\gamma$ plane and showed that the α martensite needles appeared to exists in pairs and that their long axis bisected a $\langle 110 \rangle_\gamma$ direction on the $(\bar{1}11)_\gamma$ surface of the crystal. An example of this is shown in Fig. 7. Electron micrographs of the same $(\bar{1}11)_\gamma$ orientation produced the result that each martensite needle bisecting the $\langle 110 \rangle_\gamma$ direction was joined at a bcc twin boundary. This is clearly seen in Fig. 10 where SAD patterns were taken from needles identified as A and B. These needles are in twin orientations as seen by the sterographic analysis of Fig. 10 in Fig. 11.

B. Relationship Between ε Martensite and Slip in the Austenite

The ε martensite phase was deformation induced at all temperatures (185° to 273°K) used in this study. The α martensite phase was observed only in crystals tested at 185°K. The ε martensite sheets are contained in the slip bands and their formation is possibly associated with the mechanism of slip in this alloy in the temperature range considered. The mechanism of the $\gamma \rightarrow \varepsilon$ transformation is discussed in Appendix D. The ε phase appears to cover the entire slip band, their thickness being 0.05 microns or less and their separation being of the order of 0.5 to 1 microns. This spacing between sheets seen in Fig. 3, 8 and 9 appears to be independent of temperature in the range of 180°K to 273°K. Figure 9 is an example of the ε microstructure in a specimen with the $[\bar{2}\bar{1}3]_\gamma$ tensile axis which was tested at 243°K to 5% tensile strain. No α martensite was observed at this temperature.

The large surface area of the ε martensite sheets is demonstrated by observing the slip line structure on the surface of a deformed electropolished crystal, then electropolish away the slip line structure and then etch. The slip lines will not reappear and the ε phase can therefore be observed. This procedure was applied to a crystal tested to 15% tensile strain at 242°K with a $[\bar{1}\bar{1}2]_\gamma$ tensile axis. This result is shown in Fig. 12. The polished and etched surface is the $(111)_\gamma$ plane. Even though this is a duplex slip orientation, the majority of the deformation occurred on only one slip system. Figure 12A is the as tested slip line structure, Fig. 12B the electropolished surface and Fig. 12C the etched surface exposing the thicker of the ε sheets. The circle drawn on the upper parts of these three micrographs identifes the same area. The very fine spacing of the ε sheets of 0.5 to 1 micron of course cannot be observed in this optical micrograph, however, the claim that the ε sheet can extend over the entire slipped region of the crystal is quite definitely supported. Thus plastic deformation partitions the austenite matrix with large very thin sheets of ε martensite that are parallel to the $\{111\}_\gamma$ slip planes of the crystal.

C. Why Deformation Induced ε Martensite Partitions the Austenite Matrix

It is now possible to show that ε martensite can exist in the absence of α in Fe-Ni-Cr alloys. Many studies of similar alloys[29,32,41,42] suggested that the ε phase is observed only in association with the

α martensite. The difficulty that lead to early interpretations that the ε phase must always be associated with α martensite was clarified by Goldman, et al.,[34] for Fe-Ni-Cr alloys. Using a sensitive differential thermal analysis apparatus it was observed for a Fe-11.7Ni-15Cr alloy that only one transformation temperature existed. In other words Es_γ and Ms_γ are equal or nearly equal. Es_γ and Ms_γ are the ε and α martensite start temperatures respectively. Thus, by isothermal heat treatment of these alloys it would be impossible to form the ε phase in the absence of α martensite. The Es_γ temperature could be below Ms_γ and ε martensite that is observed to be associated with the $\gamma \rightarrow \alpha$ transformation is produced because of internal stresses associated with accommodation deformation in the austenite. It has already been demonstrated that the ε phase can form over a wide temperature range in the absence of α martensite when energy is supplied to aid the transformation through an applied stress (plastic deformation). This result is also in agreement with observations by Mangonon and Thomas.[46]

Breedis and Kaufman[20] have calculated the change in free energy $\Delta F^{\alpha\rightarrow\gamma}$ and $\Delta F^{\varepsilon\rightarrow\gamma}$ using the regular solution approximation and lattice stability parameters. They found driving forces of the order of 200-400 cal per g-atom related to Ms_γ and up to 50 cal per g-atom for Es_γ. If these values of the free energy are used in Patel and Cohen's[37] model that demonstrates how the work done by an external force will raise Es_γ and Ms_γ, it is evident that much less energy supplied by the applied stress is required to initiate the $\gamma \rightarrow \varepsilon$ transformation. These new transformation start temperatures will be written as Ed_γ and Md_γ and defines the transformation start temperature due to an applied

external stress and associated plastic deformation of the crystal. Ed_γ and Md_γ are clearly not constant and may vary from Es_γ and Ms_γ to several hundred degrees above these temperatures.[37,38,39] The actual value of the transformation temperature is a function of the resolved shear stress on potential α or ε martensite habit planes. In summary, even if Es_γ is equal to Ms_γ the temperature Ed_γ will in general always be greater than Md_γ because of the smaller value for $\Delta F^{\gamma\to\varepsilon}$ and therefore much less external energy will be required to aid the $\gamma\to\varepsilon$ transformation. Because of the ease by which deformation can aid the $\gamma\to\varepsilon$ transformation it becomes quite clear as to why the austenite matrix becomes partitioned by the ε phase, with the ε sheets covering the entire $\{111\}_\gamma$ planes that have slipped.

The Ed_γ temperature has not been established for this alloy. It is in excess of 300°K. The Md_γ temperature for crystals stressed in tension with a $[001]_\gamma$ tensile axis is 190±5°K.

D. Volume Fraction Measurements of Deformation Induced ε Martensite as a Function of Crystal Orientation, Temperature and Strain

Single crystals were tested in tension with $[100]_\gamma$, $[110]_\gamma$, $[\bar{1}\bar{1}2]_\gamma$ and $[\bar{2}\bar{1}3]_\gamma$ tensile axes at 185°K and with the $[\bar{2}\bar{1}3]_\gamma$ tensile axes at 273°K and 242°K to 5% tensile strain. The volume fractions of the ε martensite was measured in each specimen by an x-ray pole figure method developed by the author.[21,25] The results showed that the volume fraction of ε martensite was about 0.02 and is independent of temperature and the direction of the tensile axis within experimental error of the

measurement (±0.005). The results are tabulated in Table VI. For the $[\bar{2}\bar{1}3]_\gamma$ specimens the ε martensite was associated with only one slip plane as would be expected. For the other specimens the ε martensite was distributed on the active slip planes. The volume fraction shown in Table VI for these specimens is the sum total of ε martensite observed on each active slip plane. It is interesting to note for the specimens tested at 185°K that the $[110]_\gamma$ specimen had ε associated with two $\{111\}_\gamma$ slip planes as expected. However ε martensite was present on only one slip plane in the $[\bar{1}\bar{1}2]_\gamma$ specimen and on only two slip planes in the $[100]_\gamma$ specimen. These results are presented in Table VII. The significance of these results will be discussed in Appendix D.

To see if these measurements were consistent with experimental observations a simple calculation was made. If a cylinder 1 cm^2 in surface area by 1 cm long was transformed to 2% ε martensite by volume, the ε sheets having a surface area equal to 1 cm^2 and a thickness of 0.05 microns, the spacing of these ε sheets along the length of the cylinder would be 2.5 microns. The spacing between ε martensite sheets observed in Fig. 3a, 8 and 9 are typically of the order of 0.5 to 1 microns in regions transformed to both ε and α martensite. It is therefore clear that a 2% by volume quanity of ε martensite is sufficient to partition the complete crystal oriented for easy glide with parallel sheets of ε martensite. The $\gamma \rightarrow \varepsilon$ transformation clearly can preceed the $\gamma \rightarrow \alpha$ transformation. Therefore

by partitioning the austenite matrix with ε, the size and variant of the habit plane of the α martensite needles is controlled in this alloy.

The fact that the quantity of ε martensite present (2% by volume at 5% tensile strain) appears to be independent of both temperature and crystal orientation strongly suggests that the amount of plastic strain is controlling the quantity of ε martensite. It is important that the volume fraction of ε and α martensite as a function of strain and temperature be measured in this single crystal alloy in the near future. A discussion of the importance of such a study is presented in Appendix E.

E. Volume Fraction Measurements of Deformation Induced α Martensite as a Function of Crystal Orientation

Quantitative volume fraction measurements of α martensite were made on tensile specimens with $[100]_\gamma$, $[1\bar{1}0]_\gamma$, $[\bar{1}\bar{1}2]_\gamma$ and $[\bar{2}\bar{1}3]_\gamma$ tensile axes. These specimens were tested in the region of 185°K to 5% tensile strain. The total volume fraction of α martensite varied from $<$ 0.002 to 0.07 for the $[100]_\gamma$ and $[\bar{2}\bar{1}3]_\gamma$ specimens respectively. These results show that Md_γ is a strong function of the resolved shear stress on potential martensite habit planes. For these experimental data it would appear that $Md_\gamma \cong 190°K$ for the $[100]_\gamma$ specimen. Md_γ must be greater than 190°K for the other three orientations. The stress strain curves and volume fraction measurements for these specimens are given in Fig. 13 and Table VII, respectively.

The data for the $[\bar{1}\bar{1}2]_\gamma$ and $[\bar{2}\bar{1}3]_\gamma$ specimens were previously reported by the author.[21]

F. Discussion of the Volume Fraction Measurements and Mechanical Property Results

In all cases ε martensite was observed only on planes that had slipped. This was confirmed by comparing slip planes defined by slip traces on two perpendicular surfaces to the x-ray measurements. If slip occurs on a particular $\{111\}_\gamma$ plane, ε martensite was always present as $\{111\}_\gamma \parallel \{0001\}_\varepsilon$. Slip is possible on only two systems for the $[\bar{1}\bar{1}2]_\gamma$ tensile axis sample. Because the crystals were two degrees from the exact $[\bar{1}\bar{1}2]_\gamma$ tensile axis, the $(1\bar{1}1)_\gamma$ $[\bar{1}01]_\gamma$ system was favored and produced twice the quantity of ε on the $(1\bar{1}1)_\gamma$ plane than was observed on the $(\bar{1}11)_\gamma$ plane (see Table VII). The majority of the α martensite was that associated with the particular K-S variant corresponding to the active $(1\bar{1}1)_\gamma$ slip direction. Although a crystal exactly with $[\bar{1}10]_\gamma$ parallel to the tensile axis should slip on two planes and four slip directions only a one degree deviation from the $[\bar{1}10]_\gamma$ was sufficient to confine slip to the $(1\bar{1}1)_\gamma$ $[\bar{1}01]_\gamma$ and $(1\bar{1}1)_\gamma$ $[011]_\gamma$ systems. The α martensite was evenly distributed between the K-S variants containing the $[\bar{1}01]_\gamma$ and $[011]_\gamma$ slip directions. The $[100]_\gamma$ sample generated slip on only two systems, the $(1\bar{1}1)_\gamma$ $[110]_\gamma$ and $(111)_\gamma$ $[1\bar{1}0]_\gamma$. Almost no α martensite was observed in this sample and the volume fraction of ε martensite was also less than in other orientations (See Table VII). It is clear from the data

in Table VII that the K-S variants favored in plastically deformed austenite crystals are those associated with both the slip plane and slip direction.

The mechanical properties of these single crystals (Figs. 13, 14 and 15) help to explain the orientation dependence of ε and α martensite formation in the polycrystal data presented by Goodchild, et al.[39] for textured 303 and 305 austenitic stainless steel. They observed that the formation of ε and α martensite was inhibited in grains with the $\langle 001 \rangle_\gamma$ parallel to the tensile axis. Grains with the $\langle 110 \rangle_\gamma$ parallel to the tensile axis contained ε and moderate amounts of α martensite. Grains with one of the $\langle 123 \rangle_\gamma$ parallel to the tensile axis contained ε martensite and the maximum amounts of α martensite. The results given in Table VII follow these same trends for α martensite, but not for ε martensite. A reduction of ε martensite was observed in the $[100]_\gamma$ tensile axis specimen, but not to the extent suggested by the polycrystals.[39] The reason almost no ε martensite is present in grains with the $\langle 100 \rangle_\gamma$ parallel to the tensile axis in polycrystal samples may be due to the orientation dependence of the flow stress observed in single crystals tested between Md_γ and Ms_γ, (Figs. 14 and 15). For single crystals, the yield and flow stress is reduced significantly when the $\gamma \rightarrow \alpha$ transformation can proceed with ease. A single crystal with a $[100]_\gamma$ tensile axis does not transform to α martensite at 185°K during straining, consequently a higher yield and flow stress are observed (Fig. 13). Epsilon martensite is not found in grains with the $\langle 001 \rangle_\gamma$ parallel to the tensile axis in polycrystalline austenitic

stainless steel because under these deformation conditions the stress in these grains does not exceed the CRSS for slip.

The reason α does not form appears to be related to the work done by the stress which can either aid or hinder the $\gamma \rightarrow \alpha$ transformation. The orientation dependence of α martensite formation follows from the criterion established by Patel and Cohen[37] showing how the work done by an external stress resolved on the habit plane (τ) and the normal to the habit plane (σ_n) of the martensite plate can raise the martensite start temperature. The work done by the stress is written as

$$U = \tau\gamma_0 + \sigma_n\varepsilon_0$$

where γ_0 is the transformation shear in the habit plane and ε_0 is the transformation shear normal to the habit plane. The values of γ_0 and ε_0 used were 0.20 and 0.04, respectively. Very simply, the effect on Ms_γ due to an applied stress is

$$\Delta F^{\gamma\rightarrow\alpha} @ Ms_\gamma = \Delta F^{\gamma\rightarrow\alpha} @ Md_\gamma + U$$

where $Ms_\gamma < Md_\gamma$. The magnitude of U depends upon the magnitude of the resolved shear stress τ and the normal stress σ_n on the potential martensite habit plane.

Goodchild et al.[39] show that the magnitude of U/σ where σ is the applied stress will indicate which martensite crystals should be favored due to the applied stress. The larger U/σ, the more the stress aids the formation of a particular martensite crystal. If it is assumed that the habit plane is the $\{112\}_\gamma$ and shear direction is the $\langle 110\rangle_\gamma$,[19,32]

crystals with the largest values of U/σ are not always observed experimentally in this alloy.

Based upon U/σ calculations, the crystal with $[\bar{2}\bar{1}3]_\gamma$ tensile axis should favor about equally ($U/\sigma \simeq 0.13$) martensite crystal formation for the following habit plane-shear directions: $(\bar{1}\bar{1}2)_\gamma$ $[\bar{1}10]_\gamma$, $(\bar{2}11)_\gamma$ $[0\bar{1}1]_\gamma$, $(\bar{1}12)_\gamma$ $[\bar{1}\bar{1}0]_\gamma$, and $(\bar{2}\bar{1}1)_\gamma$ $[011]_\gamma$. Only the $(\bar{2}11)_\gamma$ $[0\bar{1}1]_\gamma$ of this set was observed experimentally. The result is clearly seen in Fig. 16A, which was sectioned to show the $(\bar{2}11)_\gamma$ surface. Because the austenite shear direction in the $[\bar{2}\bar{1}3]_\gamma$ tensile axis crystal is the $[0\bar{1}1]_\gamma$, then it is expected that the long axis of needles would be near the $[0\bar{1}1]_\gamma$ in the $(\bar{2}11)_\gamma$ plane. This clearly was the result. Figure 16B shows the same crystal sectioned to expose the $(01\bar{1})_\gamma$ plane. It is clear that α martensite needles cut the surface in packets that appear to be confined between ε sheets parallel to the $(\bar{1}11)_\gamma$ plane. Electron microscopy of $(01\bar{1})_\gamma$ foils showed that the α martensite is confined on two sides by large ε martensite sheets that are parallel to the $(\bar{1}11)_\gamma$ plane (See Figs. 3 and 8). Figure 16C is the same crystal cut to expose the $(\bar{1}11)_\gamma$ plane. The α martensite typically appears as small, highly transformed regions that are widely separated in the austenite matrix. Accurate habit plane measurements (Table IV) from optical micrographs show that the following habit plane-shear directions $(\bar{2}11)_\gamma$ $[0\bar{1}1]_\gamma$, $(12\bar{1})_\gamma$ $[101]_\gamma$, $(1\bar{1}2)_\gamma$ $[\bar{1}\bar{1}0]_\gamma$, and $(211)_\gamma$ $[0\bar{1}1]_\gamma$ with U/σ = 0.13, 0.08, 0.08 and 0.04, respectively, are formed when the crystal is deformed plastically with the $[\bar{2}\bar{1}3]_\gamma$ tensile axis.

The difficulty at the present time is that the model of reference 37 favors the presence of α martensite habit planes that are not experimentally observed in this alloy. The metallographic results show that the austenite matrix is partitioned by the ε phase as sheets parallel to the $\{111\}_\gamma$ slip planes, and confirms earlier results of Reed in a similar alloy.[43] This partitioning appears to control both the size of the acicular α martensite crystals and the plane on which the α martensite crystals can form. Such partitioning is not accounted for in the model. If all the α martensite crystals were to form with the habit planes suggested by the theory, many needles would have to cut through the ε martensite sheet. This event has not been observed. Therefore, it is not surprising, because of ε martensite partitioning, that all the α martensite that forms due to the deformation has the $(110)_\alpha$ plane always parallel to the $\{111\}_\gamma$ slip plane(s), and that the direction of shear in the austenite plays a dominant role in determining the specific K-S variant formed.

One final point of interest is the fact that the volume fraction of α in the $[\bar{1}\bar{1}2]_\gamma$ specimen is less than half that observed in the $[\bar{2}\bar{1}3]_\gamma$ specimen. For the $[112]_\gamma$ specimen the values of U/σ are only 0.02 less than those observed for the $[\bar{2}\bar{1}3]_\gamma$ orientation. This small difference in U/σ is not believed to be the reason for this large reduction of α martensite in the $[\bar{1}\bar{1}2]_\gamma$ crystal at 5% tensile strain. The $[\bar{2}\bar{1}3]_\gamma$ tensile axis specimen is partitioned only on the $(\bar{1}11)_\gamma$ plane. The $[\bar{1}\bar{1}2]_\gamma$ crystal is partitioned on two $\{111\}_\gamma$ planes. The difference in volume fraction of α martensite observed for these two

specimens is thought to be due to the fact that partitioning by two slip systems will reduce the size of the burst of α martensite and therefore the total volume of α martensite. Thus, ε partitioning is also controlling the amount of α martensite that can form during each burst. If α could penetrate the ε interface, its significance as a controlling factor on the volume fraction of α that forms could be reduced. However, at no time has an α martensite needle been observed to pass through an ε sheet and also no evidence that ε has transformed to α has been found. These observations do not support previous studies that indicated that α martensite nucleation is aided at the intersection of ε martensite bands.[41,44]

G. Conclusions

1. The deformation induced ε martensite in this alloy forms only on $\{111\}_\gamma$ planes that slip. The ε forms as very thin sheets, 0.05 microns or less in thickness and appear to cover the entire slip plane. The orientation relationship is the $\{111\}_\gamma \parallel \{0001\}_\varepsilon$; $\langle 011\rangle_\gamma \parallel \langle \bar{2}110\rangle_\varepsilon$ (See Fig. 8C).
2. The ε martensite partitions the austenite matrix at all temperatures tested with parallel ε martensite sheets on each slip plane. At 5% tensile strain in easy glide orientation the spacing between the parallel sheets is one micron or less (See Figs. 3, 8 and 9).
3. The α martensite forms as clusters of needles bounded on both sides by parallel ε martensite sheets (See Figs. 3 and 8).

4. The α martensite in this alloy is dislocated. The habit plane is near the $\{252\}_\gamma$. Previous studies have suggested that all $\{252\}_\gamma$ martensites must be internally twinned. This study suggest that the twinning observed must have been due to accommodation deformation in the martensite and not part of the transformation shears.

5. The α martensite appears to exist in needle pairs with habits of the form $(0.333, 0.812, 0.479)_\gamma$ and $(0.479, 0.812, 0.333)_\gamma$. Needle pairs with these habit planes join at a bcc twin boundary. The AB theory has predicted this experimental result (see Tables III and IV and Fig. 10).

6. The variant of the K-S orientation relation for α martensite present in Fe-15Ni-15Cr single crystals was always the variant that contained both the austenite slip plane and slip direction. This characteristic was true for both single and multiple slip orientations (see Table VII).

7. Goodchild, et al[34] observed that grains with the $\langle 001 \rangle_\gamma$ direction parallel to the tensile axis in 303 and 305 stainless steel did not contain ε or α martensite. The single crystal results reported here may be used to explain the above observations. The $[100]_\gamma$ single crystal specimen was found to have a yield stress approximately 5 kg/mm^2 higher than was observed for the $[1\bar{1}0]_\gamma$, $[\bar{1}\bar{1}2]_\gamma$ and $[\bar{2}\bar{1}3]_\gamma$ tensile axes crystals (Fig. 5). The reason for this difference in yield stress is the fact that at 185°K, the stress aided $\gamma \rightarrow \alpha$ transformation cannot occur in the $[001]_\gamma$ specimen

because of the low shear stress on potential α martensite habit planes. It is conceivable that it is those grains in the polycrystal 303 and 305 stainless steels, which are orientated such that the applied stress aids the γ→α transformation are the grains which deform the most. Consequently $\langle 001 \rangle_\gamma$ oriented grains do not deform sufficiently to form α or ε martensite. The surrounding grains with favorable orientations for the γ→α transformation will transform to α martensite and plastically deform at stresses much lower than the yield stress for grains in the $\langle 001 \rangle_\gamma$ orientation. The absence of significant deformation in these grains explains the absence of ε martensite, and the low resolved shear stress on potential α martensite habit planes, explains the absence of α martensite.

8. Many α martensite crystal orientations that should be favored as predicted by the Patel-Cohen model are not observed experimentally. This is explained by the following; because the γ-ε transformation preceeds the γ-α transformation due to plastic deformation, the austenite matrix becomes partitioned by ε plates parallel to the slip plane(s). This partitioning blocks the formation of needles with energetically favored habit planes. The majority of needles that do form, even under the restriction of partitioning, have high U/σ values and therefore tends to support the basic concept of the model.

III. THE DEFORMATION INDUCED MARTENSITE-AUSTENITE INTERFACE

A single crystal stressed in the $[\bar{2}\bar{1}3]_\gamma$ direction at 185°K was transformed to 5% α martensite and 2% ε martensite by volume. The austenite slip system of maximum shear stress is the $(\bar{1}11)_\gamma$ $[01\bar{1}]_\gamma$. Figure 3 shows a two surface study using the electron and optical microscopes. The α martensite is confined between ε martensite plates with the $(0001)_\varepsilon \parallel (\bar{1}11)_\gamma$. The size of the acicular martensite crystals is controlled by the spacing of the ε martensite plates. These ε martensite plates are seen in Fig. 3A as dark vertical bands. The axes of the acicular crystals lie in the $(\bar{1}11)_\gamma$ plane. The ε martensite habit plane is defined as the plane perpendicular to the $(\bar{1}11)_\gamma$ containing the vector defining the crystal axis. See Table IV.

The physical nature of the interface is being revealed in some detail working with $(01\bar{1})_\gamma$ foils. Figure 8A is a bright field micrograph showing a α martensite crystal cutting the surface with its axis a few degrees out of the plane of the foil. Figure 8B is a dark field of the same area using a $(01\bar{1}1)_\varepsilon$ reflection. Fine lines light up in the interface defining a sheath surrounding the α martensite. Figure 8C is the $(200)_\gamma$ reflection that lights up the sheath as well, indicating the α martensite crystal is surrounded by alternate regions of faulted austenite and dislocated austenite. Figure 8D is the diffraction pattern from the same area and clearly shows this alloy obeys the Kurdjumov-Sachs orientation relationship. Specifically in this diffraction pattern the $(01\bar{1})_\gamma \parallel (\bar{1}11) \nparallel (\bar{2}110)_\varepsilon$ and $[\bar{1}11]_\gamma \parallel [110]_\alpha \parallel [0001]_\varepsilon$.

Efforts to image interface dislocations have been unsuccessful to date. It appears clear that the interface between the phases in this alloy is a composite of dislocated austenite and faulted austenite giving rise to hcp reflections. Also the $(110)_\alpha$ surface of the crystal is in contact with and parallel to the $(0001)_\varepsilon$ plane. The large very thin ε plates appear to control the size of the acicular α crystals and forces the long axis of the crystals to remain parallel to the austenite slip plane which is the $(\bar{1}11)_\gamma$ in this example.

ACKNOWLEDGEMENTS

The author wishes to thank Professor Gareth Thomas for continued encouragement, support and guidance during this study. Many thanks to Professor C. M. Wayman for helpful suggestions regarding the martensite shape change measurments, and to Professor R. Wenk for the use of his x-ray equipment and discussions related to the volume fraction measurements. The author would also like to thank Lutgard de Jonghe, Omer Van der Biest and Krishna Seshan for the many helpful discussions. The manuscript was expertly and graciously typed by Alice Ramirez. The alloy single crystals used in this study were grown and donated by the Advanced Materials Research and Development Laboratory of Pratt and Whitman Aircraft.

This work was performed under the auspices of the United States Atomic Energy Commission.

The most important acknowledgement is to my wife, Arleen; her love, understanding and encouragement will always be appreciated.

REFERENCES

1. A. B. Greninger and A. R. Troiano, Trans. Met. Soc. AIME 140, 307 (1940).
2. A. B. Greninger and A. R. Troiano, Trans. Met. Soc. AIME 185, 590 (1949).
3. M. S. Wechsler, D. S. Lieberman and T. A. Read, Trans. Met. Soc. AIME 197, 1503 (1953).
4. J. S. Bowles and J. K. MacKenzie, Acta Met. 2, 224 (1954).
5. A. F. Acton and M. Bevis, Met. Sci. and Eng. 5, 19 (1969-70).
6. N. D. E. Ross and A. G. Crocker, Acta Met. 18, 405 (1970).
7. E. C. Bain, Trans. Met. AIME 70, 25 (1924).
8. J. W. Christian, The Theory of Transformations in Metals and Alloys Pergamon Press, Oxford, 1952, Chapter XXII.
9. J. W. Christian, Mechanism of Phase Transformations in Crystalline Solids, Institute of Metals Monograph No. 33, Manchester, 1968, p. 129.
10. C. M. Wayman, Introduction to the Crystallography of Martensitic Transformations, MacMillan, New York, 1964.
11. C. M. Wayman, Adv. Mater. Res. 3 147 (1968).
12. D. P. Dunne and C. M. Wayman, Met. Trans. 2 2327 (1971).
13. M. Oka and C. M. Wayman, Met. Trans. AIME 242, 337 (1968).
14. S. K. Das and G. Thomas, Met. Trans. 1, 325 (1970).
15. G. Thomas and S. K. Das, J. Iron & Steel Inst. 209, 801 (1971).

16. C. M. Wayman, J. E. Hanafee and T. A. Read, Acta Met. 9, 391 (1961).

17. C. M. Wayman and A. J. Morton, Acta Met. 14, 1567 (1966).

18. D. P. Dunne and J. S. Bowles, Acta Met. 17, 201 (1969).

19. P. M. Kelly, Acta Met. 13, 635 (1965).

20. J. F. Breedis and L. Kaufman, Met. Trans. 2 2359 (1971).

21. Glen Stone, Master of Science Thesis, Lawrence Berkeley Laboratory Report No. LBL-134, University of California, Berkeley, 1971.

22. B. A. Bilby and J. W. Christian, J. Iron & Steel Inst. 197 122 (1961).

23. J. S. Bowles and A. J. Morton, Acta Met. 12, 629 (1964).

24. F. J. Schoen, Gulf General Atomic, P.O. Box 608, San Diego, Calif. 92112.

25. Glen Stone and Gareth Thomas, accepted for publication by Met. Trans., 1974. (LBL-1853)

26. P. C. Rowlands, E. O. Fearon and M. Bevis, J. of Mat. Sci. 5, 679 (1970).

27. G. Gordon, Lawrence Berkeley Laboratory, IMRD, University of California, Berkeley 94720.

28. B. Cina, J. Iron & Steel Inst. 177, 406 (1954).

29. J. F. Breedis and W. D. Robertson, Acta Met. 10, 1077 (1962).

30. P. M. Kelly and J. Nutting, J. Iron & Steel Inst. 198, 165 (1961).

31. C. J. Guntner and R. Reed, Trans. ASM 55, 399 (1962).

32. J. F. Breedis, Trans. Met Soc. AIME 230, 1583 (1964).

33. B. J. Thomas, Métaux, Corrosion, Industrie, 1969, N°s 531, novembre, et 532, decembre, p. 7-66.

34. A. J. Goldman, W. D. Robertson, and D. S. Koss, Met. Trans. AIME 230, 240 (1964).

35. H. Schumann, 25 Rostock, Klement-Gottwald-Str. 16/17, Germany.

36. Von Hermann Schumann, Archiv für das Eisenhüttenwesen, 40, 1 (1969).

37. J. R. Patel and M. Cohen, Acta Met. 1, 531 (1953).

38. R. H. Richman and G. F. Bolling, Met. Trans. 2, 2451 (1971).

39. D. Goodchild, W. T. Roberts and D. V. Wilson, Acta Met. 18, 1137 (1970).

40. L. G. Schulz, J. of Appl. Phys. 20, 1030 (1949).

41. J. A. Venables, Phil. Mag. 7, 35 (1962).

42. J. Dash and H. M. Otte, Acta Met. 11, 1169 (1963).

43. R. P. Reed, Acta Met. 10, 865 (1962).

44. R. Lagneborg, Acta Met. 12, 823 (1964).

45. R. Hall, M.S. thesis in progress, University of California, Berkeley, 1973.

46. Pat L. Mangonon, Jr. and Gareth Thomas, Met. Trans. 1, 1577 (1970).

47. P. Gaunt and J. W. Christian, Acta Met. 7, 529 (1959).

48. P. S. Kotval and R. W. K. Honeycombe, Acta Met. 16, 597 (1968).

49. J. W. Christian, Proc. R. Soc. A206, 51 (1951).

50. Hermann Schumann, Kristall und Technik, 4, 575 (1969).

51. F. Lecroisey and A. Pineau, Met. Trans. 3 387 (1972).

52. S. M. Copley and B. H. Kear, Acta Met. 16, 227 (1968).

53. Krishna Seshan, Department of Materials Science and Engineering, University of California, Berkeley 94720 (private communication).

54. John Price Hirth and Jens Lothe: Theory of Dislocations, McGraw-Hill, New York, 1968, Chapter 10.

APPENDIX A

A Computer Program to Calculate the Exact Specimen Normal from Indexed Back Reflection Laue Photographs

Back reflection Laue photographs with a specimen to film distance of 5 cm are indexed in the conventional manner. To calculate the exact specimen normal [uvw] the dot product between any three indexed poles and [uvw] will generate three equations that can be solved for [uvw]. The angle between the x-ray beam and vector normal to any diffracting plane can be obtained using the following equation:

$$\theta_i = \frac{1}{2} \text{TAN}^{-1} \left(\frac{r_i}{D}\right) \tag{1}$$

where r_i is the distance from the center of the film to the exposed spot and D is the specimen to film distance. The matrix equation for the solution of [uvw] is

$$\begin{vmatrix} h_1 & k_1 & l_1 \\ h_2 & k_2 & l_2 \\ h_3 & k_3 & l_3 \end{vmatrix} \begin{vmatrix} u \\ v \\ w \end{vmatrix} = \begin{vmatrix} \cos(\theta_1) \\ \cos(\theta_2) \\ \cos(\theta_3) \end{vmatrix} \tag{2}$$

The vectors $[h_i \; k_i \; l_i]$ are converted to unit vectors in the program. The Laue photos used in this study were indexed and many different combinations of three indexed diffraction spots were used to calculate the specimen normal. The same solution should result for any combination of three indexed poles. Table VIII shows the result of several different combinations from one Laue photograph.

The input data for PROGRAM LAUE are as follows:

Card 1:	Col 1-5	N, the number of sets of input data, Integer number right justified
Card 2:	Col 1-10	$h_1k_1l_1$ of first indexed pole.
	11-20	Decimal point must be supplied
	21-30	
	31-40	r_1 measured distance from pole to center of Laue photograph in cm.

Card 3: Same format as above, input $h_2k_2l_2$ and r_2 for second pole

Card 4: Same format as above, input $h_3k_3l_3$ and r_3 for third pole

Repeat cards 2, 3 and 4 for each set of data. Fortran listing and example of input data follows.

```
      PROGRAM LAUE(INPUT,OUTPUT,TAPE5=INPUT,TAPE6=OUTPUT)
      DIMENSION A(3),B(3),C(3),D(3),BB(3),CC(3)
      WRITE(6,5)
    5 FORMAT(1H1)
      READ(5,3) N
      DO 100 I=1,N
    3 FORMAT(I5)
C     ORIENTATION OF 5 CM LAUE PHOTOGRAPHS ONLY
C     A, B, C ARE THE INDICIES OF THREE INDEXED POLES ON THE LAUE PHOTO
C     D(1), D(2), AND D(3) ARE THE DISTANCES IN CM MEASURED FORM THE
C     CENTER OF THE LAUE PHOTOGRAPH TO POLE A, B, AND C RESPECTIVELY
      READ(5,1) A,D(1)
      READ(5,1) B,D(2)
      READ(5,1) C,D(3)
    1 FORMAT(4F10.0)
      CALL AMAG(A,X)
      D(1)=COS(ATAN(D(1)/5.0)/2.0)*X
      CALL AMAG(B,Y)
      D(2)=COS(ATAN(D(2)/5.0)/2.0)*Y
      CALL AMAG(C,Z)
      D(3)=COS(ATAN(D(3)/5.0)/2.0)*Z
      WRITE(6,4) A,D(1)
      WRITE(6,4) B,D(2)
      WRITE(6,4) C,D(3)
    4 FORMAT(10X,3F11.8,F12.8)
      CALL DET(A,B,C,AA)
      BB(1)=A(1)
      BB(2)=B(1)
      BB(3)=C(1)
      A(1)=D(1)
      B(1)=D(2)
      C(1)=D(3)
      CALL DET(A,B,C,E)
      CC(1)=E/AA
      A(1)=BB(1)
      B(1)=BB(2)
      C(1)=BB(3)
      BB(1)=A(2)
      BB(2)=B(2)
      BB(3)=C(2)
      A(2)=D(1)
      B(2)=D(2)
      C(2)=D(3)
      CALL DET(A,B,C,E)
      CC(2)=E/AA
      A(2)=BB(1)
      B(2)=BB(2)
      C(2)=BB(3)
      A(3)=D(1)
      B(3)=D(2)
      C(3)=D(3)
      CALL DET(A,B,C,E)
      CC(3)=E/AA
      CALL AMAG(CC,X)
      CC(1)=CC(1)/X
      CC(2)=CC(2)/X
      CC(3)=CC(3)/X
```

```
C       OUTPUT UNIT VECTOR NORMAL TO POLISHED SURFACE OF CRYSTAL
        WRITE(6,2) CC
        A(1)=1.0
        A(2)=1.0
        A(3)=-1.0
        CALL CROSS(A,CC,B)
        WRITE(6,2)B
        CALL CROSS(CC,B,A)
        WRITE(6,2) A
        WRITE(6,6)
      6 FORMAT(//)
      2 FORMAT(10X,3F11.8)
    100 CONTINUE
        STOP
        END
        SUBROUTINE AMAG(A,B)
        DIMENSION A(3)
        B=SQRT(A(1)*A(1)+A(2)*A(2)+A(3)*A(3))
        RETURN
        END
        SUBROUTINE DET(A,B,C,D)
        DIMENSION A(3),B(3),C(3)
        D=A(1)*(B(2)*C(3)-B(3)*C(2))+A(2)*(B(3)*C(1)-B(1)*C(3))+A(3)*(
       $B(1)*C(2)-B(2)*C(1))
        RETURN
        END
        SUBROUTINE CROSS (A,B,C)
        DIMENSION A(3),B(3),C(3)
        C(1)=A(2)*B(3)-A(3)*B(2)
        C(2)=A(3)*B(1)-A(1)*B(3)
        C(3)=A(1)*B(2)-A(2)*B(1)
        CALL AMAG(C,D)
        C(1)=C(1)/D
        C(2)=C(2)/D
        C(3)=C(3)/D
        RETURN
        END
```

```
   19
-1.        2.        2.        4.08
-3.        2.        1.        4.6
-5.        1.        3.        5.62
-1.        1.        2.        3.95
-1.        2.        2.        4.08
-3.        2.        1.        4.6
-3.        5.        3.        3.92
-1.        1.        2.        3.95
-1.        2.        2.        4.08
-3.        1.        2.        3.57
-3.        5.        3.        3.92
-1.        1.        2.        3.95
-3.        1.        3.        3.56
-3.        1.        2.        3.57
-3.        5.        3.        3.92
-2.        2.        1.        3.54
-3.        1.        3.        3.56
-3.        1.        2.        3.57
```

-2.	1.	1.	3.28
-2.	2.	1.	3.54
-3.	1.	3.	3.56
-2.	1.	2.	2.05
-2.	1.	1.	3.28
-2.	2.	1.	3.54
-1.	1.	2.	3.95
-3.	2.	1.	4.6
-5.	1.	3.	5.62
-3.	5.	3.	3.92
-1.	2.	2.	4.08
-3.	2.	1.	4.6
-3.	1.	2.	3.57
-1.	1.	2.	3.95
-1.	2.	2.	4.08
-3.	1.	3.	3.56
-3.	5.	3.	3.92
-1.	1.	2.	3.95
-2.	2.	1.	3.54
-3.	1.	2.	3.57
-3.	5.	3.	3.92
-2.	1.	1.	3.28
-3.	1.	3.	3.56
-3.	1.	2.	3.57
-2.	1.	2.	2.05
-2.	2.	1.	3.54
-3.	1.	3.	3.56
-2.	1.	1.	3.28
-2.	2.	1.	3.54
-5.	1.	3.	5.62
-2.	1.	2.	2.05
-1.	2.	2.	4.08
-5.	1.	3.	5.62
-2.	1.	1.	3.28
-3.	2.	1.	4.6
-5.	1.	3.	5.62
-2.	1.	2.	2.05
-2.	1.	1.	3.28
-3.	2.	1.	4.6

APPENDIX B.

A Computer Program to Calculate the Direction of a Trace on the Surface of a Single Crystal

The program provides quick and accurate calculations of the direction of a trace on the polished surface of the crystal. The required input are a set of orthogonal vectors that define the crystal orientation and the measured angles between these vectors and the vector parallel to the trace on the crystal surface. Two methods were used to define a set of orthogonal vectors--the first leading to the second.

The first method applied to the problem was to cut the crystal to expose two perpendicular surfaces. Each surface was orientated using 5 cm Laue back reflection photographs. The orthogonal set of reference vectors are (1) the surface normal, (2) the line of intersection of the two orientated planes obtained simply by taking the cross product of the two surface normals and (3) a second vector on the polished surface calculated by taking the cross product between the surface normal and the line of intersection. Three equations with three unknowns are obtained simply by taking the dot product between the trace and the orthogonal set of unit vectors.

$$\begin{vmatrix} h_1 & k_1 & l_1 \\ h_2 & k_2 & l_2 \\ h_3 & k_3 & l_3 \end{vmatrix} \begin{vmatrix} u \\ v \\ w \end{vmatrix} = \begin{vmatrix} 0 \\ \cos(\theta_1) \\ \cos(\theta_2) \end{vmatrix} \qquad (1)$$

The angle between the surface normal $[h_1k_1l_1]$ and the trace vector [uvw] is 90° and is defined in the program. The angle θ_1 is the angle between the trace vector and the line of intersection $[h_2k_2l_2]$ and the angle θ_2 is the angle between the second vector on the polished surface $[h_3k_3l_3]$ and the trace vector. The output is a unit vector [uvw] parallel to the trace on the crystal surface.

The second method is in fact the same as the first, except that the orthogonal set of vectors defining the crystal orientations are obtained from a known crystallographic feature on the crystal surface. In this study, it was observed using the first method described that a feature on the optical micrographs was the intersection of a ε martensite plate laying parallel to an adjacent $\{111\}_\gamma$ plane. Specifically in this experiment, the polished surface was near the $(\bar{1}11)_\gamma$ plane. This produced a line of intersection on the polished surface with a direction $[0.69551347, 0.02264272, 0.71815619]_\gamma$. This is the unit vector obtained by taking the vector product between the specimen normal $[-0.62452938, 0.51327139, 0.58865570]_\gamma$ and the $[11\bar{1}]_\gamma$ direction. When this crystallographic feature was observed, the resulting vector defining the line of intersection of the two planes was obtained to a precision of ±0.25. This result provides proof that the original method used was sound.

When possible, the specimen normal, the line of intersection of the plate on the $(11\bar{1})_\gamma$ plane and the crystal surface are used to define the crystal orientation. It is felt that the accuracy of trace calculations using a crystallographic feature is better than the original procedure (method 1). Even with this good accuracy, it appears

that sets of martensite plates with seemingly the same direction have experimental scatter up to ±1°. This scatter appears to be real and not due to experimental error (see Table IV).

The program listing to follow has been modified to resolve vectors laying on the polished surface onto the $(\bar{1}11)_\gamma$ surface. To do this, several assumptions were required. It is assumed that the long axis of the martensite needles lies exactly in the interface plane and the $(\bar{1}11)_\gamma$ plane. It is assumed that the needle has a rectangular cross section. It is assumed that the trace on the polished surface and the $[\bar{1}11]_\gamma$ direction lie in the same plane; the plane being the interface plane. All measurements are made only on martensite needles sectioned by the polished surface in such a way that both sides (traces) of the needle are parallel (see Fig. 7). The resulting output by taking the vector product between the $[\bar{1}11]_\gamma$ and the trace vector is the habit plane normal. The vector defining the long axis of the needle is simply the vector product of the $[\bar{1}11]_\gamma$ and the interface plane normal. Also in the output are the computed angles between the vectors defining the long axis and the $[101]_\gamma$ and vectors defining the interface plane normal and the $[211]_\gamma$. These calculations are given in Table IV.

The input data for PROGRAM TRACE are as follows:

Card 1:	Col 1-5	M, the number of complete data sets. Integer number right justified.
Card 2:	Col 1-5	N, the number of traces to be calculated using the set of orthogonal vector to be defined in this calculation. Integer number right justified.

Cards 3 and 4:		$\bar{A}$, $\bar{B}$, and $\bar{C}$ are the three vectors defining the orthogonal set. Decimal point must be supplied.
Col	1-10 A(1)	
	11-20 A(2)	
	21-30 A(3)	
	31-40 B(1)	
	41-50 B(2)	
	51-60 B(3)	
	61-70 C(1)	
	71-80 C(2)	
next card	1-10 C(3)	
Card 5: Col	1-7 THETA1	THETA1 and THETA2 are the angles between $\bar{B}$ and $\bar{C}$ respectively. Decimal point must be supplied.
	8-14 THETA2	

Repeat Card 5 N times for this data set.

Repeat Card 2 to Card 5 M times for each data set thereafter.

Fortran listing and example of input data follows.

```
      PROGRAM TRACE(INPUT,OUTPUT,TAPE5=INPUT,TAPE6=OUTPUT)
C     CALCULATION OF TRACE ON THE -1 1 1 PLANE WITH REFERENCE TO A
C     REFERENCE DIRECTION SUCH AS A SLIP BAND OR INTERSECTION OF TWO
C     PLANES.
      DIMENSION A(3),B(3),C(3),AA(3),BB(3),G(3),H(3),F(3)
      WRITE(6,6)
    6 FORMAT(1H1)
      READ(5,5) M
C     M IS THE NUMBER OF COMPLETE DATA SETS.
      DO 102 J=1,M
      READ(5,5) N
    5 FORMAT(I5)
      READ(5,1) A,B,C
    1 FORMAT(8F10.0/F10.0)
      WRITE(6,7) A,B,C
    7 FORMAT(10X,3F11.8/10X,3F11.8/10X,3F11.8//)
C     FOR THE CALCULATIONS USING THE INTERSECTION OF A EPISLON BAND ON THE
C     1 1 -1 SURFACE CUTTING THE -1 1 1 SURFACE LET...
C     A IS VECTOR NEAR -1 1 1 DIRECTION (THE NORMAL TO THE POLISHED
C     DIRECTION OF THE CRYSTAL)
C     B IS VECTOR NEAR 1 0 1 DIRECTION ON POLISHED SURFACE OF CRYSTAL
C     C IS VECTOR NEAR 1 2 -1 DIRECTION ONPOLISHED SURFACE OF CRYSTAL
C     N IS THE NUMBER OF TRACES TO BE CALCULATED IN A PARTICULAR DATA SET
C     THETA1 IS ANGLE BETWEEN DIRECTION OF MARTENSITE INTERFACE AND
C     1 0 1 DIRECTION ON SURFACE OF CRYSTAL
C     THETA2 IS ANGLE BETWEEN DIRECTION OF MARTENSITE INTERFACE AND
C     1 2 -1 DIRECTION ON SURFACE OF CRYSTAL
      CALL AMAG(A,X)
      CALL AMAG(B,Y)
      CALL AMAG(C,Z)
      DO 101 I=1,3
      A(I)=A(I)/X
      B(I)=B(I)/Y
      C(I)=C(I)/Z
  101 CONTINUE
      CALL DET(A,B,C,D)
      DO 100 I=1,N
      READ(5,2) THETA1,THETA2,ALPHA
    2 FORMAT(2F7.2,5X,A10)
      WRITE(6,8) THETA1, THETA2,ALPHA
    8 FORMAT(10X,F7.2,5X,F7.2,5X,A10)
      THETA1=COS(THETA1*3.141592654/180.)
      THETA2=COS(THETA2*3.141592654/180.)
      AA(1)=A(1)
      AA(2)=B(1)
      AA(3)=C(1)
      A(1)=0.0
      B(1)=THETA1
      C(1)=THETA2
      CALL DET(A,B,C,DD)
      BB(1)=DD/D
      A(1)=AA(1)
      B(1)=AA(2)
      C(1)=AA(3)
      AA(1)=A(2)
      AA(2)=B(2)
      AA(3)=C(2)
```

```
      A(2)=0.0
      B(2)=THETA1
      C(2)=THETA2
      CALL DET(A,B,C,DD)
      BB(2)=DD/D
      A(2)=AA(1)
      B(2)=AA(2)
      C(2)=AA(3)
      AA(1)=A(3)
      AA(2)=B(3)
      AA(3)=C(3)
      A(3)=0.0
      B(3)=THETA1
      C(3)=THETA2
      CALL DET(A,B,C,DD)
      BB(3)=DD/D
      CALL AMAG(BB,CC)
      A(3)=AA(1)
      B(3)=AA(2)
      C(3)=AA(3)
      BB(1)=BB(1)/CC
      BB(2)=BB(2)/CC
      BB(3)=BB(3)/CC
      F(1)=-1.0/SQRT(3.0)
      F(2)=-F(1)
      F(3)=F(2)
    3 FORMAT(10X,4F12.8)
C     OUTPUT UNIT VECTOR ON POLISHED SURFACE IN DIRECTION OF INTERFACE
C     LINE
      WRITE(6,3) BB
      CALL CROSS(F,BB,G)
      CALL CROSS(F,G,H)
      F(1)=1.0/SQRT(2.0)
      F(2)=0.0
      F(3)=F(1)
      CALL DOT(F,H,ANG)
C     OUTPUT UNIT VECTOR ON -1 1 1 SURFACE IN DIRECTION OF INTERFACE LINE
C     AND ANGLE BETWEEN 101 DIRECTION
      WRITE(6,4) H,ANG
      F(1)=2.0/SQRT(6.0)
      F(2)=1.0/SQRT(6.0)
      F(3)=F(2)
C     OUTPUT OF VECTOR NORMAL TO INTERFACE PLANE AND ANGLE BETWEEN 211 DIRECTION
      CALL DOT(F,G,ANG)
      WRITE(6,4) G,ANG
    4 FORM+T(10X,3F11.8,5X,F8.2)
      WRITE(6,9)
    9 FORMAT(//)
  100 CONTINUE
  102 CONTINUE
      STOP
      END
      SUBROUTINE DOT(A,B,ANG)
      DIMENSION A(3),B(3)
      ANG=+COS((A(1)*B(1)+A(2)*B(2)+A(3)*B(3))/SQRT(A(1)*A(1)+A(2)*A(2)+
     $A(3)*A(3))/SQRT(B(1)*B(1)+B(B)*B(2)+B(3)*B(3)))*180.0/3.141592654
      RETURN
```

```
      END
      SUBROUTINE CROSS (A,B,C)
      DIMENSION A(3),B(3),C(3)
      C(1)=A(2)*B(3)-A(3)*B(2)
      C(2)=A(3)*B(1)-A(1)*B(3)
      C(3)=A(1)*B(2)-A(2)*B(1)
      CALL AMAG(C,D)
      C(1)=C(1)/D
      C(2)=C(2)/D
      C(3)=C(3)/D
      RETURN
      END
      SUBROUTINE AMAG(A,B)
      DIMENSION A(3)
      B=SQRT(A(1)*A(1)+A(2)*A(2)+A(3)*A(3))
      RETURN
      END
      SUBROUTINE DET(A,B,C,D)
      DIMENSION A(3),B(3),C(3)
      D=A(1)*(B(2)*C(3)-B(3)*C(2))+A(2)*(B(3)*C(1)-B(1)*C(3))+A(3)*(
     $B(1)*C(2)-B(2)*C(1))
      RETURN
      END

    1
   28
-.62452938 .51327139 .58865570 .69551347 .02264272 .71815619 .35528026 .85792761
-.37112821
   9.17  99.17      322-1
   5.33  84.67      322-2
   5.67  84.33      322-3
   9.58  99.58        322-4
  67.08 157.08      322-5
  55.33 145.33      322-6
  67.92 157.92      322-7
  54.83 144.83      329-1
  69.75 159.75      329-2
  69.08 159.08      329-3
  56.33 146.33      329-4
  69.33 159.33      329-5
  69.33 159.33      329-6
55.92   145.92      329-7
   8.25  98.25      329-8
   8.92  98.92      329-9
   5.42  84.58      329-10
  10.17 100.17      336-1
   8.50  98.50      336-2
  11.75 101.75      336-3
  10.67 100.67      336-4
   3.58  86.42      336-5
   4.50  85.50      336-6
   7.47 97.47       337-1
 55.92 145.92       337-2
 68.31 158.31       337-3
 56.28 146.28       337-4
  3.75 86.25        337-5
```

APPENDIX C.

A Computer Program to Calculate the Magnitude and Direction of the Shape Change Associated with the $\gamma \rightarrow \alpha$ Martensitic Transformations

The magnitude and direction of the shape change are calculated using the method described by Bowles and Morton.[23] The specimen normal is the $(001)_\gamma$. The reference vector used to calculate the angle required to rotate the result from the J basis to the austenite basis is the $[100]_\gamma$. The geometry of the measurement is shown in Fig. 5. The input data are the direction of the fiducial line (F), the angle between the fiducial line and the transformed line (ALPHA), and the angle between the nomal of the tilted α martensite crystal and the $(001)_\gamma$ surface (PHI). The angle PHI is measured such that the nomal to the tilted surface, the $(001)_\gamma$ and the habit plane nomal all lie on the same great circle. The unit vector defining the habit plane nomal is also required. The output is the magnitude of the shape change and a unit vector defining the direction of the shape change.

The input data for PROGRAM SHAPE are as follows:

Card 1:	Col. 1-3	N the number of habits plane nomals to be tested for each measured ALPHA and PHI	
	Col. 4-6	M the number of values of ALPHA and PHI	
Card 2:	Col. 1-10	u	direction of fiducial line
	Col. 11-20	v	
	Col. 21-30	w	
Card 3:	Col. 1-10	ALPHA	
	Col. 11-20	PHI	

Card 4:	Col 1-10	h	Habit plane normal
	Col 11-20	k	
	Col 21-30	l	

Repeat Card 4 N times	This sequence repeated M times
Repeat Card 3	
Repeat Card 4 N times	

Fortran listing and example of input data follows.

```
      PROGRAM SHAPE(INPUT,OUTPUT,TAPE5=INPUT,TAPE6=OUTPUT)
      REAL J1(3),J2(3),J3(3),H(3),F(3),F1(3),MD(3),ROT(3,3),MDD(3),HH(3)
      J3(1)=F1(3)=0.0
      J3(2)=F1(2)=0.0
      J3(3)=F1(1)=1.0
      READ(5,4) N,M
    4 FORMAT(I3,I3)
      READ(5,1) F
      DO 100 K=1,M
      READ(5,1) ALPHA,PHI
      WRITE(6,1) ALPHA,PHI,F
    1 FORMAT(8F10.5)
      ALPHA=ALPHA*3.14159/180.
      PHI=PHI*3.14159/180.
      DO 100 I=1,N
      READ(5,1) H
      WRITE(6,1) H
      CALL CROSS (H,J3,J1)
      CALL CROSS(J3,J1,J2)
      CALL DOT(J3,H,BETA)
      CALL DOT(J1,F,ROW)
      ROWP=ROW+ALPHA
      CALL DOT(J1,F1,THETA)
      A=1.0/TAN(PHI)
      B=COS(BETA)+SIN(BETA)*A
      C=1.0289176
      MD(3)=C/B
      MD(2)=C*A/B-1.0/SIN(BETA)
      AA=1.0/TAN(ROW)
      MD(1)=C*A/(B*TAN(ROWP))-AA/SIN(BETA)
      CALL AMAG(MD,D)
C     D IS THE MAGNITUDE OF THE SHAPE STRAIN.
      MD(3)=MD(3)/D
      MD(2)=MD(2)/D
      MD(1)=MD(1)/D
      WRITE(6,3) MD,D
    3 FORMAT(5X,F10.6,5X,F10.6,5X,F10.6,5X,F10.6)
      ROT(1,1)=ROT(2,2)=COS(THETA)
      ROT(1,2)=-SIN(THETA)
      ROT(2,1)=SIN(THETA)
      ROT(1,3)=ROT(2,3)=ROT(3,1)=ROT(3,2)=0.0
      ROT(3,3)=1.0
      CALL GMPRD(ROT,MD,MDD,3,3,1)
      WRITE(6,2) MDD
    2 FORMAT(5X,F10.6,5X,F10.6,5X,F10.6)
       ROT(1,1)=ROT(1,3)=ROT(2,2)=ROT(2,3)=ROT(3,1)=ROT(3,2)=0.0
      ROT(1,2)=ROT(3,3)=1.0
      ROT(2,1)=-1.0
      CALL GMPRD(ROT,MDD,MD,3,3,1)
      CALL GMPRD(ROT,MD,MDD,3,3,1)
      CALL GMPRD(ROT,H,HH,3,3,1)
      CALL GMPRD(ROT,HH,H,3,3,1)
      WRITE(6,2) MDD
      WRITE(6,2) H
      WRITE(6,5)
    5 FORMAT(//)
  100 CONTINUE
```

```
      STOP
      END
      SUBROUTINE GMPRD(A,B,R,N,M,L)
      DIMENSION A(9),B(9),R(9)
      IR=0
      IK=-M
      DO 10 K=1,L
      IK=IK+M
      DO 10 J=1,N
      IR=IR+1
      JI=J-N
      IB=IK
      R(IR)=0
      DO 10 I=1,M
      JI=JI+N
      IB=IB+1
   10 R(IR)=R(IR)+A(JI)*B(IB)
      RETURN
      END
      SUBROUTINE DOT(A,B,ANG)
      DIMENSION A(3),B(3)
      ANG=ACOS((A(1)*B(1)+A(2)*B(2)+A(3)*B(3))/SQRT(A(1)*A(1)+A(2)*A(2)+
     $A(3)*A(3))/SQRT(B(1)*B(1)+B(B)*B(2)+B(3)*B(3)))
      RETURN
      END
      SUBROUTINE CROSS (A,B,C)
      DIMENSION A(3),B(3),C(3)
      C(1)=A(2)*B(3)-A(3)*B(2)
      C(2)=A(3)*B(1)-A(1)*B(3)
      C(3)=A(1)*B(2)-A(2)*B(1)
      CALL AMAG(C,D)
      C(1)=C(1)/D
      C(2)=C(2)/D
      C(3)=C(3)/D
      RETURN
      END
      SUBROUTINE AMAG(A,B)
      DIMENSION A(3)
      B=SQRT(A(1)*A(1)+A(2)*A(2)+A(3)*A(3))
      RETURN
      END
```

```
  4   8
  -1.0      -1.0      0.0
  -5.5      -9.0
-0.479    -0.812    0.333
-0.333    -0.812    0.479
-0.812    -0.479    0.333
-0.812    -.333     0.479
   6.6      11.0
-0.479    -0.812    0.333
-0.333    -0.812    0.479
-0.812    -0.479    0.333
-0.812    -.333     0.479
   5.5       9.0
-0.479    -0.812    0.333
-0.333    -0.812    0.479
```

-0.812	-0.479	0.333
-0.812	-.333	0.479
-6.6	-11.0	
-0.479	-0.812	0.333
-0.333	-0.812	0.479
-0.812	-0.479	0.333
-0.812	-.333	0.479
5.5	-9.0	
-0.479	-0.812	0.333
-0.333	-0.812	0.479
-0.812	-0.479	0.333
-0.812	-.333	0.479
-6.6	11.0	
-0.479	-0.812	0.333
-0.333	-0.812	0.479
-0.812	-0.479	0.333
-0.812	-.333	0.479
-5.5	9.0	
-0.479	-0.812	0.333
-0.333	-0.812	0.479
-0.812	-0.479	0.333
-0.812	-.333	0.479
6.6	-11.0	
-0.479	-0.812	0.333
-0.333	-0.812	0.479
-0.812	-0.479	0.333
-0.812	-.333	0.479

APPENDIX D

The Mechanism of the $\gamma \rightarrow \varepsilon$ Deformation Induced Phase Transformation

The objective of this discussion is to present data that indicates that the critical resolve shear stress (CRSS) acting on $\{111\}_\gamma$ planes in $\langle 112 \rangle_\gamma$ directions can dictate the variants of ε martensite that can form by plastic deformation in low stacking fault energy materials. The results showed that slip and ε martensite were observed on only two of the expected four $\{111\}_\gamma$ planes for the $[100]_\gamma$ tensile axis specimen and on only one of the expected two $\{111\}_\gamma$ planes for the $[\bar{1}\bar{1}0]_\gamma$ tensile axis specimen. There are of course experimental reasons that could cause these results. These are errors in cutting the crystals (crystal orientation) and poor axial alignment and during tensile testing. The ideal tensile axes wanted and actual tensile axes obtained in these single crystals were usually within two degrees of each other. The crystal orientation and Schmidt factors for all the slip systems possible in these crystals are presented in Tables IX and X. Great care was excercised to control the axial alignment of the crystals. However this is always a difficult problem when testing small crystals; in this study the gauge length of the specimens were between 10 and 15 mm. With these problems in mind, it appears the fact that slip and therefore ε martensite are not forming on specific $\{111\}_\gamma$ planes, and the fact that the total volume fraction of ε associated with the $[100]_\gamma$ is less than that observed for other orientations tested may be consistent with previous studies.

Gaunt and Christian[47] have studied the f.c.c. to h.c.p. transformation in cobalt and cobalt-nickel alloys. The f.c.c. to h.c.p. martensitic transformation occurs in this alloy by both quenching below the martensite start temperature and by elastic and plastic strain above this temperature. The h.c.p. phase exists as sheets parallel to {111} f.c.c. planes. An important observation was the fact that the {111} f.c.c. plane that exhibited the presence of the h.c.p. phase was <u>not necessarily the {111} f.c.c. plane of highest resolved shear stress</u>. Kotual and Honeycombe[48] studied the f.c.c. to h.c.p. ($\alpha \rightarrow \zeta$) transformation in the Copper-Germanium system. This transformation is also formed under stress and by thermal activation. They established the orientation relationship as $(111)_\alpha \parallel (0001)_\zeta$ and $[\bar{1}10]_\alpha \parallel [11\bar{2}0]_\zeta$, the same relationship is now clearly established for the $\gamma \rightarrow \varepsilon$ transformation in low stacking fault energy Fe-Ni-Cr alloys. Kotual and Honeycombe calculated the angle of tilt that should be observed on the specimen surface if the ζ phase was forming by the motion of $\frac{a}{6}\langle 112\rangle_\alpha$ Shockley partials on alternate $\{111\}_\alpha$ planes, which results in a half-twin shear $1/(2\sqrt{2})$ as first proposed by Christian.[49] Three different tilt angles associated with each of the three $a/6\langle 112\rangle_\alpha$ shears on a $\{111\}_\alpha$ plane were obtained. <u>The significant result obtained when the $\alpha \rightarrow \zeta$ transformation is induced by stress was the fact that for any given set of $\{111\}_\alpha$ planes, surface tilts associated with only one $a/6\langle 112\rangle$ shear was observed</u>. Other studies using Fe-Ni-Cr-C polycrystalline alloys tend to support this behavior but add little to the basic understanding as to why the state of stress tends to control which variant of the h.c.p. phase that forms.[50,51]

Copley and Kear[52] have calculated the dependence of the width of a dissociated dislocation on dislocation velocity and have shown that the dynamic width of a Shockley pair is dependent on the CRSS on each dislocation. When the leading partial has the highest Schmidt factor its possible for one partial to glide out of the crystal leaving the partial with the lower CRSS behind. The crystal now has a large intrinsic stacking fault. For the case where the trailing partial has the highest Schmidt factor the partials glide together due to the applied stress. Continued motion of these partials would cause the formation of an extrinsic stacking fault. If the energy of the extrinsic fault is enough larger than the entrinsic fault, it is possible the extrinsic fault would not form in the crystal, and that plastic deformation in these low stacking fault energy single crystals will be due to the motion of leading Shockley partical dislocation that have higher Schmidt factors than the trailing Shockley particals. A figure from Copley and Kear's paper[52] showing how the orientation dependence of the tensile axis will control the spacing between Shockley partials as a function of dislocation velocity is given in Fig. 19. In this figure D' is the force per unit length of dislocation line, v* is a velocity near the shear wave velocity, v the dislocation velocity and ΔX the spacing between Shockley partial dislocations.

Krishna Seshan[53] was ask to review the single crystal results presented in this thesis to see if the observed selectivity of ε martensite formation as a function of the direction of the tensile axis is consistant with Copley and Kears results and previous studies of the f.c.c. $\rightarrow$ h.c.p. transformation already discussed. Seshan

concluded that if only one kind of stacking fault can form in the material, these single crystal results were consistant with Copley and Kears calculations.[52] Hirth and Lothe[54] discuss the formation of stacking faults in f.c.c. metals. Throughout this discussion it becomes clear that extrinsic faults are rarely found in f.c.c. metals. It is therefore possible that only intrinsic faults are forming in this Fe-15Ni-15Cr alloy and a detailed study of faults could form the basis of an interesting research project.

APPENDIX E

The Volume Fraction of ε and α Martensite as a Function of Strain

Gunther and Reed[31] have measured the volume fraction of α and ε martensite in a polycrystalline Fe-18Cr-9Ni alloy deformed at 77°K. They observed that the volume fraction of ε martensite increased rapidly to a maximum of 0.35 at 9% tensile strain and then decreases to 0.10 at 26% tensile strain, the apparent strain at fracture. The volume fraction of α at this strain was 0.90. These results suggested that the ε→α transformation was occurring. However Breedis and Kaufman[20] have demonstrated that the ε→α transformation should not occur in these Fe-Ni-Cr alloys at temperatures below 500°K. Also no known electron microscopy studies have shown α martensite in a region of a specimen that was at one time clearly ε martensite. The variation of ε and α martensite as a function of strain and temperature is of considerable interest. A separate study was initiated to make measurements of the volume fraction of ε and α martensite as a function of strain to fracture in this alloy,[45] but this work has not yet been completed.

It appears that the quantity of ε martensite present in Fe-15Ni-15Cr single crystals increases from zero to 8-9 percent by volume in about 10% tensile strain. The quantity of ε then remains nearly constant in specimen that initially had the $[\bar{2}\bar{1}3]_\gamma$ tensile axis, but shows a sharp decrease in the $[\bar{1}\bar{1}2]_\gamma$ tensile axis specimens. This is shown in

Fig. 17. This reduction of ε is in agreement with polycrystal stainless steel results of Guntner and Reed.[31] If plastic deformation in the austenite is responsible for the $\gamma \rightarrow \varepsilon$ transformation it is necessary to ask why the amount of ε stops increasing even tough the amount of plastic strain increases significantly. One possibility is that the $\varepsilon \rightarrow \gamma$ transformations begins to occur at a rate equal to or greater than the $\gamma \rightarrow \varepsilon$ transformation. The popular mechanism for the $\gamma \rightarrow \varepsilon$ transformation is that of slip in the austenite of every other $(111)_\gamma$ plane, thus forming the regular hcp structure. The $\varepsilon \rightarrow \gamma$ transformation could occur in the reverse manner.

A second possibility is that as soon as the matrix is partitioned by the ε, the majority of plastic deformation, at least to the strains tested to in this program, occurs on the basal plane of the new hcp phase. Large slip steps at small tensile strains would support this mode of deformation. The surface of specimens tested to 15% tensile strain at 242°K and 5% tensile strain at 185°K are presented in Fig. 18A and B respectively. The results clearly indicate large slip steps.

One final piece of perhaps unconvincing data is the somewhat larger then expected temperature dependence of the flow stress observed in this alloy when only the $\gamma \rightarrow \varepsilon$ transformation occurs (242° and 273°K). Materials with the fcc crystal structure usually exhibit a weak temperature dependence of the flow stress. These crystals tested at 273°K and 242°K (a 31° temperature difference) exhibited a 2 kg/mm^2 increase in the tensile flow stress with decreasing temperature. This is large for a

fcc metal and suggests the possibility of a different mechanism for slip in this alloy. This behavior is shown for the $[\bar{1}\bar{1}2]_\gamma$ and $[\bar{2}\bar{1}3]_\gamma$ tensile specimens in Fig. 14 and 15 respectively.

Whatever the case may be, this phenomenon should be studied using in situ tensile testing of thick foils in the high voltage electron microscope. It is quite possible the study could be carried out at room temperature in this alloy. There is no reason to expect that the ε phase will not form at room temperature in single crystal foils although this point has not been checked.

Table I. Calculated solutions that produce $\{252\}_\gamma$ α martensite habit planes where the magnitude of one shear is zero.

S SHEAR	T SHEAR	MAGNITUDE S SHEAR	MAGNITUDE T SHEAR	MAGNITUDE SHAPE CHANGE	SHAPE CHANGE VECTOR	HABIT PLANE NORMAL	ANGULAR DEVIATION FORM K-S RELATIONSHIP PLANE	DIRECTION	Key*
(1 1 0) [-1 1 1]	(1 0 1) [1 1 -1]	.00000000	-.25210794	.28539530	-.15804210 -.54153953 .82568616	-.34059760 -.81154891 -.47474377	.39	1.14	(2)
(1 1 0) [-1 1 1]	(1 0 1) [1 1 -1]	-.02000000	.26360641	.28207180	-.09526621 -.54832164 .83082353	-.34904589 -.81829585 -.45668246	1.23	.96	(2)
(1 1 0) [-1 1 1]	(-1 0 1) [1 -1 1]	.04000000	.23321870	.29224581	-.57116323 -.19516451 .79729755	-.76299505 -.38754428 -.51734707	1.50	1.12	(1)
(1 1 0) [-1 1 1]	(-1 0 1) [1 -1 1]	.02000000	.24291902	.28803745	-.55660692 -.17784509 .81151701	-.78784512 -.36438389 -.49651229	.91	1.12	(1)
(1 1 0) [-1 1 1]	(-1 0 1) [1 -1 1]	.00000000	.25210794	.28539530	-.54153953 -.15804210 .82568616	-.81154891 -.34059760 -.47474377	.39	1.14	(1)
(1 1 0) [-1 1 1]	(-1 0 1) [1 -1 1]	-.02000000	.26070952	.28432186	-.52605668 -.13588413 .83952360	-.83366441 -.31663806 -.45248645	.20	1.15	(1)
(1 1 0) [-1 1 1]	(-1 0 1) [1 -1 1]	-.04000000	.26866393	.28478504	-.51026401 -.11160749 .85274522	-.85387367 -.29295701 -.43020453	.61	1.18	(1)
(1 1 0) [-1 1 1]	(-1 0 1) [1 -1 1]	-.06000000	.27593192	.28672272	-.49427364 -.08554141 .86508742	-.87200101 -.26995998 -.40833302	1.00	1.21	(1)
(1 1 0) [-1 1 1]	(-1 0 1) [1 -1 1]	-.08000000	.28249626	.29005020	-.47820031 -.05808138 .87632814	-.88800642 -.24797284 -.38723904	1.37	1.25	(1)

*Key: (1) $(111)_\gamma \parallel (011)_\alpha$; $[01\bar{1}]_\gamma \parallel [\bar{1}\bar{1}1]_\alpha$

(2) $(111)_\gamma \parallel (011)_\alpha$; $[10\bar{1}]_\gamma \parallel [\bar{1}1\bar{1}]_\alpha$

Table II. Calculated two shear solutions that produce {252} α martensite habit planes.

S SHEAR	T SHEAR	MAGNITUDE S SHEAR	MAGNITUDE T SHEAR	MAGNITUDE SHAPE CHANGE	SHAPE CHANGE VECTOR	HABIT PLANE NORMAL	ANGULAR DEVIATION FORM K-S PLANE	ANGULAR DEVIATION RELATIONSHIP DIRECTION	Key*
(1 1 0) [1 -1 1]	(1 0 1) [1 1 -1]	.14000000	-.29163118	.26415648	-.08922845 -.55010180 .83031698	.17076391 -.88389193 -.43540183	1.19	.79	(2)
(1 1 0) [1 -1 1]	(-1 0 1) [1 -1 1]	.06000000	.28091268	.25663259	-.60424815 -.05025460 .79520981	-.80934514 -.31858294 -.49342209	.40	1.49	(1)
(1 1 0) [1 -1 1]	(-1 0 1) [1 -1 1]	.04000000	.27166559	.26555575	-.58311913 -.08863132 .80753735	-.81027732 -.32725027 -.48616656	.40	1.35	(1)
(1 1 0) [1 -1 1]	(-1 0 1) [1 -1 1]	.02000000	.26203627	.27517099	-.56213502 -.12457413 .81760962	-.81099138 -.33448317 -.48001457	.39	1.23	(1)
(1 1 0) [1 -1 1]	(-1 0 1) [1 -1 1]	.00000000	.25210794	.28539530	-.54153953 -.15804210 .82568616	-.81154891 -.34059760 -.47474377	.39	1.14	(1)
(1 1 0) [1 -1 1]	(-1 0 1) [1 -1 1]	-.02000000	.24194201	.29615715	-.52151179 -.18907801 .83203062	-.81199165 -.34582630 -.47018479	.39	1.05	(1)
(1 1 0) [1 -1 1]	(-1 0 1) [1 -1 1]	-.04000000	.23158463	.30739447	-.50217628 -.21777921 .83689378	-.81234855 -.35034352 -.46620730	.39	.98	(1)
(1 1 0) [1 -1 1]	(-1 0 1) [1 -1 1]	-.06000000	.22107096	.31905323	-.48361300 -.24427587 .84050447	-.81264012 -.35428180 -.46270989	.38	.92	(1)
(1 1 0) [1 -1 1]	(-1 0 1) [1 -1 1]	-.08000000	.21042825	.33108625	-.46586708 -.26871546 .84306576	-.81288118 -.35774339 -.45961272	.38	.86	(1)
(1 1 0) [1 -1 1]	(-1 0 1) [1 -1 1]	-.10000000	.19967786	.34345234	-.44895701 -.29125188 .84475437	-.81308262 -.36080828 -.45685231	.38	.81	(1)
(1 1 0) [1 -1 1]	(-1 0 1) [1 -1 1]	-.12000000	.18883674	.35611546	-.43288160 -.31203824 .84572197	-.81325258 -.36353983 -.45437763	.38	.77	(1)
(1 1 0) [1 -1 1]	(-1 0 1) [1 -1 1]	-.14000000	.17791854	.36904406	-.41762555 -.33122224 .84609735	-.81339723 -.36598880 -.45214726	.38	.73	(1)
(1 1 0) [1 -1 1]	(-1 0 1) [1 -1 1]	-.16000000	.16693432	.38221047	-.40316378 -.34894335 .84598907	-.81352132 -.36819627 -.45012729	.38	.69	(1)
(1 1 0) [1 -1 1]	(-1 0 1) [1 -1 1]	-.18000000	.15589315	.39559040	-.38946478 -.36533138 .84548812	-.81362853 -.37019585 -.44828970	.38	.66	(1)

Table II. Continued.

S SHEAR	T SHEAR	MAGNITUDE S SHEAR	MAGNITUDE T SHEAR	MAGNITUDE SHAPE CHANGE	SHAPE CHANGE VECTOR	HABIT PLANE NORMAL	ANGULAR DEVIATION FORM K-S RELATIONSHIP PLANE	ANGULAR DEVIATION FORM K-S RELATIONSHIP DIRECTION	Key*
(-1 1 0) [1 1 -1]	(1 0 1) [1 1 -1]	.18000000	-.15589315	.39559040	-.36533138 -.38946478 .84548812	-.37019585 -.81362853 -.44828970	.38	.66	(2)
(-1 1 0) [1 1 -1]	(1 0 1) [1 1 -1]	.16000000	-.16693432	.38221047	-.34894335 -.40316378 .84598907	-.36819627 -.81352132 -.45012729	.38	.69	(2)
(-1 1 0) [1 1 -1]	(1 0 1) [1 1 -1]	.14000000	-.17791854	.36904406	-.33122224 -.41762555 .84609735	-.36598880 -.81339723 -.45214726	.38	.73	(2)
(-1 1 0) [1 1 -1]	(1 0 1) [1 1 -1]	.12000000	-.18883674	.35611546	-.31203824 -.43288160 .84572197	-.36353983 -.81325258 -.45437763	.38	.77	(2)
(-1 1 0) [1 1 -1]	(1 0 1) [1 1 -1]	.10000000	-.19967786	.34345234	-.29125188 -.44895701 .84475437	-.36080828 -.81308262 -.45685231	.38	.81	(2)
(-1 1 0) [1 1 -1]	(1 0 -1) [1 1 -1]	.08000000	-.21042825	.33108625	-.26871546 -.46586708 .84306576	-.35774339 -.81288118 -.45961272	.38	.86	(2)
(-1 1 0) [1 1 -1]	(1 0 1) [1 1 -1]	.06000000	-.22107096	.31905323	-.24427587 -.48361300 .84050447	-.35428180 -.81264012 -.46270989	.38	.92	(2)
(-1 1 0) [1 1 -1]	(1 0 1) [1 1 -1]	.04000000	-.23158463	.30739447	-.21777921 -.50217628 .83689378	-.35034352 -.81234855 -.46620730	.39	.98	(2)
(-1 1 0) [1 1 -1]	(1 0 1) [1 1 -1]	.02000000	-.24194201	.29615715	-.18907801 -.52151179 .83203062	-.34582630 -.81199165 -.47018479	.39	1.05	(2)
(-1 1 0) [1 1 -1]	(1 0 1) [1 1 -1]	.00000000	-.25210794	.28539530	-.15804210 -.54153953 .82568616	-.34059760 -.81154891 -.47474377	.39	1.14	(2)
(-1 1 0) [1 1 -1]	(1 0 1) [1 1 -1]	-.02000000	-.26203627	.27517099	-.12457413 -.56213502 .81760962	-.33448317 -.81099138 -.48001457	.39	1.23	(2)
(-1 1 0) [1 1 -1]	(1 0 1) [1 1 -1]	-.04000000	-.27166559	.26555575	-.08863132 -.58311913 .80753735	-.32725027 -.81027732 -.48616656	.40	1.35	(2)
(-1 1 0) [1 1 -1]	(1 0 1) [1 1 -1]	-.06000000	-.28091268	.25663259	-.05025460 -.60424815 .79520981	-.31858294 -.80934514 -.49342209	.40	1.49	(2)
(1 1 0) [1 -1 1]	(0 1 1) [1 -1 1]	-.28000000	.26490374	.27227523	-.56827832 -.11425590 .81486523	-.81079984 -.33248350 -.48172435	.39	1.26	(1)

Table II. Continued.

S SHEAR	T SHEAR	MAGNITUDE S SHEAR	MAGNITUDE T SHEAR	MAGNITUDE SHAPE CHANGE	SHAPE CHANGE VECTOR	HABIT PLANE NORMAL	ANGULAR DEVIATION FORM K-S RELATIONSHIP PLANE	DIRECTION	Key*
(1 1 0) [1 -1 1]	(0 1 1) [1 -1 1]	-.30000000	.24114693	.29701041	-.51998972 -.19138060 .83245670	-.81202202 -.34619930 -.46985773	.39	1.05	(1)
(1 1 0) [1 -1 1]	(0 1 1) [1 -1 1]	-.32000000	.21457950	.32636666	-.47266707 -.25944912 .84218288	-.81279271 -.35644879 -.46077356	.38	.88	(1)
(1 1 0) [1 -1 1]	(0 1 1) [1 -1 1]	-.34000000	.18597553	.35948725	-.42879541 -.31722717 .84587317	-.81329282 -.36420871 -.45376956	.38	.76	(1)
(1 1 0) [1 -1 1]	(0 1 1) [1 -1 1]	-.36000000	.15590833	.39557192	-.38948307 -.36530977 .84548904	-.81362839 -.37019324 -.44829211	.38	.66	(1)

*Key: (1) $(111)_\gamma \parallel (011)_\alpha$; $[01\bar{1}]_\gamma \parallel [\bar{1}\bar{1}1]_\alpha$

(2) $(111)_\gamma \parallel (011)_\alpha$; $[10\bar{1}]_\gamma \parallel [\bar{1}1\bar{1}]_\alpha$

0 0 0 0 5 6 0 3 7 3 1

Table III. Calculated two shear solutions that produced {252} twin related α martensite habits.

S SHEAR	T SHEAR	MAGNITUDE S SHEAR	MAGNITUDE T SHEAR	MAGNITUDE SHAPE CHANGE	SHAPE CHANGE VECTOR	HABIT PLANE NORMAL	ANGULAR DEVIATION FORM K-S RELATIONSHIP PLANE	DIRECTION	Key*
(1 0 1) [1 1 -1]	(0 1 1) [1 1 -1]	-.16000000	-.39912727	.27993985	-.82166551 .55232436 .14072523	.47742097 .81127190 .33750128	.39	1.18	(2)
(1 0 1) [1 1 -1]	(0 1 1) [1 1 -1]	-.18000000	-.35482363	.25591349	-.79405752 .60603014 .04690537	.49409428 .80925374 .31777228	.40	1.50	(2)
(1 0 1) [1 1 -1]	(0 1 1) [1 1 -1]	-.24000000	.02803047	.26914863	-.10264092 -.57507847 .81163391	-.33016068 -.81057169 -.48370182	.39	1.30	(2)
(1 0 1) [1 1 -1]	(0 1 1) [1 1 -1]	-.26000000	.01913433	.29731264	-.19219104 -.51945279 .83260519	-.34633012 -.81203264 -.46974296	.39	1.04	(2)
(1 0 1) [1 1 -1]	(0 1 1) [1 1 -1]	-.28000000	.07004022	.33162087	-.26974067 -.46510932 .84315675	-.35788534 -.81289076 -.45948525	.38	.86	(2)
(1 0 1) [1 1 -1]	(0 1 1) [1 1 -1]	-.30000000	.12352425	.37076472	-.33363642 -.41567650 .84610861	-.36629248 -.81341466 -.45186991	.38	.72	(2)
(-1 0 1) [1 -1 1]	(0 1 1) [1 -1 1]	.30000000	-.12352425	.37076472	-.41567650 -.33363642 .84610861	-.81341466 -.36629248 -.45186991	.38	.72	(1)
(-1 0 1) [1 -1 1]	(0 1 1) [1 -1 1]	.28000000	-.07004022	.33162087	-.46510932 -.26974067 .84315675	-.81289076 -.35788534 -.45948525	.38	.86	(1)
(-1 0 1) [1 -1 1]	(0 1 1) [1 -1 1]	.26000000	-.01913433	.29731264	-.51945279 -.19219104 .83260519	-.81203264 -.34633012 -.46974296	.39	1.04	(1)
(-1 0 1) [1 -1 1]	(0 1 1) [1 -1 1]	.24000000	.02803047	.26914863	-.57507847 -.10264092 .81163391	-.81057169 -.33016068 -.48370182	.39	1.30	(1)
(-1 0 1) [1 -1 1]	(0 1 1) [1 -1 1]	.18000000	.35482363	.25591349	.60603014 -.79405752 .04690537	.80925374 .49409428 .31777228	.40	1.50	(1)
(-1 0 1) [1 -1 1]	(0 1 1) [1 -1 1]	.16000000	.39912727	.27993985	.55232436 -.82166551 .14072523	.81127190 .47742097 .33750128	.39	1.18	(1)

*Key: (1) $(111)_\gamma \parallel (011)_\alpha$; $[01\bar{1}]_\gamma \parallel [\bar{1}\bar{1}1]_\alpha$

(2) $(111)_\gamma \parallel (011)_\alpha$; $[10\bar{1}]_\gamma \parallel [01\bar{1}]_\alpha$

Table IV. Measurements of the α martensite needle axis and habit Plane normal assuming the habit plane is perpendicular to a $\{111\}_\gamma$ plane.

Unit Vector Defining the Long Axis of Martensite Needles on the $(\bar{1}11)_\gamma$ Plane			Unit Vector Defining the Interface Plane Normal for Martensite Needles on the $(\bar{1}11)_\gamma$			Angle Between Intetface Normal and $(211)_\gamma$ Direction
h	k	ℓ	h	k	ℓ	
-0.63798142	0.12229693	-0.76027835	0.50955508	0.80728565	-0.29773058	51.39
-0.63433004	0.12805297	-0.76238300	0.51409345	0.80639265	-0.29229920	50.98
-0.64605652	0.10935841	-0.75541493	0.49927712	0.80913992	-0.30986280	52.30
-0.64019198	0.11878404	-0.75897601	0.50677500	0.80781001	-0.30103501	51.63
-0.62901910	0.13632438	-0.76534348	0.52057818	0.80503561	-0.28445743	50.39
-0.64387846	0.11287727	-0.75675514	0.50208285	0.80865653	-0.30657368	52.05
-0.61447222	0.15840100	-0.77287322	0.53767142	0.80098426	-0.26331284	48.81
-0.62446647	0.14332271	-0.76778918	0.52603069	0.80381918	-0.27778848	49.89
-0.74501901	-0.08318268	-0.66183633	0.33408584	0.81224830	-0.47816247	65.85
-0.74698423	-0.08799094	-0.65899329	0.32966836	0.81174150	-0.48207314	66.19
-0.74554175	-0.08445573	-0.66108602	0.33291765	0.81211692	-0.47919927	65.94
-0.73449311	-0.05839400	-0.67609911	0.35663221	0.81440580	-0.45777359	64.10
-0.74011221	-0.07143354	-0.66867867	0.34481964	0.81336579	-0.46854616	65.02
-0.73554564	-0.06080464	-0.67474100	0.35445632	0.81422937	-0.45977305	64.27
0.09102861	0.74821292	-0.65718431	0.81140647	0.32687015	0.48453632	6.40
0.10291886	0.75292631	-0.65000745	0.80998418	0.31586174	0.49412244	7.24
0.12874635	0.76263407	-0.63388773	0.80628224	0.29164351	0.51463873	9.07
0.11930364	0.75916950	-0.63986586	0.80773344	0.30054674	0.50718670	8.40
0.12282893	0.76047440	-0.63764547	0.80720488	0.29722946	0.50997542	8.65
0.12282893	0.76047440	-0.63764547	0.80720488	0.29722946	0.50997542	8.65
0.10843235	0.75505982	-0.64662748	0.80926454	0.31072710	0.49853744	7.63
-0.07606209	0.66600086	-0.74206295	0.81294602	0.47234471	0.34060131	5.35
-0.08314634	0.66185772	-0.74500406	0.81225203	0.47813285	0.33411917	5.84
-0.06187563	0.67413562	-0.73601126	0.81414868	0.46066021	0.35348847	4.35
-0.06769479	0.67082492	-0.73851970	0.81368549	0.46546815	0.34821734	4.76
-0.06769479	0.67082492	-0.73851970	0.81368549	0.46546815	0.34821734	4.76
-0.06258547	0.67373371	-0.73631919	0.81409442	0.46124782	0.35284660	4.40

	h	k	ℓ	
Specimen Normal	-0.62452938	0.51327139	0.58865570	± 0.1°
Second Surface Normal	0.02682327	0.70555316	-0.70814917	± 0.1°
Line of Intersection Between Specimen Surface and Second Surface	0.7807972	0.4275636	0.4555712	

Table V. Shape change calculations that correspond to Fig. 6A, 6B and 6C. The specimen normal and direction of fiducial line use in these calculations are respectively the $[001]_\gamma$ and $[110]_\gamma$. The photomicrograph was rotated about the $[110]_\gamma$, $[\bar{1}10]_\gamma$ and $[001]_\gamma$ to show that symmetrical solutions exist.

Needle Code	Projected Deviation of Fiducial Line (degrees)	Measured Surface Tilt (degrees)	Surface Tilt used for this Calculation (degrees)	Magnitude of Shape Change	Direction of Shape Change $\begin{bmatrix} h \\ k \\ l \end{bmatrix}$	Habit Plane Normal $\begin{bmatrix} h \\ k \\ l \end{bmatrix}$
A	5.5±0.2°	9.0±1°	10.0	0.223	0.125475 -0.521830 0.844787	0.812 0.333 0.479
B	-6.6±0.2°		-11.0	0.277	-0.140576 0.551343 -0.822350	0.812 0.479 0.333
A	5.5±0.2°	-9.0±1°	- 9.0	0.226	-0.562850 0.158440 -0.811232	0.479 0.812 0.333
B	-6.6±0.2°		+11.0	0.250	0.556964 -0.114648 0.822586	0.333 0.812 0.479
A	-5.5±0.2°	9.0±1°	10.0	0.223	0.521830 -0.125475 0.844787	0.333 0.812 0.479
B	6.6±0.2°		-11.0	0.277	-0.551343 0.140576 -0.822350	0.479 0.812 0.333

Table V. Continued.

Needle Code	Projected Deviation of Fiducial Line (degrees)	Measured Surface Tilt (degrees)	Surface Tilt used for this Calculation (degrees)	Magnitude of Shape Change	Direction of Shape Change $\begin{bmatrix} h \\ k \\ l \end{bmatrix}$	Habit Plane Normal $\begin{bmatrix} h \\ k \\ l \end{bmatrix}$
A	-5.5±0.2°	-9.0±1°	-9.0	0.226	-0.158440 0.562850 -0.811232	0.812 0.479 0.333
B	6.6±0.2°		11.0	0.250	0.114648 -0.556964 0.822586	0.812 0.333 0.479
C	8.8±0.2°	- 6±1°	-6.0	0.238	-0.823889 0.136474 -0.550075	.333 .812 .479
D	-7.2±0.2°		11.0	0.242	0.553593 0.137058 0.821432	.479 .812 .333
C	8.8±0.2°	- 6±1°	-6.0	0.213	-0.824453 -0.090215 -0.558693	.479 .812 .333
D	-7.2±0.2°		12.0	0.272	0.55743 -0.124679 0.820802	.333 .812 .479

Table V. Continued.

Needle Code	Projected Deviation of Fiducial Line (degrees)	Measured Surface Tilt (degrees)	Surface Tilt used for this Calculation (degrees)	Magnitude of Shape Change	Direction of Shape Change $\begin{bmatrix} h \\ k \\ l \end{bmatrix}$	Habit Plane Normal $\begin{bmatrix} h \\ k \\ l \end{bmatrix}$
C	-8.8±0.2°	-6±1°	-6	0.213	0.090215 0.824453 -0.55869	0.812 0.479 0.333
D	7.2±0.2°		12.0	0.271	0.124679 -0.557439 0.820802	0.812 0.333 0.479
C	-8.8±0.2°	-6±1°	-6.0	0.238	-0.136474 0.823889 -0.550075	0.812 0.333 0.479
D	7.2±0.2°		11.0	0.242	-0.137078 -0.553593 0.821432	0.812 0.479 0.333
C	8.8±0.2°	6±1°	7.0	0.242	-0.152874 -0.815919 0.557589	0.812 0.333 0.479
D	7.2±0.2°		-12.0	0.304	-0.132069 0.548712 -0.825513	0.812 0.479 0.333
C	-8.8±0.2°	6±1°	7.0	0.252	0.815919 0.152874 0.557589	0.333 0.812 0.479
D	7.2±0.2°		-12.0	0.304	-0.548712 0.132069 -0.825513	0.479 0.812 0.333

Table V. Continued

Needle Code	Projected Deviation of Fiducial Line (degrees)	Measured Surface Tilt (degrees)	Surface Tilt used for this Calculation (degrees)	Magnitude of Shape Change	Direction of Shape Change $\begin{bmatrix} h \\ k \\ l \end{bmatrix}$	Habit Plane Normal $\begin{bmatrix} h \\ k \\ l \end{bmatrix}$
E	6.5±0.2°	15°±2°	10.0	0.220	-0.146879 -0.547233 0.823992	0.812 0.479 0.333
E	6.5±0.2°	-15°±2°	-11.0	0.276	-0.546507 0.144836 -0.824835	0.479 0.812 0.333

Table VI. Volume fraction of ε martensite in single crystals tested to 5% tensile strain. The error associated with these measurements is ±0.005.

	Temperature °K		
Tensile axis	185°	242°	273°
$[\bar{2}\bar{1}3]_\gamma$	0.021	0.025	0.020
$[\bar{1}\bar{1}2]_\gamma$	0.028	-	-
$[110]_\gamma$	0.027	-	-
$[100]_\gamma$	0.015	-	-

TABLE VII

Summary of volume fraction measurements for Fe-15^{w}/o Ni-15^{w}/o Cr alloy tested to 5% tensile strain at 185°K

Symbol		Variant of the KS orientation Relationship		$[\bar{2}\bar{1}3]$ Tensile axis C_α	$[\bar{1}\bar{1}2]$ Tensile axis C_α	$[\bar{1}10]$ Tensile axis C_α	$[100]$ Tensile axis C_α
[X]	1	$(\bar{1}11)_\gamma \parallel (110)_\alpha$;	$[\bar{1}\bar{1}0]_\gamma \parallel [\bar{1}11]_\alpha$	0.0072	0.0018	not observed	
[X]	2		$[\bar{1}\bar{1}0]_\gamma \parallel [\bar{1}1\bar{1}]_\alpha$	0.0033	0.0006	not observed	Same
[X]	3		$[\bar{1}0\bar{1}]_\gamma \parallel [\bar{1}11]_\alpha$	0.0011	not observed	not observed	very weak
[X]	4		$[\bar{1}0\bar{1}]_\gamma \parallel [\bar{1}1\bar{1}]_\alpha$	not observed	not observed	not observed	peaks observed
[X]	5		$[01\bar{1}]_\gamma \parallel [\bar{1}11]_\alpha$	0.0137*	≈0.0006	not observed	just above back-
[X]	6		$[01\bar{1}]_\gamma \parallel [\bar{1}1\bar{1}]_\alpha$	0.0421*	0.0019	not observed	ground
■	1	$(1\bar{1}1)_\gamma \parallel (110)_\alpha$;	$[\bar{1}01]_\gamma \parallel [\bar{1}11]_\alpha$	not observed	0.0132*	0.0044	
■	2		$[\bar{1}01]_\gamma \parallel [\bar{1}1\bar{1}]_\alpha$	not observed	0.0056	0.0105*	
■	3		$[011]_\gamma \parallel [\bar{1}11]_\alpha$	not observed	not observed	0.0112*	
■	4		$[011]_\gamma \parallel [\bar{1}1\bar{1}]_\alpha$	not observed	not observed	0.0032	
■	5		$[110]_\gamma \parallel [\bar{1}11]_\alpha$	not observed	0.0020	≈0.0003	
■	6		$[110]_\gamma \parallel [\bar{1}1\bar{1}]_\alpha$	not observed	0.0041	not observed	
			TOTAL α	0.0674	0.0298	0.0296	≈0.002
				C_ε	C_ε	C_ε	C_ε
⊙	1	$(111)_\gamma \parallel (0001)_\varepsilon$		not observed	not observed	not observed	0.0102
⊙	2	$(1\bar{1}1)_\gamma \parallel (0001)_\varepsilon$		not observed	0.0194	0.0270	0.0045
⊙	3	$(\bar{1}11)_\gamma \parallel (0001)_\varepsilon$		0.0214	0.0091	not observed	not observed
⊙	4	$(11\bar{1})_\gamma \parallel (0001)_\varepsilon$		not observed	not observed	not observed	not observed
			TOTAL ε	0.0214	0.0285	0.0270	0.0147
			TOTAL α + ε	0.0888	0.0583	0.0566	0.0167

* The majority of α martensite is always associated with the active austenite slip plane and direction.

Table VIII. Example of Calculations obtained by using PROGRAM LAUE to calculate the surface normal of a single crystal using five combination of Indexed poles from the same Laue back reflection photograph.

Indexed Pole $(hkl)_\gamma$	r_i cm	Unit vector of specimen normal $[unw]_\gamma$
$(\bar{1}2\bar{2})$	4.60	[0.02720366, 0.70525724, -0.70842938]
$(02\bar{1})$	3.89	
$(01\bar{2})$	3.82	
$(02\bar{1})$	3.89	[0.02952808, 0.70521071, -0.70838263]
$(01\bar{2})$	3.82	
$(13\bar{5})$	3.21	
$(\bar{1}2\bar{2})$	4.60	[0.02873764, 0.70639197, -0.70723725]
$(13\bar{5})$	3.21	
$(01\bar{2})$	3.82	
$(\bar{1}2\bar{2})$	4.60	[0.02682377, 0.70555316, -0.70814917]
$(02\bar{1})$	3.89	
$(12\bar{2})$	3.71	
$(13\bar{5})$	3.21	[0.02832692, 0.70577667, -0.70786784]
$(\bar{1}5\bar{3})$	3.72	
$(\bar{1}2\bar{2})$	4.60	

Table IX. Schmid factors and measured directions of the tensile axis before and after testing for the $[100]_\gamma$ and $[\bar{1}10]_\gamma$ tensile axis specimens.

Slip Systems	Ideal $[100]_\gamma$	*Actual @ zero Strain	**Actual @ 4.75% Strain	Ideal $[\bar{1}10]_\gamma$	*Actual @ zero strain	**Actual @ 5.0% strain
(1 1 1) [1 -1 0]	.408248	.415202	.431676	0.	-.011276	-.054441
(1 1 1) [0 -1 1]	0.	.012486	.020101	0.	-.005506	-.025251
(1 1 1) [-1 0 1]	-.408248	-.402716	-.411575	0.	.005770	.029191
(1 1 1) [1 -2 1]	.235702	.246926	.260833	0.	-.009689	-.046010
(1 1 1) [-1 -1 2]	-.235702	-.225300	-.226018	0.	.000152	.002275
(1 1 1) [-2 1 1]	-.471405	-.472225	-.486851	0.	.009841	.048285
(-1 1 1) [1 1 0]	-.408248	-.400955	-.380137	0.	.001174	.017465
(-1 1 1) [1 0 1]	-.408248	-.413330	-.397224	-.408248	-.402352	-.376961
(-1 1 1) [0 -1 1]	0.	-.012375	-.017087	-.408248	-.403526	-.394426
(-1 1 1) [2 1 1]	-.471405	-.470128	-.448809	-.235702	-.231620	-.207555
(-1 1 1) [1 -1 2]	-.235702	-.245781	-.239202	-.471405	-.465274	-.445361
(-1 1 1) [-1 -2 1]	.235702	.224347	.209607	-.235702	-.233653	-.237806
(-1 -1 1) [-1 1 0]	.408248	.400770	.381047	0.	.008957	.021061
(-1 -1 1) [0 1 1]	0.	-.001761	-.031438	0.	.004596	.011725
(-1 -1 1) [1 0 1]	-.408248	-.402531	-.412485	0.	-.004361	-.009336
(-1 -1 1) [-1 2 1]	.235702	.230368	.201846	0.	.007824	.018929
(-1 -1 1) [1 1 2]	-.235702	-.233418	-.256299	0.	.000136	.001379
(-1 -1 1) [2 -1 1]	-.471405	-.463786	-.458146	0.	-.007689	-.017550
(1 -1 1) [1 1 0]	.408248	.415017	.432586	0.	-.001145	-.015915
(1 -1 1) [-1 0 1]	-.408248	-.413145	-.398133	-.408248	-.412482	-.415488
(1 -1 1) [0 1 1]	0.	.001872	.034452	-.408248	-.413627	-.431402
(1 -1 1) [-2 -1 1]	-.471405	-.478139	-.479616	-.235704	-.237486	-.230694
(1 -1 1) [-1 1 2]	-.235704	-.237488	-.209971	-.471405	-.476955	-.488952
(1 -1 1) [1 2 1]	.235702	.240691	.269645	-.235702	-.239469	-.258259

*$[0.999763, -0.013002, 0.0174531]_\gamma$ *$[-0.705993, 0.708002, 0.017524]_\gamma$

**$[0.997842, 0.017615, 0.063259]_\gamma$ **$[-0.690949, 0.719926, 0.65542]_\gamma$

Table X. Schmid factors and measured directions of the tensile axes before and after testing for the $[\bar{1}\bar{1}2]_\gamma$ and $[\bar{2}\bar{1}3]_\gamma$ tensile axes specimens.

Slip Systems	Ideal $[\bar{1}\bar{1}2]_\gamma$	*Actual @ zero Strain	**Actual @ 4.85% Strain	Ideal $[\bar{2}\bar{1}3]_\gamma$	*Actual @ zero strain	**Actual @ 5.1% strain
(1 1 1) [1 -1 0]	0.	-.000061	-.003031	0.	-.001758	.003346
(1 1 1) [0 -1 1]	0.	-.001573	-.026786	0.	.007037	-.030823
(1 1 1) [-1 0 1]	0.	-.001512	-.023755	0.	.008795	-.034169
(1 1 1) [1 -2 1]	0.	-.000943	-.017215	0.	.003048	-.015864
(1 1 1) [-1 -1 2]	0.	-.001731	-.029179	0.	.009141	-.037523
(1 1 1) [-2 1 1]	0.	-.000838	-.011965	0.	.006092	-.021659
(-1 1 1) [1 1 0]	-.272166	-.256036	-.223984	-.349927	-.346890	-.320341
(-1 1 1) [1 0 1]	.136083	.134620	.117870	.116642	.121964	.112263
(-1 1 1) [0 -1 1]	.408248	.390656	.341854	.466569	.468854	.432604
(-1 1 1) [2 1 1]	-.078567	-.070099	-.061265	-.134687	-.129861	-.120134
(-1 1 1) [1 -1 2]	.314270	.303268	.265422	.336718	.341109	.314579
(-1 1 1) [-1 -2 1]	.392837	.373367	.326687	.471405	.470970	.434713
(-1 -1 1) [-1 1 0]	0.	-.032244	-.097820	.174964	.174226	.084397
(-1 -1 1) [0 1 1]	.272166	.254524	.200229	.349927	.355685	.286172
(-1 -1 1) [1 0 1]	.272166	.286768	.298049	.174964	.181458	.201775
(-1 -1 1) [-1 2 1]	.157135	.128333	.059126	.303046	.305944	.213948
(-1 -1 1) [1 1 2]	.314270	.312515	.287681	.303046	.310120	.281717
(-1 -1 1) [2 -1 1]	.157135	.184182	.228555	0.	-.174421	-.232598
(1 -1 1) [1 1 0]	-.272166	-.288341	-.324835	-.174964	.004175	.067768
(1 -1 1) [-1 0 1]	.408248	.422900	.439674	.291606	.294627	.348207
(1 -1 1) [0 1 1]	.136083	.134559	.114839	.116642	.120206	.115609
(1 -1 1) [-2 -1 1]	.392837	.410635	.441389	.269374	.270805	.335328
(1 -1 1) [-1 1 2]	.314270	.321849	.320148	.235702	.239504	.267784
(1 -1 1) [1 2 1]	-.078567	-.088786	-.121241	-.033672	-.031301	-.067544

*$[-0.384854, -0.433220, 0.814989]_\gamma$ *$[-0.529029, -0.261995, 0.807147]_\gamma$

**$[-0.349804, -0.495862, 0.794832]_\gamma$ **$[-0.490865, -0.365358, 0.790927]_\gamma$

0 0 0 0 3 9 0 5 7 8 7

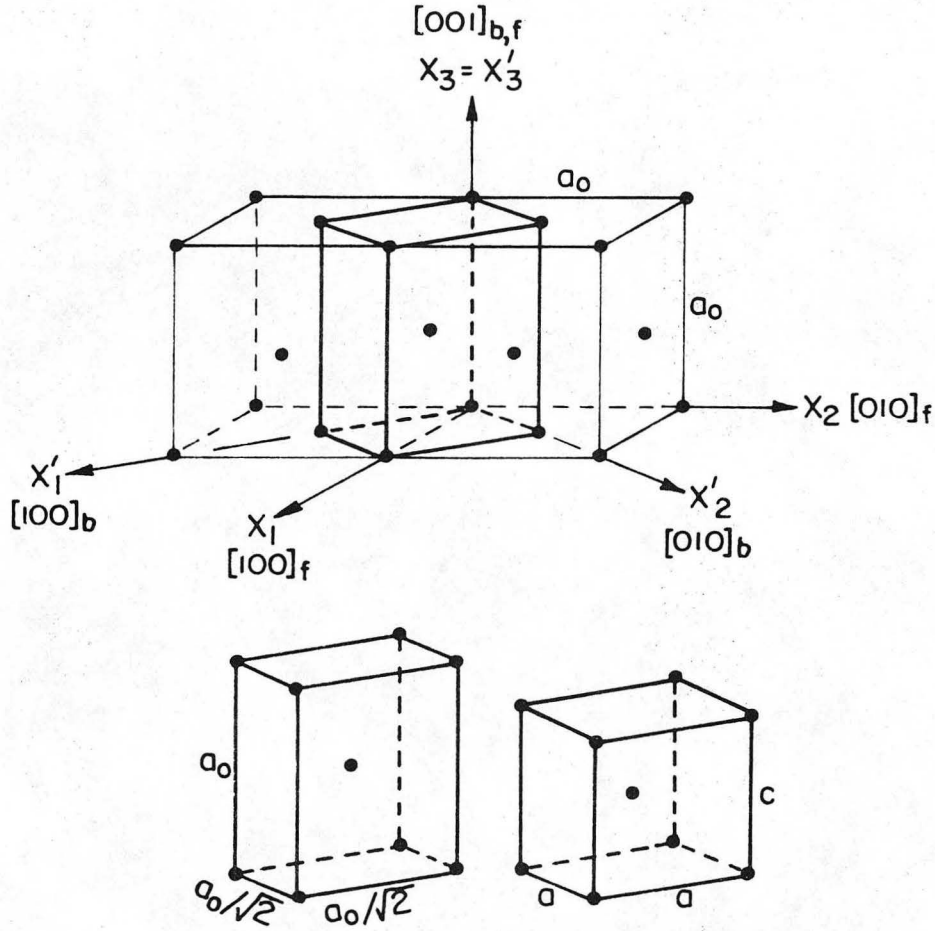

XBL 737-1525

Fig. 1. Lattice correspondence and lattice deformation for the $\gamma \rightarrow \alpha$ martensitic phase transformation in iron alloys (after Bain[7] and Wayman[10]).

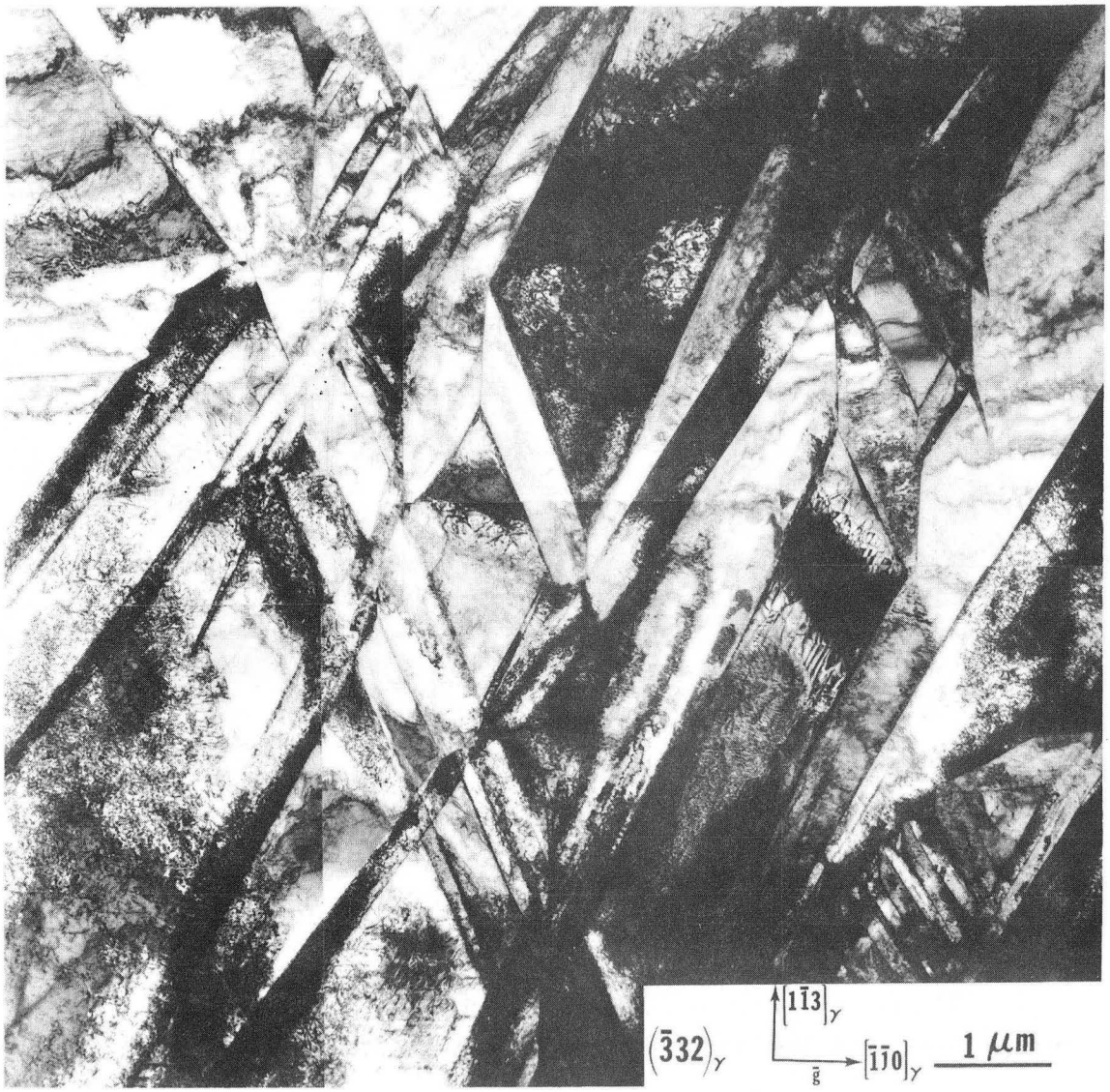

XBB 735-3371

Fig. 2. Montage showing a large area transformed to ε and α martensite. The ε cannot be seen because it is parallel to the plane of the figure. The α appears as needles joining at straight $\{112\}_\alpha$ twin boundaries. There are no twins observable inside the α martensite crystals.

0 0 0 0 3 9 0 5 7 8 8

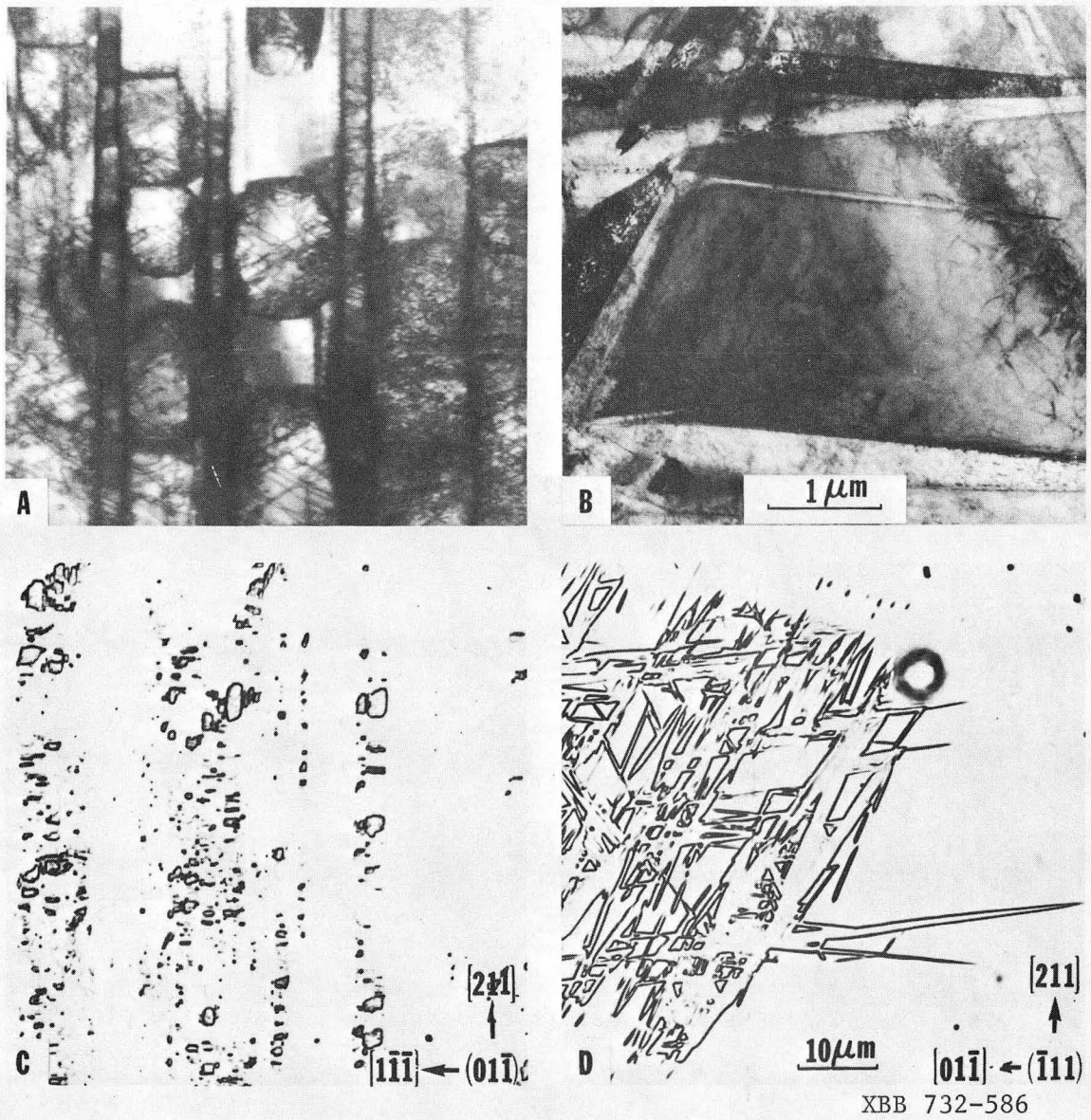

XBB 732-586

Fig. 3. Two surface analysis using the optical and electron microscopes. The crystal was sectioned to expose the $(01\bar{1})_\gamma$ and $(\bar{1}11)_\gamma$ surfaces. This micrograph clearly proves the α martensite geometry is acicular in this alloy. There are no twins observable inside the α martensite crystals.

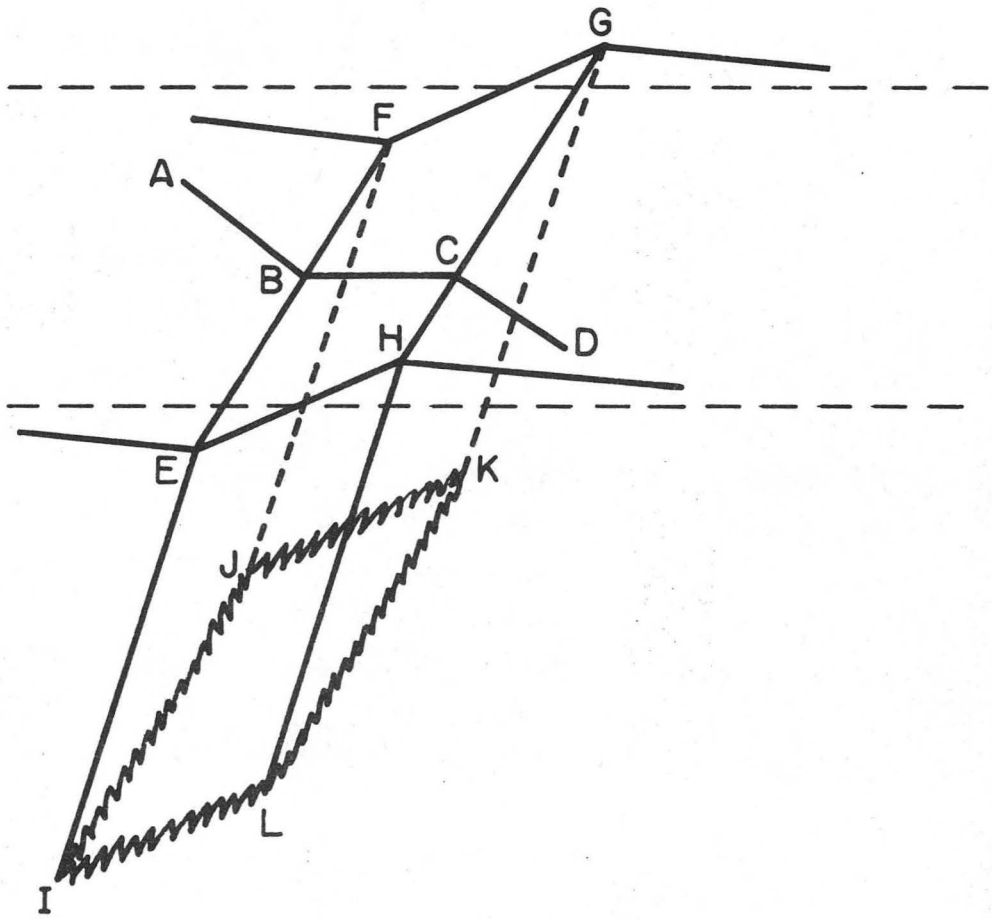

XBL 737-1524

Fig. 4. The shape deformation due to a martensite plate. Surface EFGH remains plane and tilted about EF and GH. The scratch ABCD, originally a straight line, remains continuous. The interfaces EFJI and HGKL are undistorted and no line in these interfaces is rotated by more than a small fraction of a degree (after Wayman[10] and Bilby and Christian[22]).

0 0 0 0 3 9 0 3 7 8 9

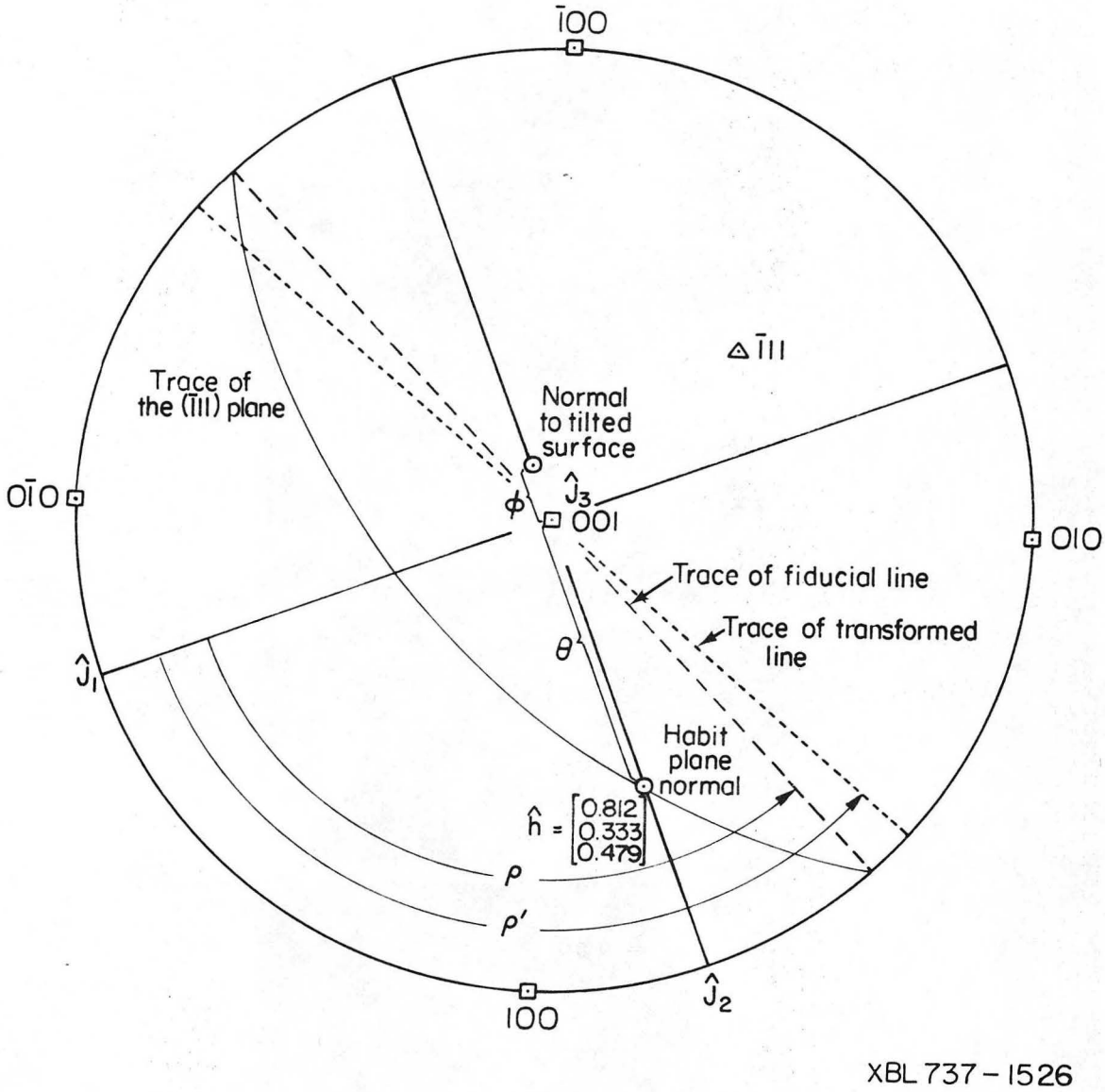

XBL 737-1526

Fig. 5. Sterographic projection showing how the J basis is defined, the position of the normal to the tilted surface and habit plane. All angles are positive as shown. (After Bowles and Morton.[23])

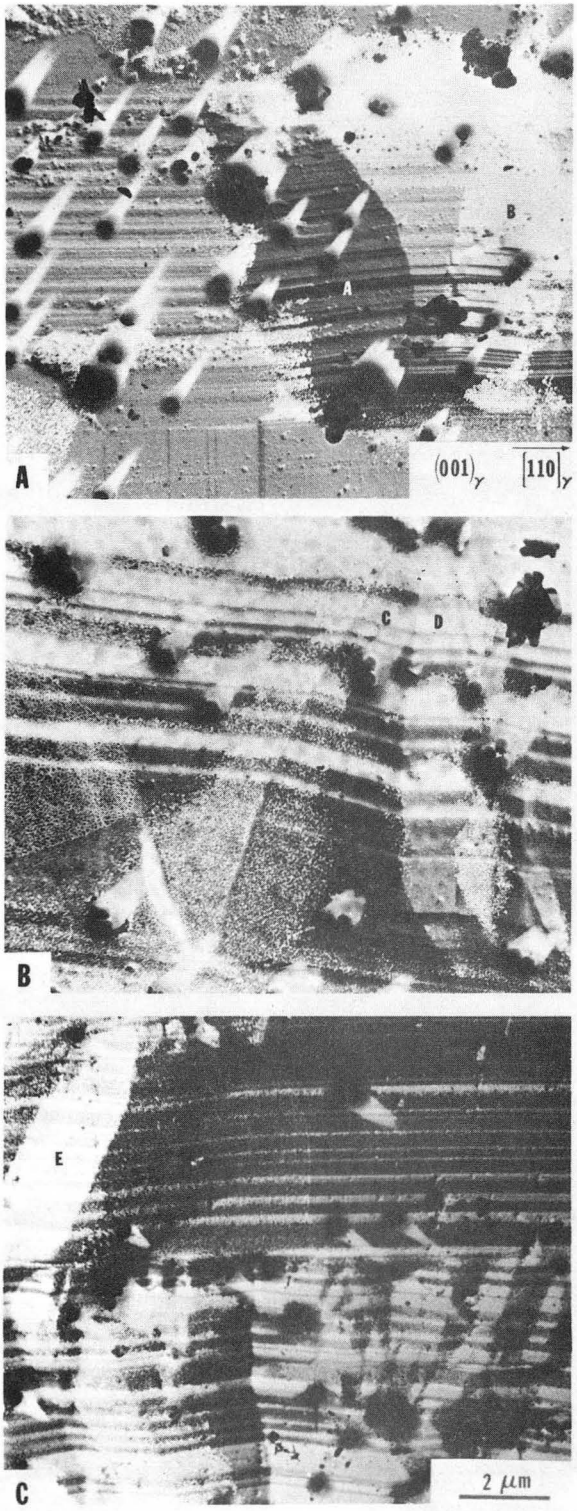

XBB 747-4731

Fig. 6. Gold shadowed carbon replicas of α martensite needles cutting the $(001)_\gamma$ surface. The fiducial lines used in shape change calculations are $[110]_\gamma$ slip traces. The results of shape change calculations from these electron micrographs are given in Table V.

0 0 0 0 3 9 0 3 7 9 0

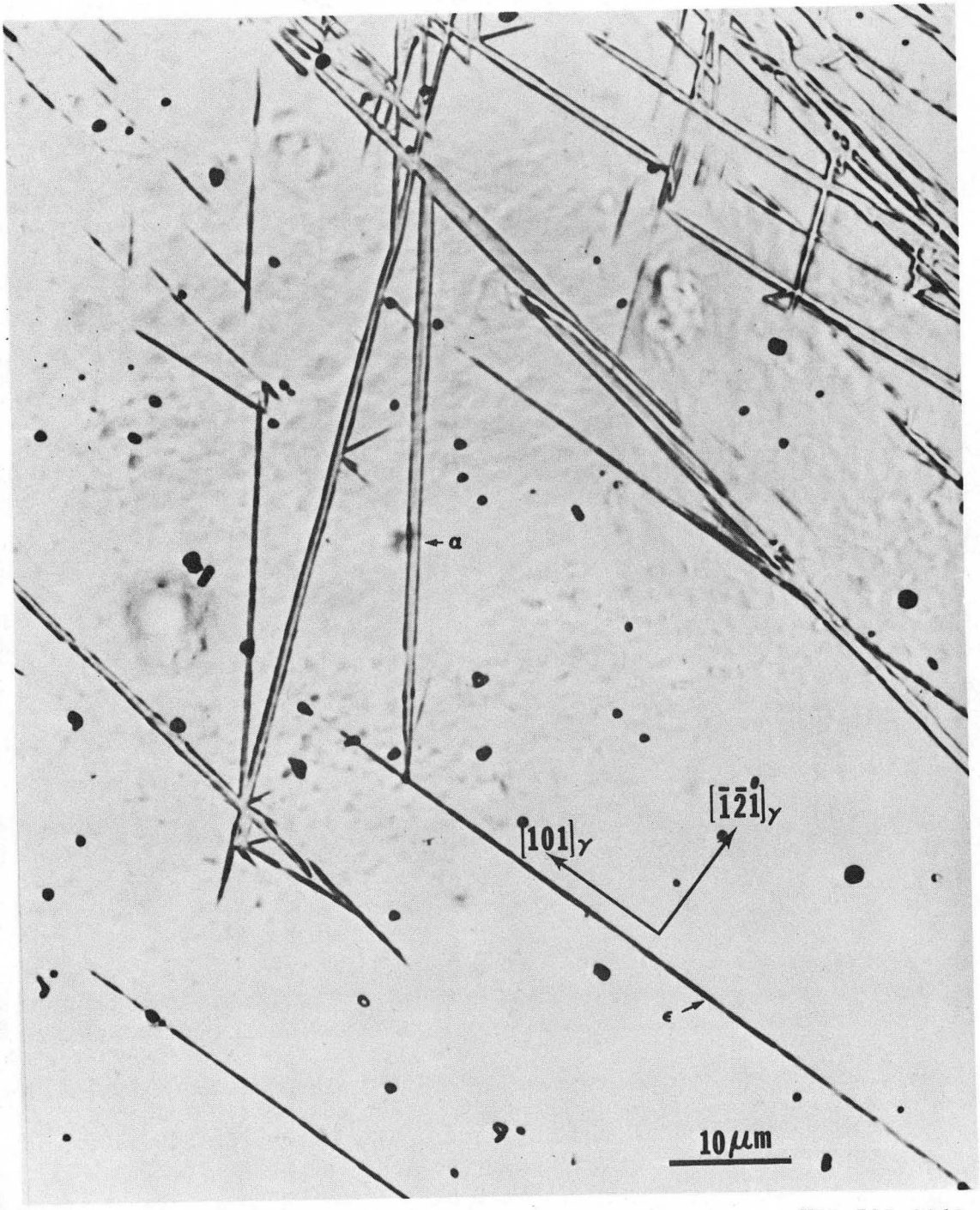

XBB 735-3369

Fig. 7. Optical micrograph of $(\bar{1}11)_\gamma$ surface showing the deformation induced α martensite needles bisecting $\langle 110 \rangle_\gamma$ directions. This is a typical example of the microstructure used to calculate the needle axis and habit plane normal.

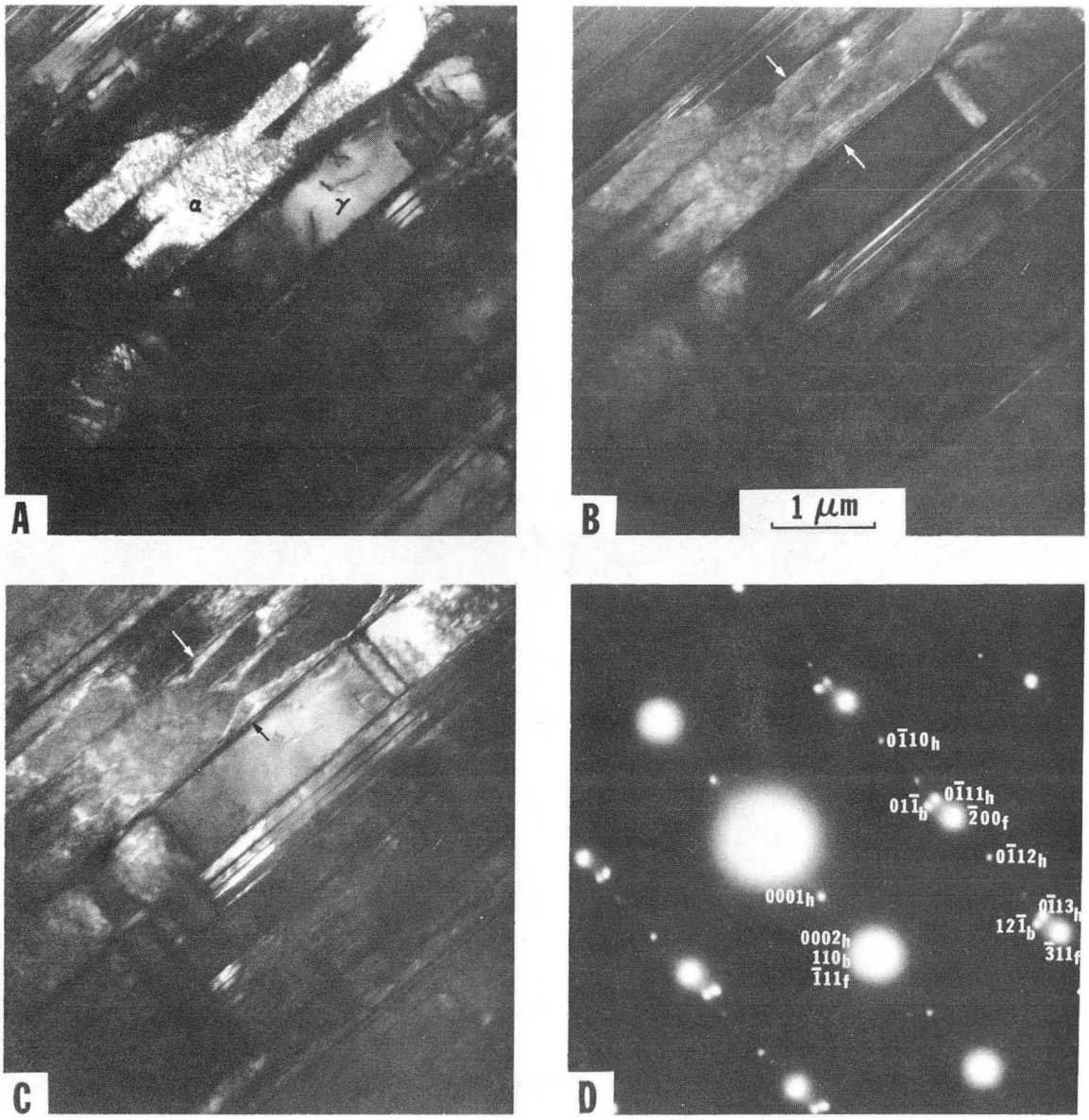

XBB 734-2477

Fig. 8. Electron micrographs identifying the deformation induced ε martensite phase, showing the K-S orientation relationship between γ(f)-ε(h)-α(b) and revealing the structure of the γ-ε-α interface, A is the bright field image. B is the dark field image using the $(0\bar{1}11)_\varepsilon$ reflection, C is the dark field image using the $(\bar{2}00)_\gamma$ reflection and D is the electron diffraction pattern of the three superimposed phases.

0 0 0 0 3 9 0 3 7 9 1

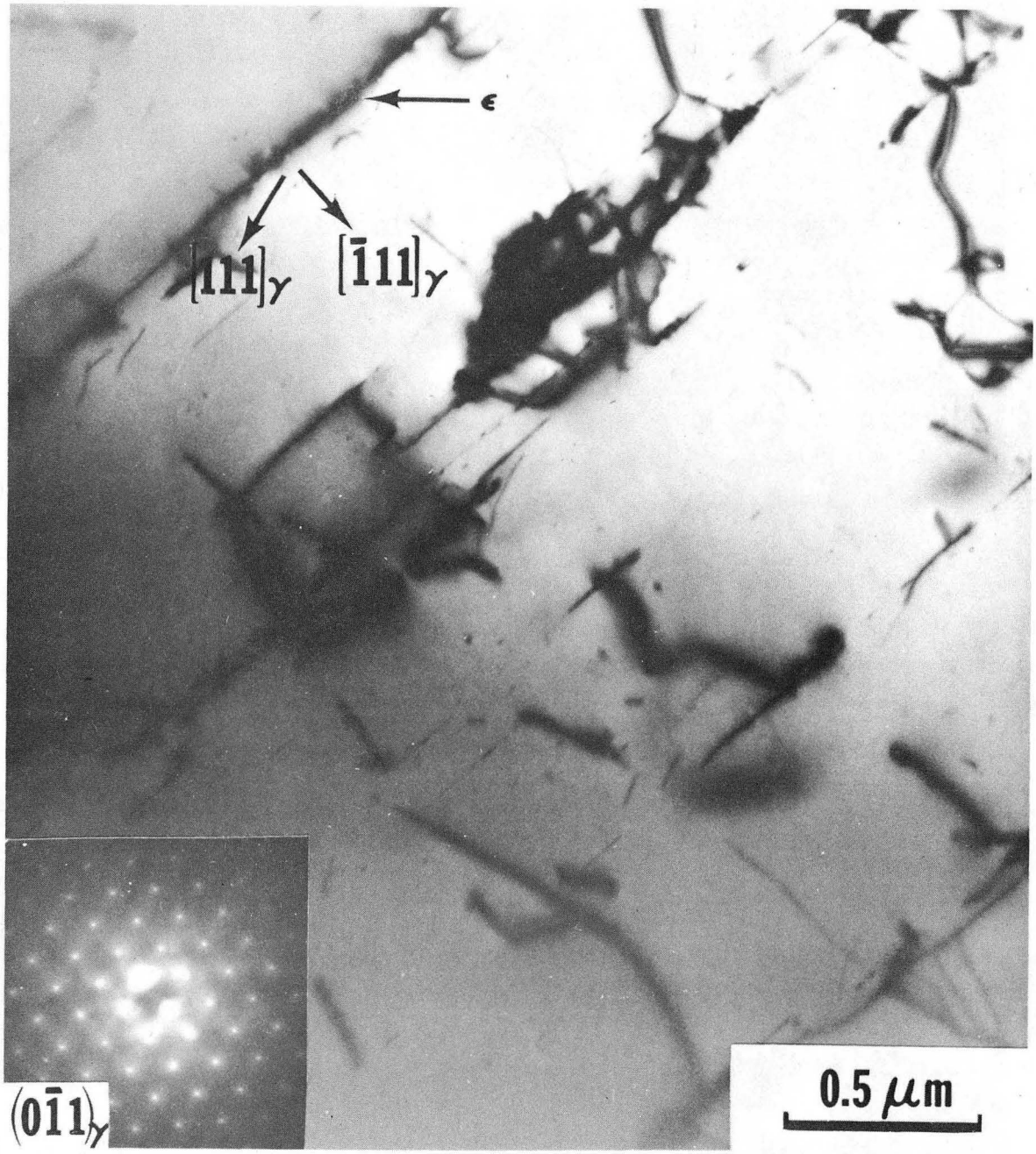

XBB 737-4664

Fig. 9. Electron micrographs showing the deformations induced ε phase in a crystal containing no α martensite. In this example sheets of ε are laying on $(\bar{1}11)_\gamma$ planes.

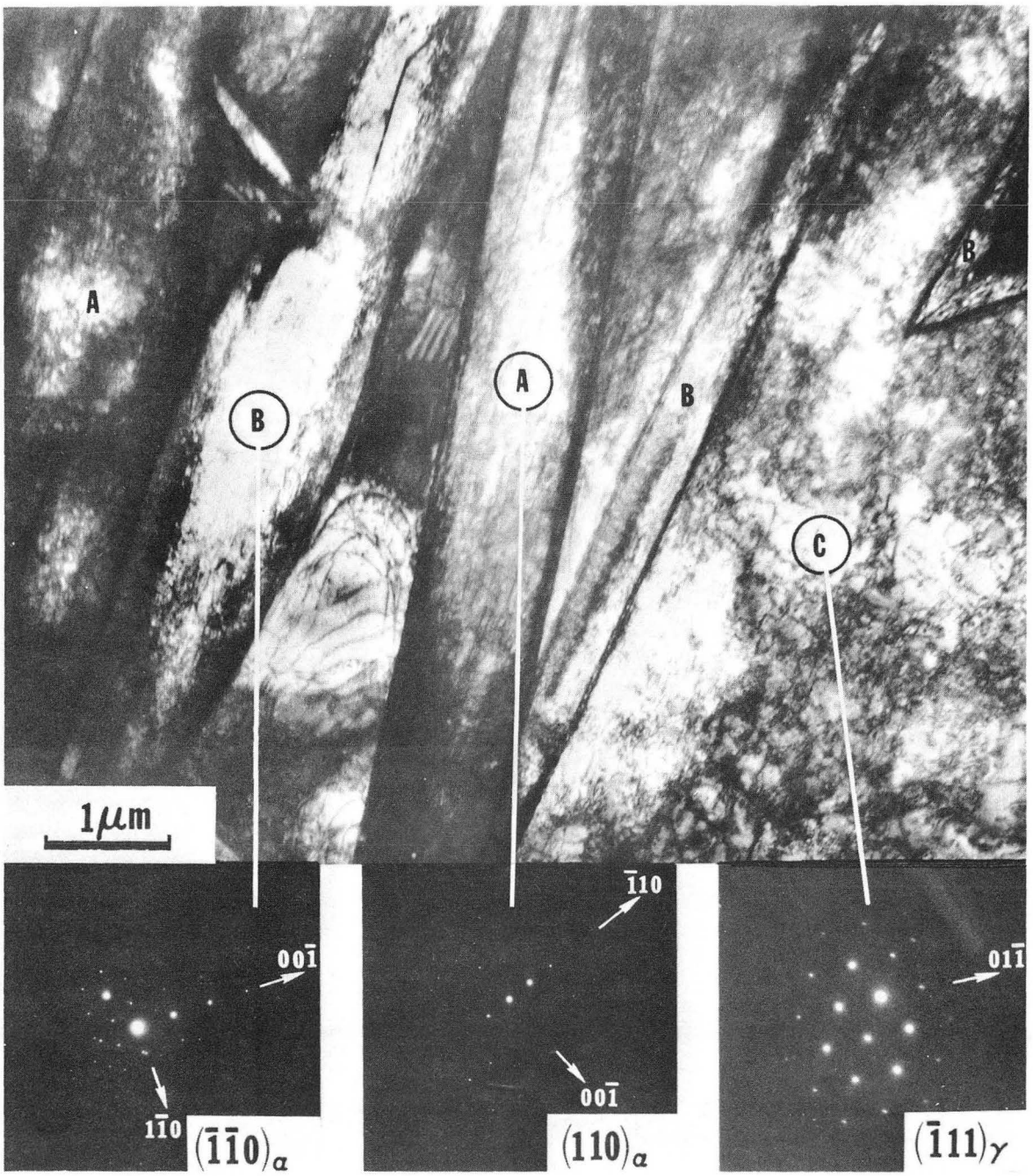

XBB 737-4665

Fig. 10. Electron micrographs showing that each α martensite needle pair join at a $\{112\}_\alpha$ twin boundary. Needles marked A and B are the same orientation. The region marked C is the austenite.

0 0 0 0 3 9 0 3 7 9 2

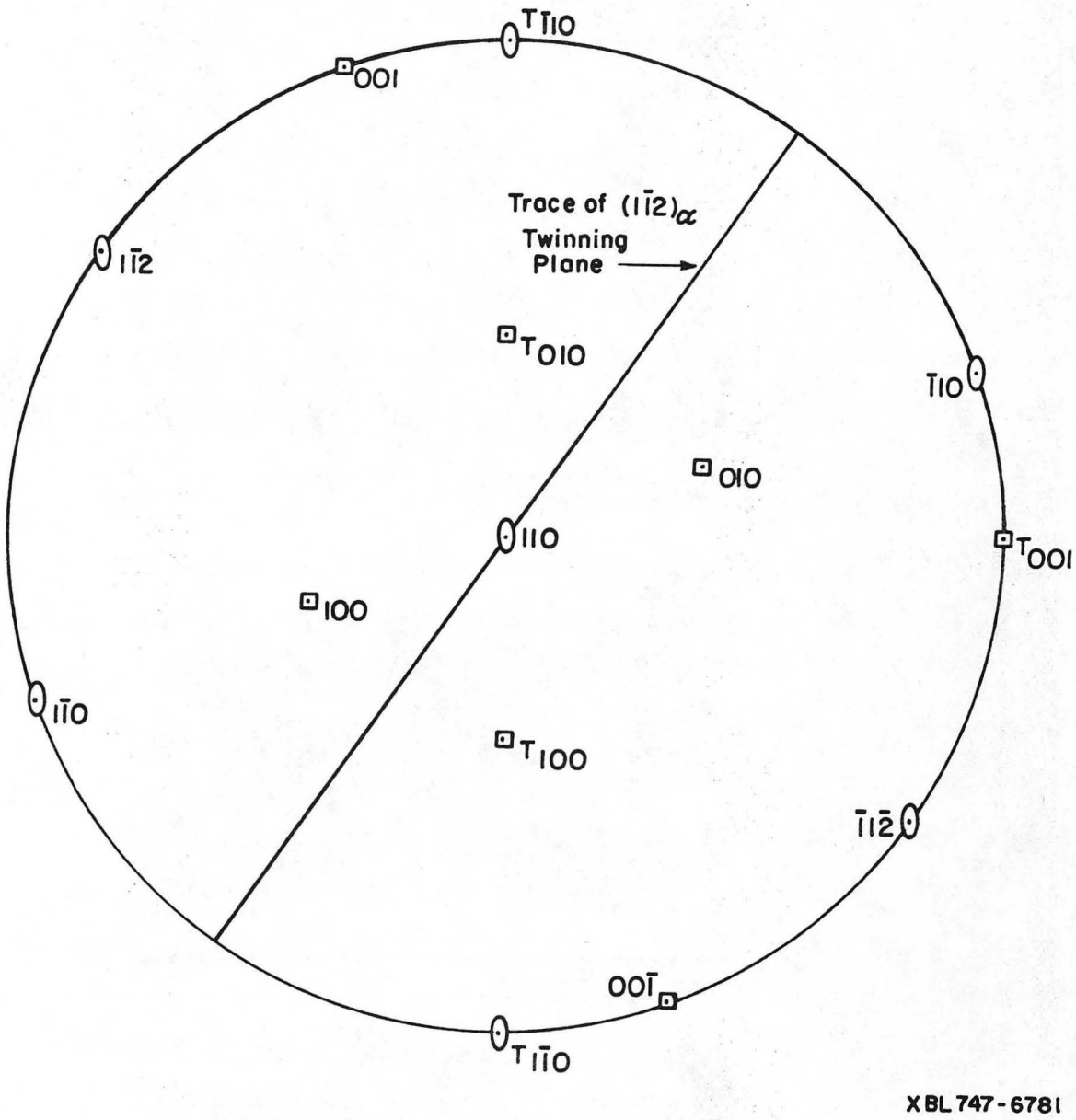

Fig. 11. Sterographic analysis of Fig. 10 showing that the needles A and B join at a $(11\bar{2})_\alpha$ twin boundary.

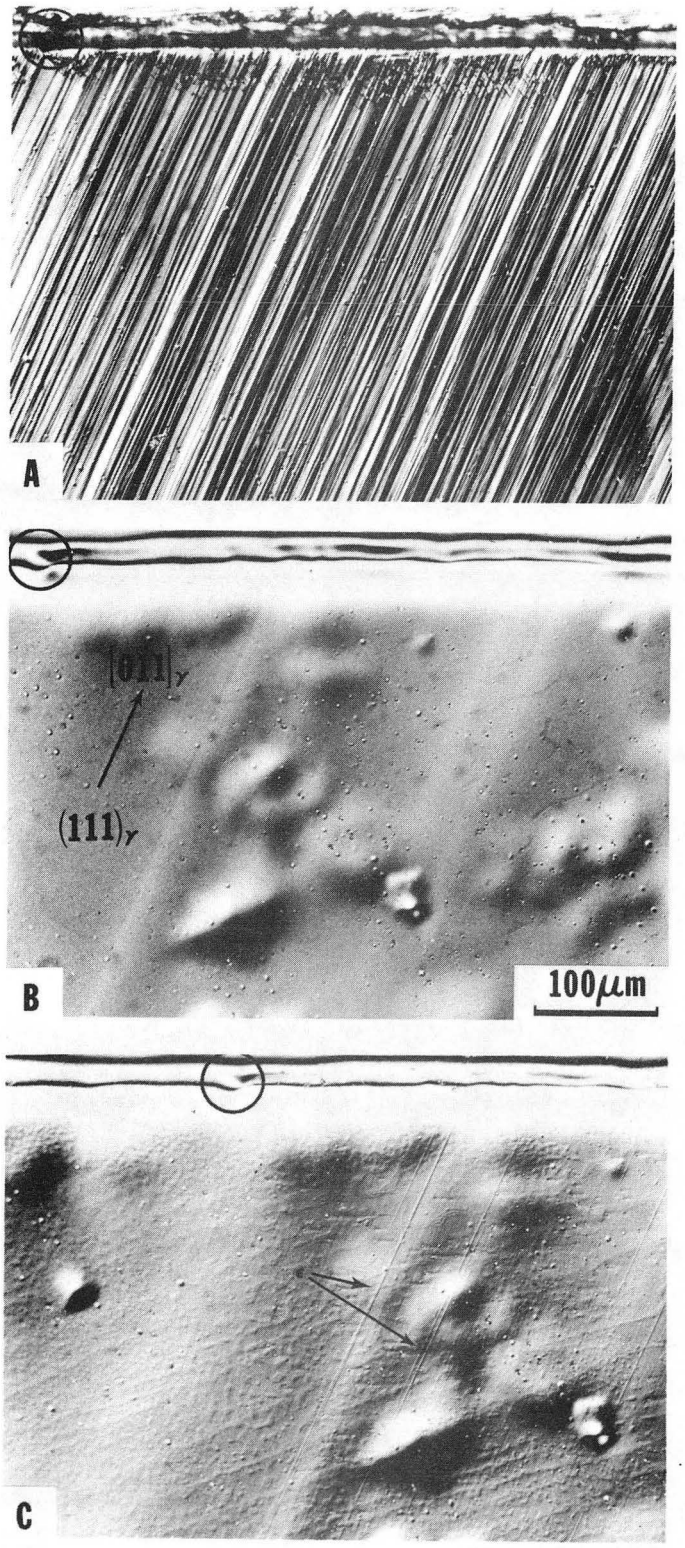

XBB 737-4790

Fig. 12. Optical micrographs of a $(111)_\gamma$ surface of a crystal tested at 242°K showing (A). The slip line structure, (B) same area after electropolishing, and (C) same area after etching to reveal the ε martensite. The circle over the scratch placed on the specimen for a reference identifies the same region of the crystal in each micrograph.

0 0 0 0 3 9 0 5 7 9 3

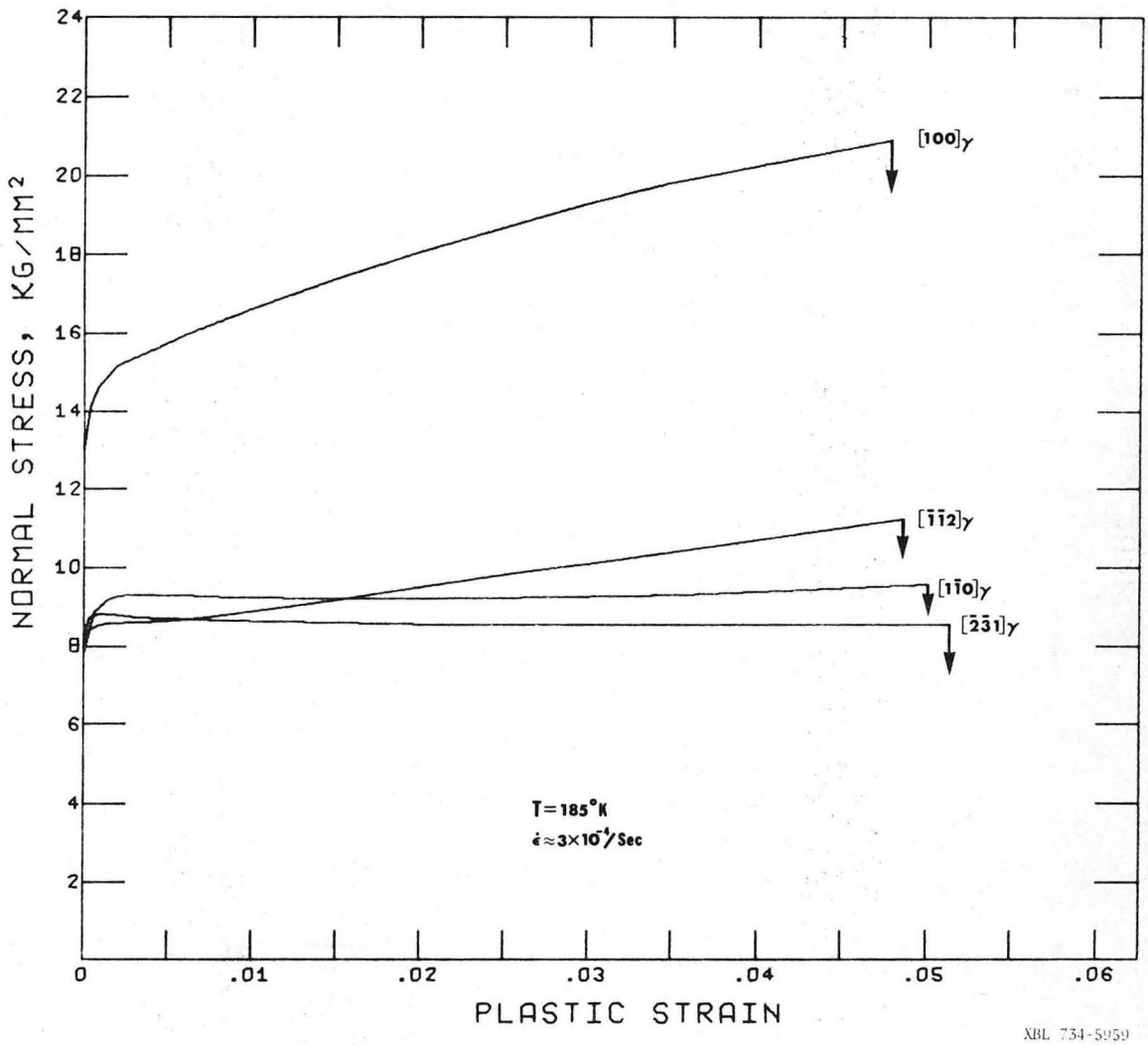

Fig. 13. Stress-strain curves for each crystal tested at 185°K to approximately 5% tensile strain.

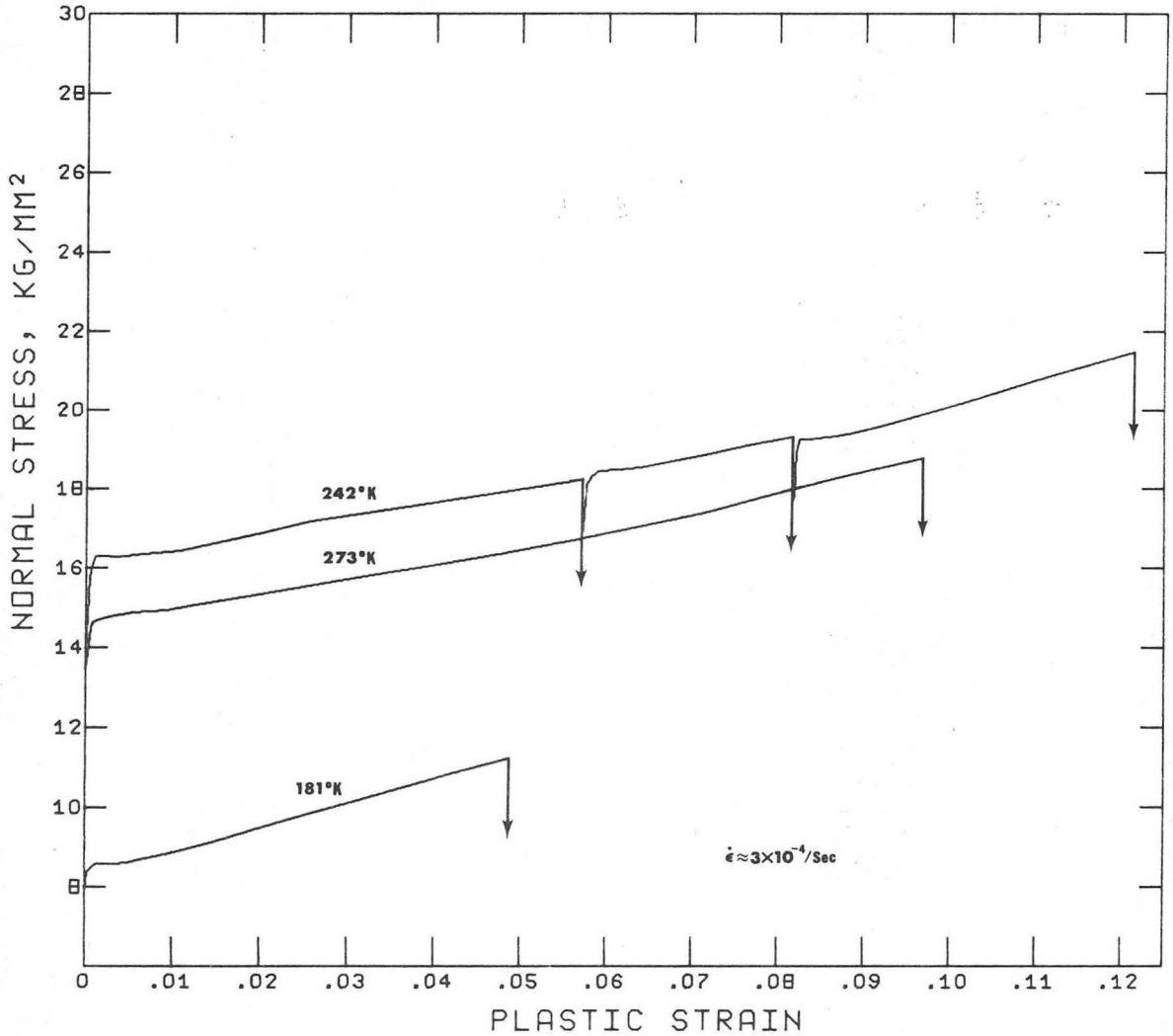

XBL 7011-6953

Fig. 14. Stress-strain curves for $[\bar{1}\bar{1}2]_\gamma$ tensile axis specimens tested at 181°, 242° and 273°K.[21,25]

0 0 0 0 3 9 0 5 7 9 4

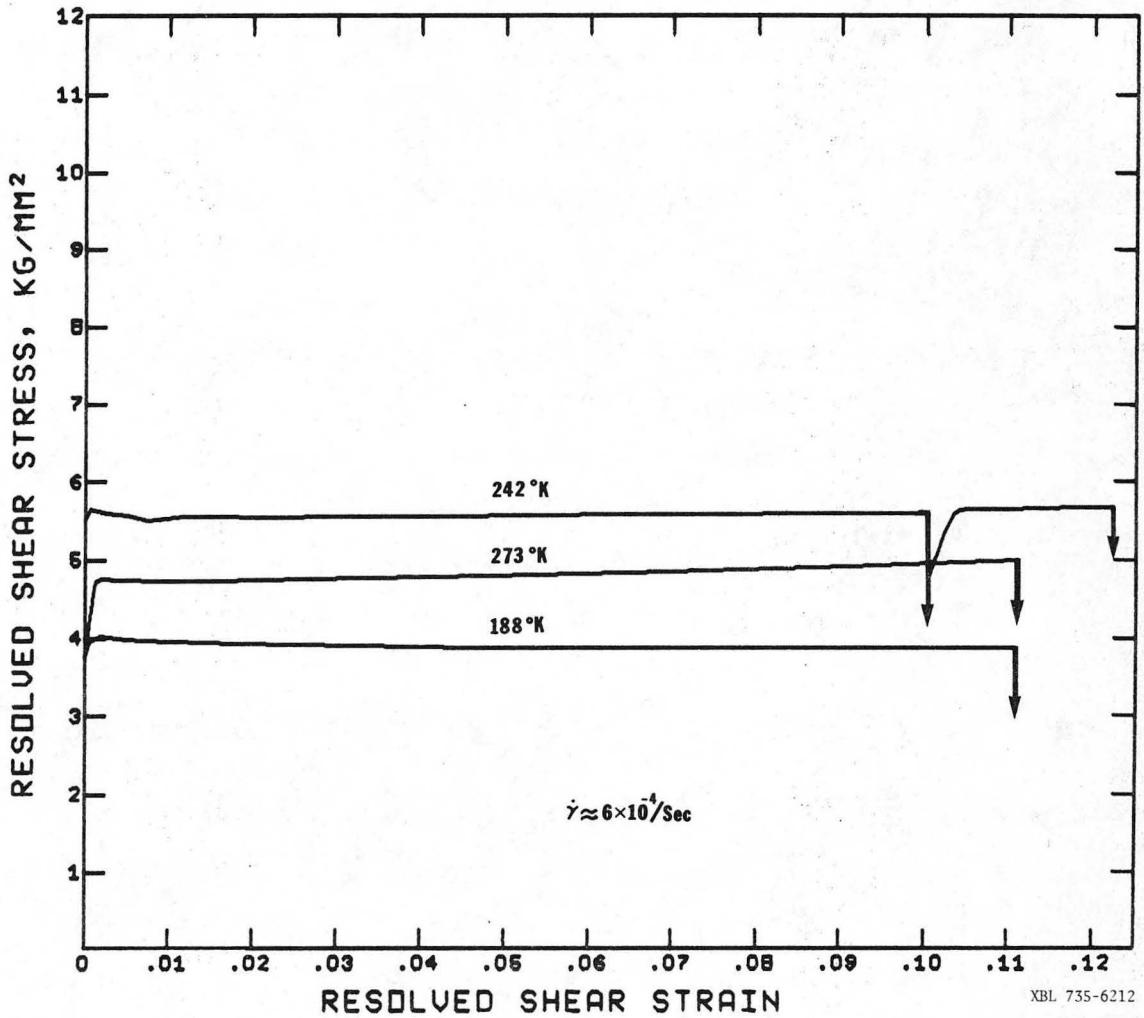

Fig. 15. Stress-strain curves for $[\bar{2}\bar{1}3]_{\gamma}$ tensile axis specimens tested at 188°, 242° and 273°K.[21,25]

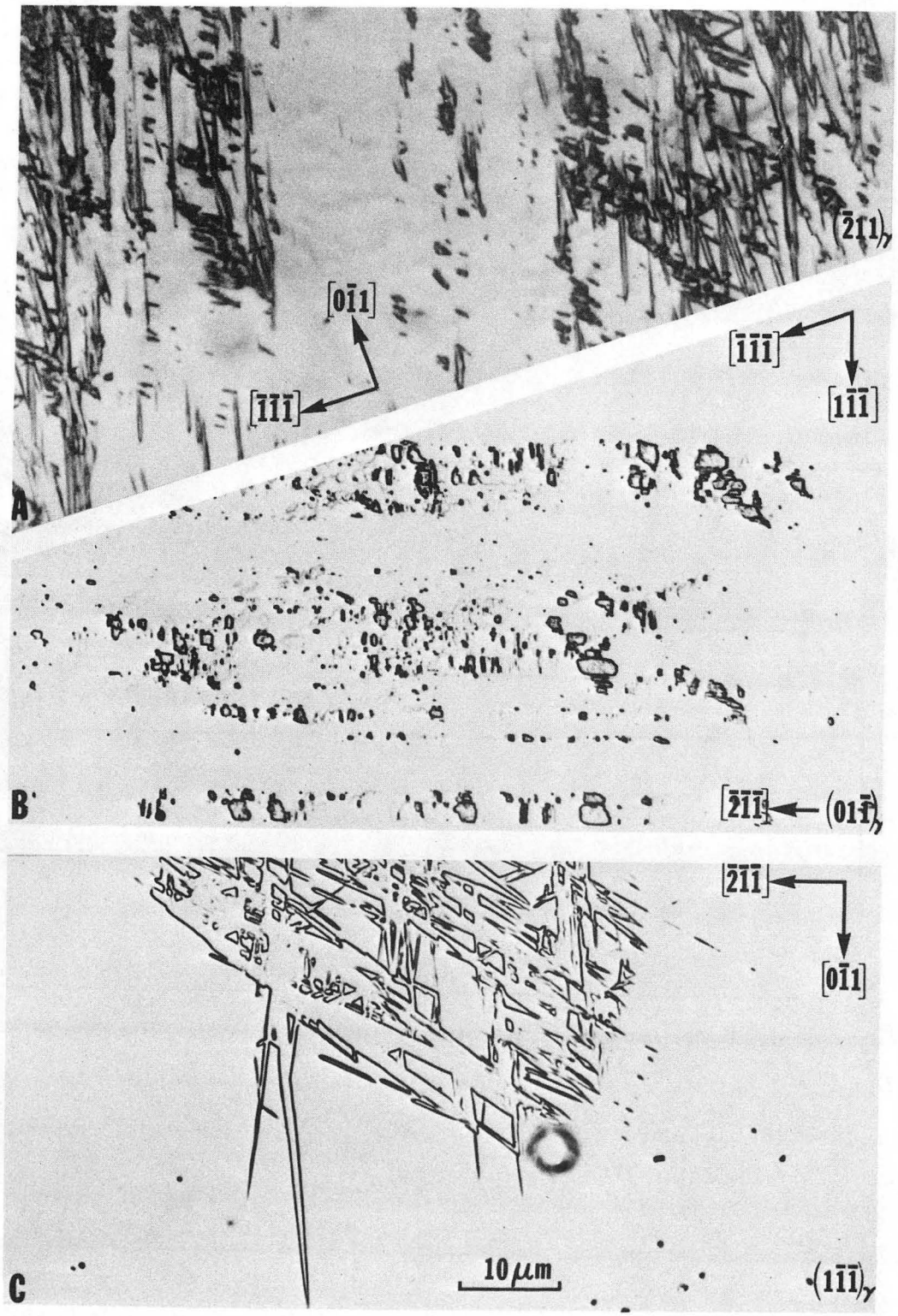

XBB 734-2476

Fig. 16. Three surface analysis showing (A) the $(\bar{2}11)_\gamma$ surface, (B) the $(01\bar{1})_\gamma$ surface, and (C) the $(1\bar{1}\bar{1})_\gamma$ surface of a $[\bar{2}\bar{1}3]_\gamma$ tensile axis specimen tested to 5% tensile strain at 185°K.[25]

0 0 0 0 3 9 0 5 7 9 5

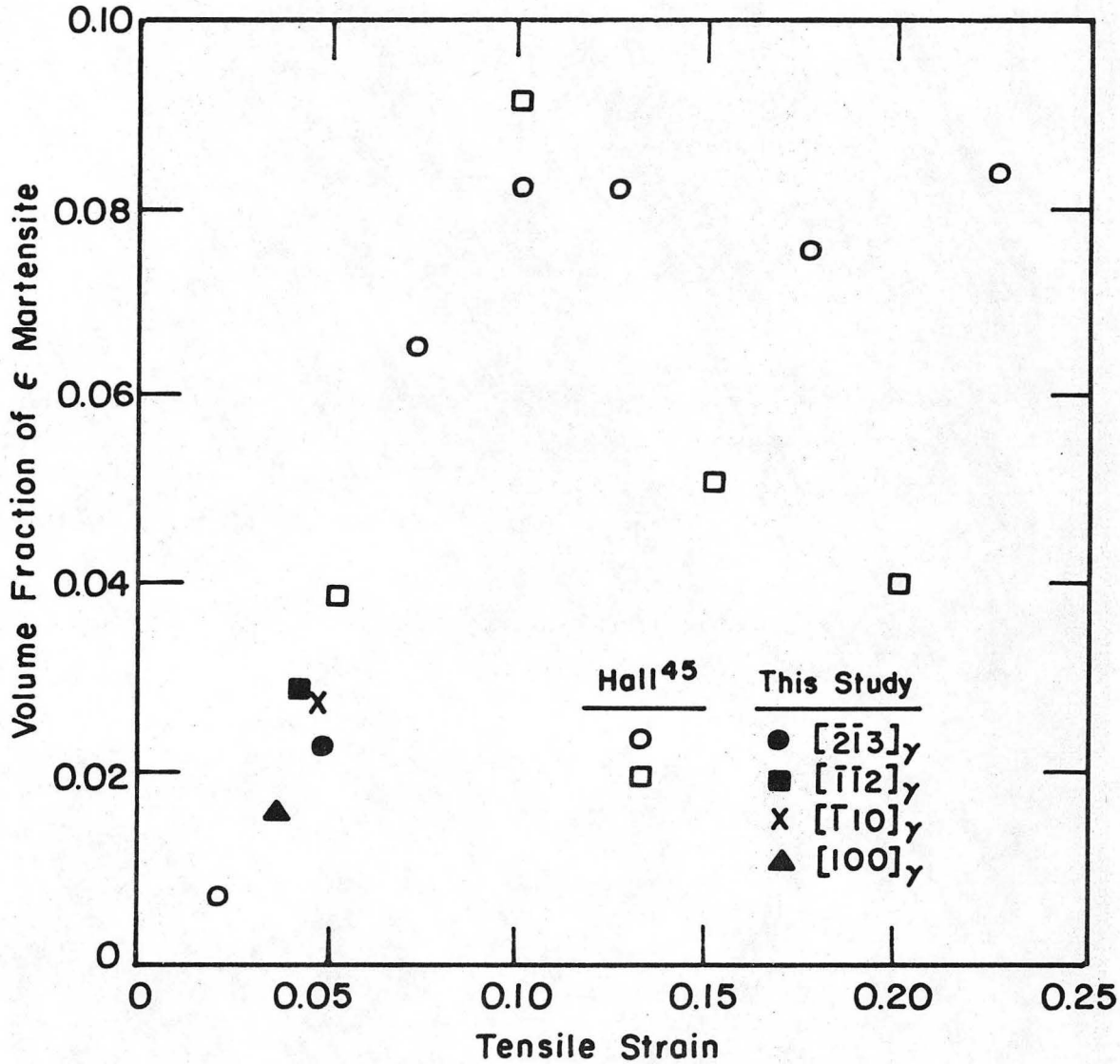

XBL 747-6780

Fig. 17. The variation of the volume fraction of deformation induced ε martensite as a function of tensile strain and orientation of the tensile axis.

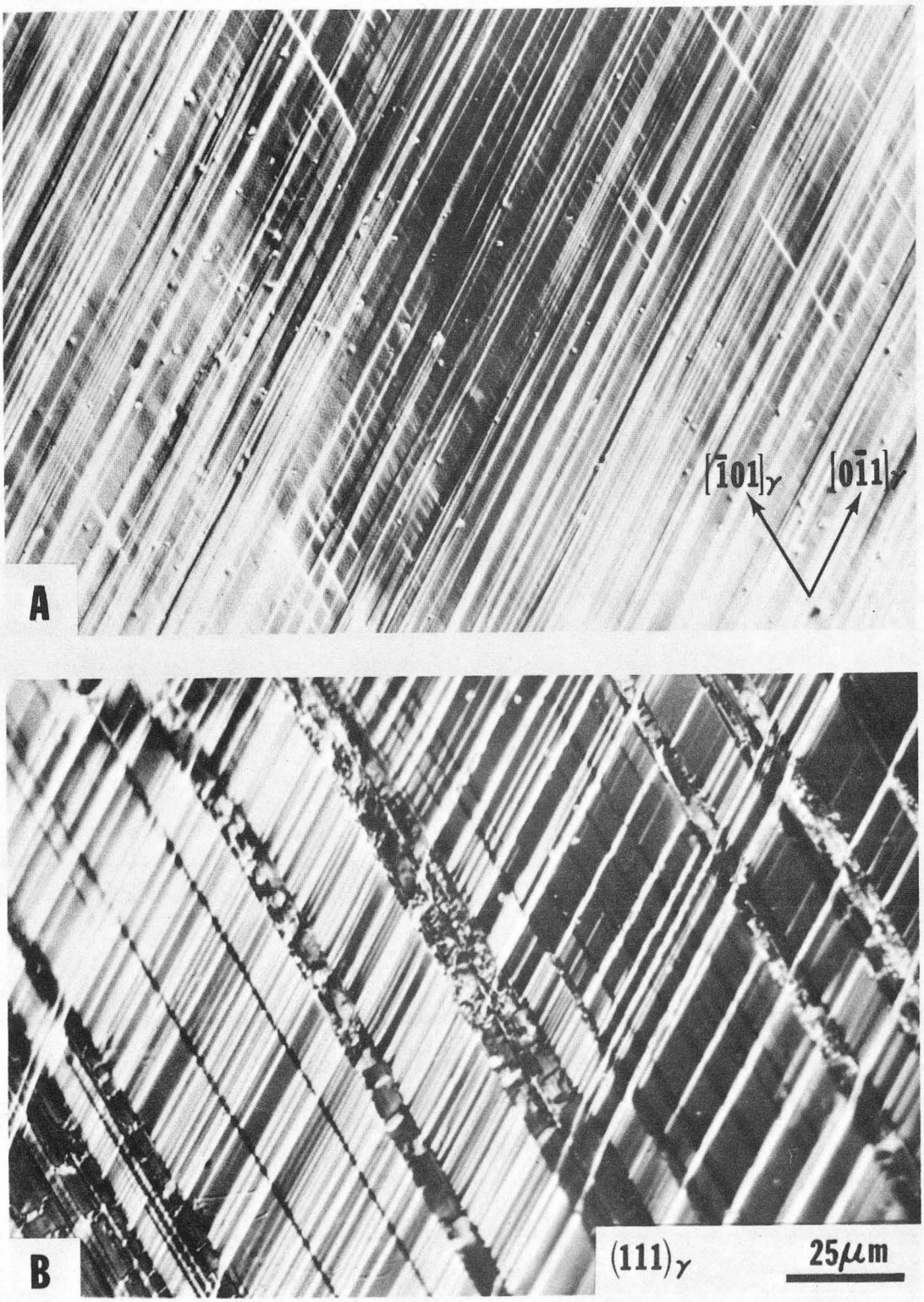

XBB 747-4730

Fig. 18. The slip line structure of (A) a $[\bar{1}\bar{1}2]_\gamma$ tensile axis specimen tested to 15% tensile strain at 242°K and (B) a specimen of the same orientation tested to 5% tensile strain at 185°K. Note the large slip steps in each of these crystals. The specimen tested at 185°K transformed partially to α martensite.

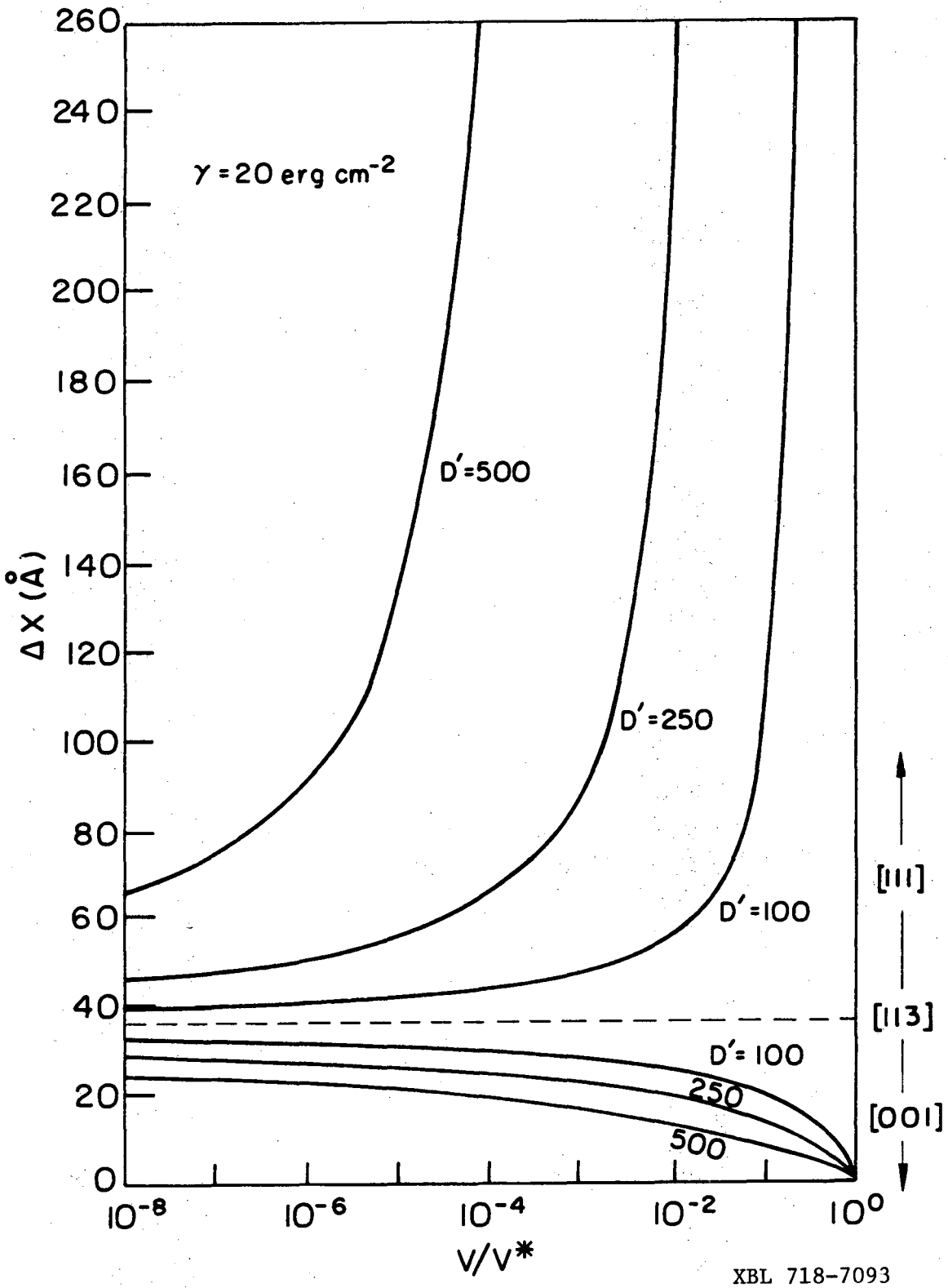

XBL 718-7093

Fig. 19. Plot showing the dynamic separation of partial dislocations as a function of resolved shear stress on the following and leading partials for crystals with $[111]_\gamma$, $[113]_\gamma$ and $[001]_\gamma$ tensile axes.[52]

LEGAL NOTICE

This report was prepared as an account of work sponsored by the United States Government. Neither the United States nor the United States Atomic Energy Commission, nor any of their employees, nor any of their contractors, subcontractors, or their employees, makes any warranty, express or implied, or assumes any legal liability or responsibility for the accuracy, completeness or usefulness of any information, apparatus, product or process disclosed, or represents that its use would not infringe privately owned rights.

TECHNICAL INFORMATION DIVISION
LAWRENCE BERKELEY LABORATORY
UNIVERSITY OF CALIFORNIA
BERKELEY, CALIFORNIA 94720